GROWTH AND CHARACTERIZATION OF GALLIUM ARSENIDE GROWN BY

CONVENTIONAL AND CURRENT-CONTROLLED LIQUID PHASE EPITAXY

by

RONALD PAUL GALE

B.S., Cornell University
1972

M.Engr., Cornell University
1973

Submitted in partial fulfillment
of the requirements for the
degree of

DOCTOR OF PHILOSOPHY

at the

MASSACHUSETTS INSTITUTE OF TECHNOLOGY

JUNE 1978

Signature of Author..
Department of Materials Science and Engineering
May 5, 1978

Certified by..
Thesis Supervisor

Accepted by...
Chairman, Departmental Committee on Graduate Students

GROWTH AND CHARACTERIZATION OF GALLIUM ARSENIDE GROWN BY

CONVENTIONAL AND CURRENT-CONTROLLED LIQUID PHASE EPITAXY

by

RONALD PAUL GALE

Submitted to the Department of Materials Science and Engineering
on May 5, 1978, in partial fulfillment of the requirements
for the degree of Doctor of Philosophy.

ABSTRACT

GaAs epitaxial layers were grown from a Ga solution by conventional and current-controlled liquid phase epitaxy (LPE), and were characterized with respect to growth and segregation behavior. The growth experiments were carried out at temperatures ranging from 700 to 875°C using furnace cooling rates below 2°C/min with and without applied currents of densities up to 20 A/cm^2. Gallium solutions were doped with tin or tellurium such that epilayers exhibited charge carrier concentrations from 2×10^{16} to 4×10^{17} cm^{-3}, as measured by the capacitance-voltate technique utilizing a mercury Schottky diode probe. The carrier concentration data were related to the growth behavior. Growth rates and layer morphology were determined from interface demarcation introduced during growth by periodic currnet pulses. The growth rates associated with conventional and current-controlled LPE ranged from 0.02 to 2.3 μm/min.

A theoretical and experimental analysis of growth associated with conventional LPE in the present configuration indicates the presence of equilibrium conditions at the growth interface and free convection in solution. Layer thicknesses were found to correspond to growth dictated by the Ga-As liquidus assuming a 50% deposition efficiency. The initial transient growth behavior could be fitted to a model which permitted the determination of a theoretical momentum boundary layer thickness which was, for horizontal heat flow, found to depend on the Grashof number.

Current-controlled LPE of GaAs was carried out in two different exper-imental configurations involving growth with and without a GaAs source.

The growth behavior for both methods was found to involve solute transport and thermal effects, which include diffusion, convection, electromigration, Peltier cooling, and Joule heating. An analysis of growth without a source was carried out on the basis of a theoretical model presently developed. It indicated that growth without a source was primarily due to electromigration of As. The analysis yielded, in addition, values for both the diffusivity (D_{As} = 0.32 exp[-9700/T] cm^2/sec) and the differential electromigration mobility (μ_{As} = 0.32 exp[-2330/T] cm^2/V-sec) of As in Ga over the temperature range from 700 to 850°C. The value for μ_{As} at 850°C)0.04 cm^2/V-sec) was confirmed by independent electromigration experiments. Applying these results to growth under steady-state current-controlled conditions (with a source), it was found that thermal effects tended to reduce the growth rate by up to 40% from those predicted for electromigration (at 10 A/cm^2 and 850°C). The Joule and Peltier effects were thus found to significantly affect steady-state current-controlled growth.

Using interface demarcation, the nature and origin of non-uniform growth were investigated. It was found that thickness variations in conventional LPE are due to variations in the momentum boundary layer near the substrate-solution interface, while thickness variations in current-controlled LPE without a source were primarily due to variations in the original growth interface. It was observed that during conventional LPE and the initial transient of current-controlled LPE, a significant reduction occurred in the amplitude of the morphological variations of the layers.

The growth interface temperature was determined to be the controlling parameter for segregation of Sn and Te at or near 850°C. Variations in layer carrier concentrations could be attributed solely to changes in the interface temperature, and were found to be unaffected by the growth rate (R < 2 μm/min) or by the application of an electric current (up to 10 A/cm^2 for Sn-doping to 20 A/cm^2 for Te-doping). By analyzing the effect of current on segregation in layers grown with both current polarities, it was concluded that local equilibrium conditions exist at the growth interface during current-controlled LPE. The value for the equilibrium distribution coefficient of Sn at 850°C in GaAs was determined to be 6.7 x 10^{-4}.

Thesis Supervisor: August F. Witt

Title: Professor of Materials Science and Engineering

TABLE OF CONTENTS

LIST OF FIGURES

LIST OF TABLES

ACKNOWLEDGMENTS

Appreciation is extended to the staff of the Electronic Materials Group, including J.C. Baker, J. DiMaria, P. Merrick, P. Jastrzebski, and especially to G. Landahl who has been extremely helpful throughout the present work and has done an exceptional job of typing this manuscript.

Financial support from the National Science Foundation (MRL) is gratefully acknowledged. The author would also like to thank both the Materials Science Center Central Facility for the use of certain laboratory equipment, and the IBM Watson Research Center for a fellowship during 1976-77.

Special thanks are extended to C.O. Bozler and R. McClelland of MIT Lincoln Laboratory for discussions on GaAs and for the use of their C-V Profiler which was instrumental in the completion of the present work.

I would like to thank each member of my family for the love, encouragement, and support which I have always appreciated. My wife, Carrie, has been a constant source of love and understanding, and has provided a great deal of help in the preparation of this manuscript.

To Carrie this thesis is dedicated.

1. INTRODUCTION

The role of semiconductor crystal growth in the manufacture of electronic devices is becoming increasingly important due to the greater demands on compositional and crystalline perfection of materials made by new and smaller devices. The needed control of these material properties is not presently available with bulk growth from the melt. However, using wafers cut from melt-grown crystals as substrates, epitaxial layers have been grown (from the liquid and vapor phases) which exhibit the necessary properties and have been fabricated into operating devices. The use of epitaxy allows control over layer composition and leads to better crystalline perfection in the layer compared to the substrate, partially due to the lower growth temperatures possible and the slower growth rates used.

In many specific applications, the use of liquid phase epitaxy (LPE) has certain advantages over vapor phase epitaxy (VPE). The growth apparatus is simpler for the former, and avoids the use of corrosive gases. Higher growth rates are possible for LPE, and there is more of a variety of possible dopants that can be introduced into the layer from solution. The stoichiometry of the compound is fixed by the equilibrium phase diagram. Because of these advantages, liquid phase epitaxy is most widely used presently for the growth of GaP, GaAs, III-V ternaries, and garnets.

GaAs grown by LPE is particularly important because of its optical and electrical properties. Gallium arsenide has a direct band gap which is ideally suited for solar cell applications. The high electron mobilities in high purity layers enables the material to be used in microwave frequency applications. The matching lattice constant of GaAs and

AlAs has led to the growth of heterojunction lasers, which are an important part of the developing optical communication systems. For all of these device applications it is required that the material can perform at or near its theoretical limits. More stringent requirements for epitaxial growth have brought out specific problems associated with liquid phase epitaxial growth of gallium arsenide. To understand the origin of these problems, it is desirable to first review the basic physical processes that are involved in LPE growth.

Liquid phase epitaxy of GaAs is growth of the compound from Ga-rich or As-rich solutions at temperatures below the melting point of GaAs and above the eutectic temperatures of Ga and As, respectively. Because of the high vapor pressure of As at temperatures above its melting point and material handling difficulties, gallium-rich solutions are normally used for LPE. Growth from solution is achieved by exceeding the solubility limit of As in the liquid, given by the liquidus curve in the equilibrium phase diagram. This can be accomplished in one of two ways represented by arrows from point A in Figure 1.1. The solution may be cooled below its liquidus temperature (A → B), and/or the local concentration of arsenic at the growth interface may be increased (A → C). The latter method involves transport of As to the interface and will be discussed in terms of kinetics in Chapter 2 and Section 5.1.

There are many different techniques and apparatus utilized for LPE growth, but basically they are all variations of the two aforementioned processes. Any one of the various techniques employed has specific advantages but all have inherent deficiencies. For example, when the temperature of the system is changed upon continuous cooling, the dopant distri-
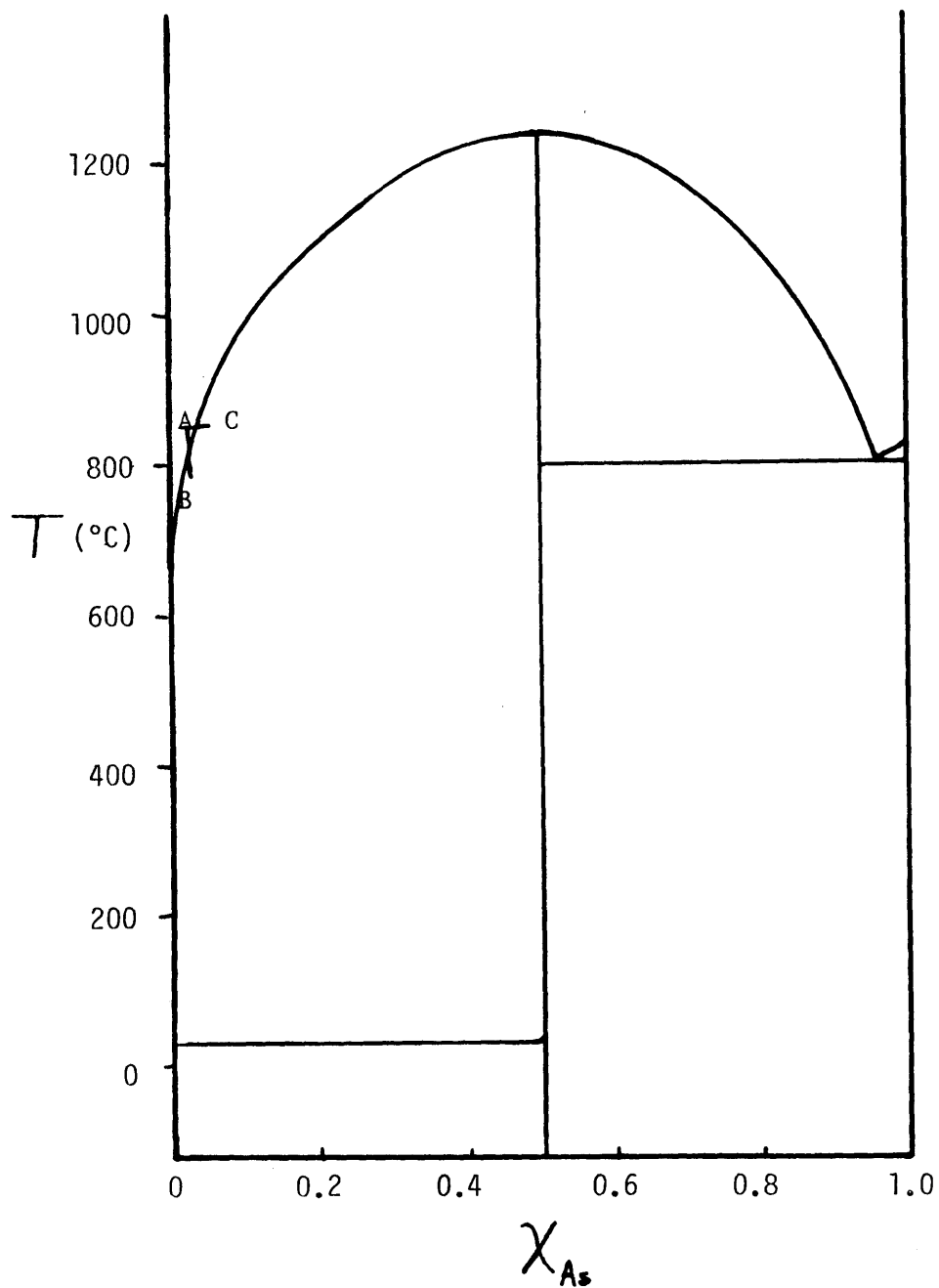
Figure 1.1: Gallium-arsenic phase diagram. (Point A is in the liquid field, points B and C are in the two-phase field of liquid and GaAs compound.)

bution coefficient also changes, leading to inhomogeneous doping. If step-cool growth is used instead, deposition is at constant temperature after the temperature drop (ΔT) has been imposed, but the maximum layer thickness is limited by ΔT which is in turn limited by solution under-cooling. Steady state growth by an imposed temperature gradient across a source/solution/substrate system is isothermal (to a first approxima-tion) but is slow due to the rate-limiting diffusion of As across the solution.

When the prediction of growth due to an applied electric current across the growth interface was confirmed by Kumagawa et al[1] with the isothermal growth of InSb, an added parameter and added control over LPE growth was introduced. The possibility of isothermal growth at reason-able growth rates as well as dopant modulation were suggested, and are investigated in the present work for the LPE growth of GaAs.

2. LITERATURE REVIEW

2.0 Introduction

The extensive literature concerned with LPE in general and LPE of GaAs in particular is evidence of the progress made in this field in recent years. It reflects advances in the controllability of epitaxial layer properties and the wide range of applications of this process to device fabrication. The summary of the pertinent literature presented in this chapter is divided into sections dealing with particular aspects of LPE which are relevant to the approach or the interpretation of the results of the present work. First presented is the historical development of the different types of LPE growth apparatus (2.1) followed by a review of work on growth behavior and layer morphology (2.2) and segregation behavior (2.3). The effects of an electric field on solidification are reviewed in Section 2.4 with particular attention paid to LPE. Finally, various needs and deficiencies relating to LPE of GaAs are discussed.

2.1 Development of Growth Apparatus

To adequately control the basic properties of LPE layers, the growth apparatus used must perform the following functions:

(1) contain a solution of some known composition;

(2) permit establishment of contact between the solution and a substrate surface;

(3) permit reproducible growth on the substrate;

(4) permit separation of the solution from the epitaxially grown layer.

In addition, the apparatus should not contaminate the solution or layer.

In first introducing LPE of GaAs, Nelson[2] used a tipping furnace, a relatively simple apparatus useful for single-layer growth. In this arrangement the solution and substrate are spatially separated at the onset but occupy the same compartment. At the desired temperature and furnace cooling rate, the system is tilted allowing the solution to flow onto the substrate. After the period of growth, isolation of the layer is achieved by re-establishing the original system position. In order to increase the control over temperature and timing of the growth process, Rupprecht[3] designed the vertical dipping technique. In this technique the solution is in a crucible in the center of a vertical furnace, while the substrate is mounted vertically on a rod which permitted lowering of the substrate into the supersaturated solution for growth. This technique has been modified by a horizontally mounted rotating substrate,[4,5] and a source/solution/substrate vertical configuration with a constant thermal gradient applied to induce growth by As diffusion from the source to the substrate.[6,7] When analyzing the epilayers grown by these techniques, the following basic problems have been identified: thickness non-uniformity, compositional changes, and regions where the solution was incompletely removed from the substrate surface. Neither of these techniques is readily modified to permit successive deposition of layers of different composition (e.g., multi-layer structures for lasers).

The sliding boat, introduced by Panish et al[8] in 1969, overcame some of these problems and developed into the most widely used growth apparatus for LPE of GaAs. The solution is contained in a bin (see Fig. 2.1), the bottom of which can slide when pulled by a rod. The sub-
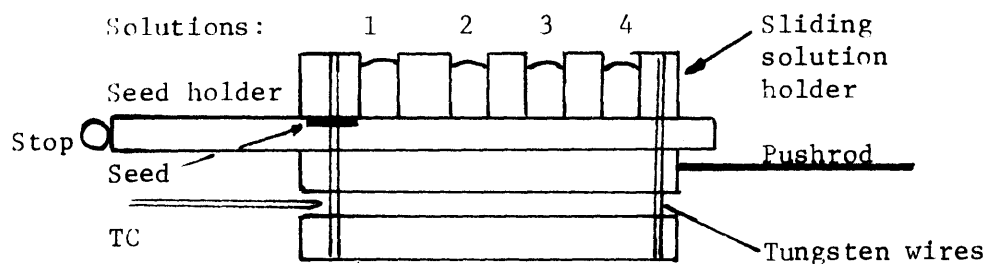
Figure 2.1:   LPE sliding boat, after Panish et al.[8] The seed
holder is held stationary by the stop, while the
other parts of the boat (held together by tungsten
wires) are translated by the push rod.

strate is positioned in a recess in the slider and can be pulled under the solution for growth, and pulled further to terminate growth. With proper clearance below the substrate and the bin's lower edge, the substrate/ layer surface is, after growth, wiped completely clear of solution. Multiple bins permit growth of multiple layer structures with good thickness uniformity due to control over solution shapes[9] and thermal fields. In a further development a source crystal was added to the slider next to the substrate[9,10] which allows each solution to be saturated prior to contact with the substrate. The sliding boat technique is utilized in the present work and is described in detail in Section 4.1, Growth Apparatus and Procedures.

2.2 Growth Behavior and Morphology

The important differences in the various types of growth apparatus are the available controls over the growth conditions which affect epitaxial layer properties. These conditions include diffusion and convection in solution, interface kinetics, and constitutional supercooling. Theoretical and experimental results reported in the literature relating each of these effects to growth behavior or layer morphology are presented.

The effects of solute (As) transport in solution have been shown to dominate LPE growth rate behavior.[11-21] Tiller and Kang[11] determined expressions for growth velocities under conditions of diffusive transport, fluid flow, and interface attachment for variable cooling rates. Small and Barnes,[12] and later Minden[13] treated LPE by assuming diffusion-limited growth with equilibrium conditions at the interface and a liquidus

of constant slope. Crossley and Small,[14] using computer simulated
growth with solution mixing, boundary layer diffusion, and homogeneous
nucleation, obtained qualitative agreement of layer thickness with exper-
iment. They indicated that the growth behavior of systems with vertical
substrate geometry suggested the presence of solution mixing, while a
bulk diffusion model was applicable to systems with the solution over a
horizontal substrate. Ghez[15] extended Minden's analysis to include the
temperature dependence of the liquidus concentration, while Rode[16]
later included the temperature dependence of the diffusion constant
using numerical methods. Rode's comparison of a diffusion-limited growth
model to experiment yielded quantitative agreement and a value for the
diffusion constant of As in Ga over a temperature range from 800 to 900°C.
Other experimental results investigating the functional dependence of
layer thickness on time of growth,[17-19] liquidus slope,[20] and cooling
rates[18,21,22] were in agreement with diffusion-limited growth theories
assuming equilibrium conditions at the interface.[12-16]

The influence of interface kinetics on growth rates, assuming a first
order reaction, was calculated by Tiller and Kang[11] and Ghez and Lew.[23]
The magnitude and the time-dependency of the growth rate was reported to
change with finite values of an interface rate constant and non-zero
values of the reaction's activation energy. However, experimental results
on GaAs indicated infinitely fast interface kinetics.[13] This was con-
sistent with the undercooling of less than 0.15°C[16] and 0.25°C[14]
required to initiate growth of GaAs at 800°C.

Interface kinetics and thermal fields in the solution have been shown to affect the morphology of epitaxial layers. The appearance of surface terraces has been attributed to constitutional supercooling[24,25] and interface attachment to low-index planes[26-28] (i.e., substrate orientation). Smooth surface layers have been grown with constitutional supercooling which was reported to affect the morphology of thicker layers.[13,26] Calculations have been reported for thermal gradients necessary to prevent constitutional supercooling for various solution heights[13] and growth durations.[29] However, interface instability is a more complex phenomenon that also involves surface energies, thermal properties of liquid and solid, and surface kinetics.[30,31] Other processes relating to morphology which are as yet unresolved are nucleation,[23,28,32,33] surface reconstruction,[34,35] and faceting.[36]

2.3 Segregation Behavior

Segregation behavior has been previously studied by first identifying and reducing background impurities,[37-42] and determining the empirical behavior of intentional doping.[6,43-46] High purity layers (10^{14} cm^{-3} range) were first grown by Kang and Greene[37] and improved results (10^{13} cm^{-3} range) have since been reported by other workers.[38-42] Contamination has been identified and reduced for oxygen,[33,38-40] silicon,[41] and graphite.[43]

The behavior of various dopants in LPE growth of GaAs has been the cause of several problems in the distribution of carriers in the layers.[43-46] Kang and Greene[40] reported carrier concentration gra-

dients due to a temperature dependence in the distribution coefficients of Sn, Te, and Se.[43] Goodwin et al[44] found that layers doped with Si could be alternately n- and p-type during one run. Sudlow et al[45] identified the cause of dopant gradients in GaP as partially due to variations with temperature of the distribution coefficient of the dopant Te, S and Zn. The distribution coefficient of Sn was reported to be independent of layer concentrations up to 10^{18} cm^{-3}.[33] Distribution coefficients were found dependent on substrate orientation.[45] Zschauer and Vogel[46] treated these and other seemingly anomalous segregation behavior in a model which assumes that the solution is in equilibrium with the layer surface, not the layer bulk. Segregation behavior in LPE of GaAs has had to be dealt with by empirical methods lacking a basic understanding of the processes involved.

2.4 Current-Controlled Growth

The application of an electric current across a solution-solid growth interface results in thermoelectric heating or cooling at the interface (Peltier effect), field-aided mass transport in solution (electromigration), and resistive (Joule) heating of the system. These effects may in turn alter the morphology, and growth and segregation behavior during solidification.

A general theory of segregation in the presence of an electric field was presented by Pfann and Wagner.[47] By assuming that electromigration provided a constant flux of solute toward (or away from) the growth interface, they obtained an expression for the distribution coefficient by modifying the Burton, Prim and Slichter model.[48] Verhoeven[49] derived

the electromigration flux assuming a specie's mobility and found qualitative agreement with experiments for segregation changes of Bi in Sn. Several workers[50] reported phenomenological models of electromigration that included interactions of ions with the applied field and the con-. ducting electrons. The latter effect, electron "wind" or "drag", was suggested as the dominant one in several metal alloy systems,[51] and used to explain anomalous behavior seen in experimental results.[52]

The application of an applied electric field during the growth of semiconductors was first discussed with regard to p-n junction formation in Ge.[53] Singh, Witt and Gatos[54] developed the technique of introducing interface demarcation lines during growth of InSb from the melt. By applying current pulses at known intervals across the solid-melt interface, they obtained from the resulting Peltier cooling an accelerated growth rate[55] with an associated segregation striation marking the interface which could be made visible after a subsequent polish and etch. They extended the technique to the LPE of InSb,[1] causing a layer to be grown due to Peltier cooling at the interface while the furnace maintained a constant temperature. They also showed that interface demarcation could be used for LPE of InSb, and later LPE of GaAs.[56] Isothermal growth utilizing an electric current across the substrate-solution interface was subsequently reported for GaAs,[57-60] InP,[61] (GaAl)As,[62] and garnets.[63] However, there was disagreement over the dominant growth mechanism, some work indicating Peltier cooling,[62] other work supporting electromigration.[58] In addition, the exact nature of the segregation effect causing the demarcation lines was not known.[56]

2.5 Summary of Problems and Deficiencies in LPE

As the technique of liquid phase epitaxy has developed, so too have its applications to different devices and different materials.[64,65] More stringent requirements are introduced to LPE, and characteristics of the epilayers that were once acceptable later become limitations. Thickness control and uniformity, necessary in laser structures, have not been completely characterized for LPE. Uniform doping composition in epilayers, required for GaAs microwave devices, cannot be easily achieved for conventional LPE.

The introduction of current-controlled LPE as a growth technique differing significantly from conventional LPE offers several potential improvements in epitaxial layer characteristics. Growth rates can be controlled by the magnitude of the applied current.[57] Growth can be carried out isothermally, resulting in constant dopant concentrations in the layers. In addition, there is the potential for the modulation of dopant incorporation by current or temperature control, the latter parameter being independent of growth with an applied current. Thus, there are needs and reasons to further investigate current-controlled LPE in order to further improve LPE in general.

3. APPROACH

Current-controlled liquid phase epitaxy is a new approach to overcome some of the problems inherent to conventional LPE. Because growth can thus be carried out at a constant temperature, the segregation behavior must be expected to differ significantly from conventional LPE. Moreover, because growth is dependent on an applied current, growth rates may be varied quickly and accurately. The use of an electric current suggests these and other possibilities for additional control over the material parameters of epilayers. This study was carried out in order to investigate potential advantages of current-controlled growth over conventional LPE. With the ultimate application of this technique to device fabrication in mind, two areas of research were analyzed: growth behavior and morphology, and segregation behavior.

The investigation of the growth behavior and growth interface morphology is primarily concerned with the study of growth rates, and their functional dependence on experimental variables. To determine the effects of individual growth parameters such as diffusion, convection, Peltier cooling, and electromigration on current-controlled LPE, a series of layers was grown by this technique from solutions with no GaAs source present. The resulting non-steady-state growth behavior, found to be highly sensitive to the parameters under study, was characterized by interface demarcation and compared to a model developed for this purpose. Steady-state current-controlled LPE is then analyzed with the previously determined parameters of growth.

The segregation behavior is studied with respect to two n-type dopants, Sn and Te, which are known to behave in a different manner during LPE of GaAs. Charge carrier concentrations in the solid, determined in lieu of dopant concentrations for segregation studies, were obtained from capacitance-voltage measurements which were able to provide profiles into the layer beneath the surface. Used in conjunction with interface demarcation, the carrier concentration profiles provided a direct comparison of segregation behavior for different microscopic growth rates within the same epilayers.

This thesis is structured around these two areas of study. Each is discussed in a separate chapter (five and six) which includes the relevant background and theory, experimental results, and discussion. Chapter seven is devoted to electromigration of As in Ga, examined through a set of classical experiments without growth taking place. Chapter eight is a summary of results and conclusions, followed by recommendations for further study. The experimental apparatus and procedures for growth and characterization are described first in the next chapter.

4. EXPERIMENTAL TECHNIQUES AND PROCEDURES

4.1 Growth Apparatus and Procedures

4.1.1 Growth cell

LPE layers were grown in a sliding boat similar to the one introduced by Panish et al,[8] but modified to permit both conventional and current-induced growth. The lower half of the boat (see Fig. 4.1), with its primary function the accomodation of the GaAs substrate, was stationary. The substrate was positioned on a graphite pedestal whose height was adjusted such that the substrate's upper surface (growth surface) was level with the upper surface of the lower boron nitride (BN) plate (L-BN in Fig. 4.1b). This BN plate (HBR grade, Union Carbide) fitted firmly into the bulk of the lower part of the boat (high purity graphite, HPD-3-2, Poco) and also held a GaAs source crystal laterally displaced 0.625 inches from the center of the substrate. The upper portion of the boat (herein called the slider) which confined the solution was con-structed to slide over the lower BN plate on another attached BN plate (U-BN). The slider was guided by a BN support on either side of the boat. These boron nitride plates were used to insulate the slider from the lower position of the boat to permit transmission of electric current of known density across the solution-solid interface only. To achieve a uniform current distribution across the solution-substrate interface the solution well was lined by boron nitride (S-BN) and a tight-fitting graphite plug was used as an electrode. All components contacting the substrate and the solution were removable to permit periodic cleaning by a vacuum bakeout at 1200°C. Two stainless steel rods screwed into the
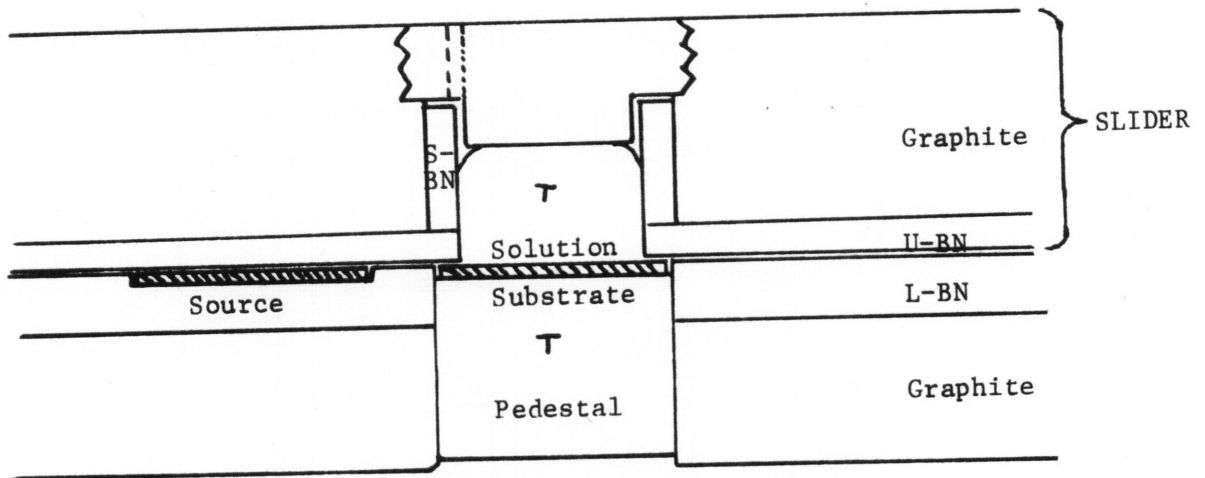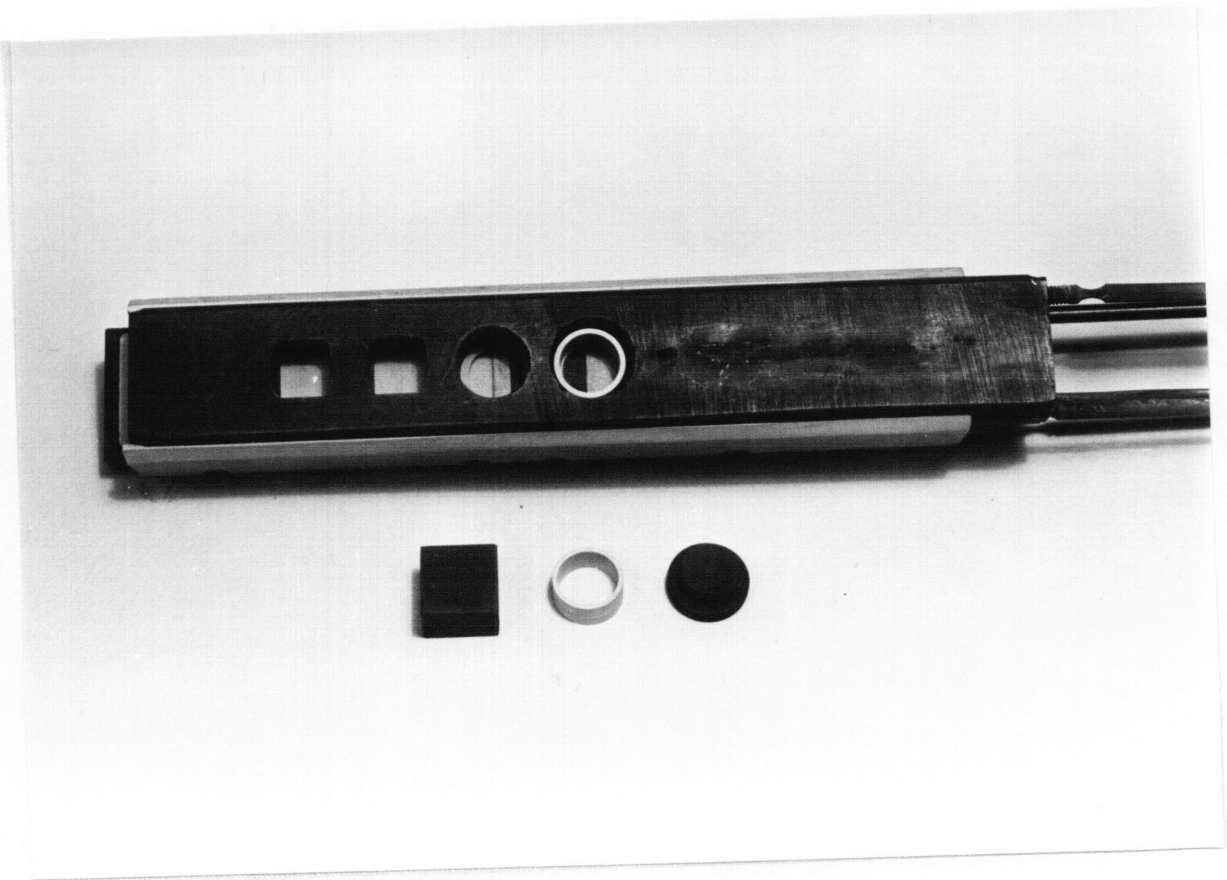
Figure 4.1: Photograph and schematic of the LPE boat. The slider enables the Ga solution to be equilibrated with the GaAs source, contacted to the GaAs substrate for growth, and isolated from the layer. Two thermocouple positions are indicated by "T".

upper and lower graphite pieces extended out of the furnace tube and served as current leads and as pushrods.

Two chromel-alumel thermocouples (marked by "T" in Fig. 4.1b) were used to monitor the substrate and solution temperatures during growth. The substrate temperature was measured by a stationary thermocouple 6.4 mm below and 1.6 mm to one side of the growth interface (6.5 mm total distance). The temperature of the solution was determined by a mobile thermocouple normally positioned 1.6 mm beside the solution and 6.4 mm above the growth interface.

4.1.2 Furnace system

The growth cell was positioned in a quartz tube (1.5" I.D.) in the center of a 26 inch Marshall furnace. End caps, in addition to providing a vacuum seal (with Viton O-rings), allowed for feed and exhaust of a gas flow through the furnace tube. The gas flow system, shown schematically in Fig. 4.2, was designed to maintain a protective inert atmosphere for the growth system. The system was capable of supplying three prepurified (<1 ppm O_2) gases directly to the furnace tube (nitrogen, argon or hydrogen), but normally hydrogen was used after passage through a palladium purifier (Serfass Hydrogen Purifier). At the exit end of the furnace tube a bubbler was used to determine the flow rate and to keep the pressure in the tube slightly above one atmosphere.

4.1.3 Instrumentation

The Marshall furnace was controlled by a Leeds and Northrup series

- 32 -
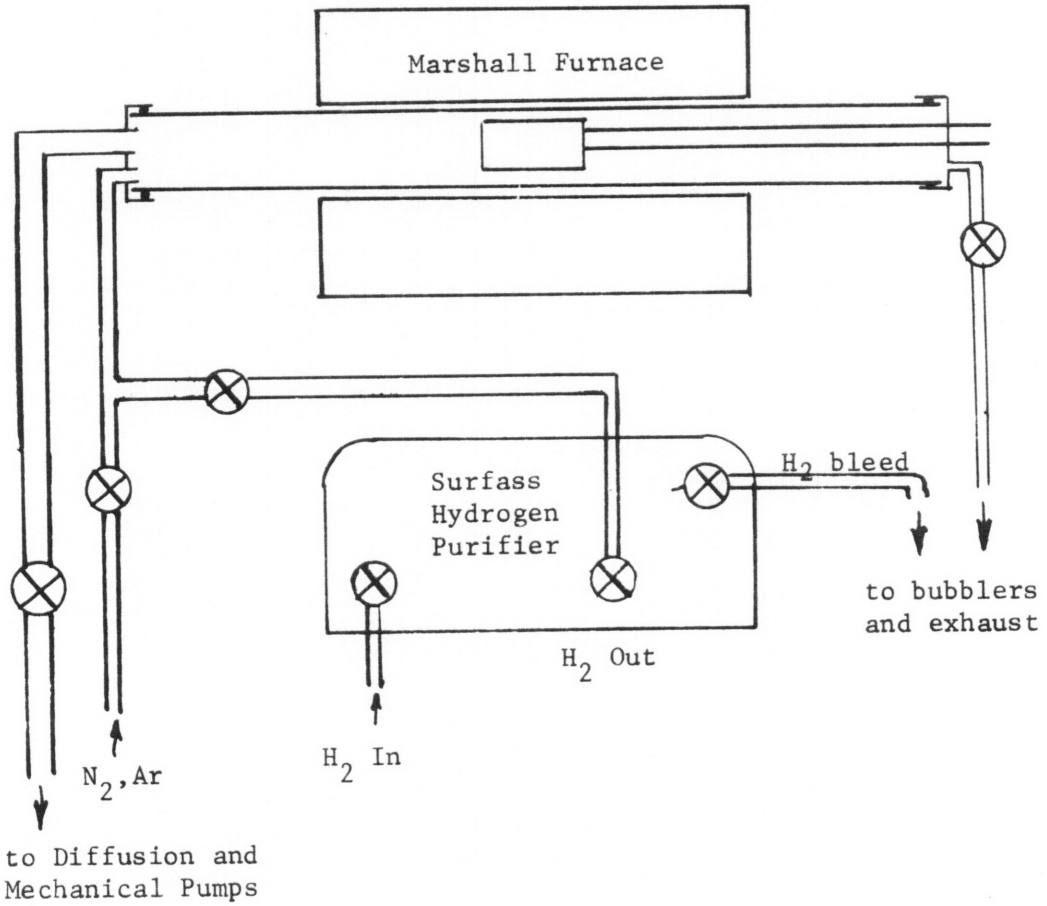
Figure 4.2:   Schematic and photograph of the LPE growth system.

60 CAT unit driving a Barber-Colman 621A SCR Power Controller. The furnace temperature was monitored by a platinum/platinum-rhodium (S type) thermocouple placed near the furnace windings and electronically compensated to 0°C by an L&N 10877 Set Point unit. The Set Point Unit had motorized control for delay as well as ramp cooling or heating. The furnace power control was sensitive to changes smaller than 0.02°C in the furnace temperature. For current-controlled growth, two parallel Keithley power supplies wired in a master/slave configuration were used as the current source, controlled by a DC signal and/or a pulse generator. The maximum current used was 40 amps at a maximum slewing rate of 250 A/msec.

4.1.4 Growth procedures

Solutions were prepared from gallium (AluSuisse, 99.9999%), undoped polycrystalline GaAs (Laser Diode, nominally $n = 10^{14}$ cm^{-3}), and dopants of Sn (United Minerals and Chemicals, 99.9999%) and Te (source unknown, 99.9999%[66]). In preparation for experiments the gallium was melted first and poured into the well of the slider and baked at 850°C for twenty hours in a purified hydrogen atmosphere to remove any volatile impurities that may have been leached from the boat. After cooling, the boat was removed to a nitrogen atmosphere where etched GaAs and dopant (if any) were added and the solution capped with the graphite plug. An etched GaAs source wafer (0.50" square) used for equilibration of the solution prior to growth was placed in a recess in the lower BN plate near the substrate position. The slider was then positioned 1.25 inches

to the left of center of the lower portion of the boat isolating the solution from the substrate and source.

Gallium arsenide substrates were cut into 0.50 inch squares with a string saw from (100) orientated wafers (Laser Diode, highly doped Si or Te, or Cr/semi-insulating; one side prepolished). The upper surfaces (to be used for growth) were polished eight minutes on a polytex pad with a solution of 5.3% sodium hypochloride (100% Chlorox bleach). The substrates were subsequently washed in hot acetone, hot trichloroethylene, acetone, and methanol, rinsed in distilled water and dried with nitrogen. Immediately prior to a growth experiment the substrate was washed in a soap solution, rinsed, and treated in the following solutions for the indicated times:

1. Hot 50% HCl for 10 minutes, rinsed;

2. Hot 50% HF for 10 minutes, rinsed and dried;

3. 5:1:1 $H_2SO_4:H_2O_2:H_2O$ for 2 minutes at 20°C;

4. Water quench and rinse for 2 minutes, dried.

A current contact was then fabricated on the substrate's rear (prepolished) surface in one of several ways. In early experiments the substrate was contacted either directly to the graphite pedestal or with a thin (<0.05 mm) or thick (1.5 mm) layer of gallium separating the substrate and pedestal. In later experiments a thin layer of gallium was spread over the pedestal and the rear surface of the substrate, separated by a piece of Ge (1.5mm thick) or more often, a piece of Ta foil (0.010"). The effects of the different contacting methods are discussed in Section 5.2. With the substrate in position, the pedestal was inserted into the boat and held in place by a set screw.

After insertion of the loaded boat into the furnace tube, the system was subjected to three cycles of slow evacuation (to $\lesssim 10^{-2}$ torr) and backfilling with purified hydrogen. The hydrogen flow was set to approximately 500 cc/min (STP) for thirty minutes to two hours, after which the furnace was brought to temperature over a period of two hours and the flow of H_2 reduced to 100 cc/min (STP). One hour after the temperature of the furnace had reached equilibrium the slider was moved to position the solution over the GaAs source. The solution was subsequently equilibrated for two hours and the slider moved again to establish solution-substrate contact, which was monitored through a resistance measurement.

The growth procedures used varied with the nature of each experiment. Thus, for example, to insure complete wetting of the substrate surface by the solution, one of three backmelting procedures were used:

    (1)   application of three consecutive 40 Amp pulses across the solid-solution interface,

    (2)   application of an AC current,

    (3)   increase in the furnace temperature by 2-5°C.

In the latter two cases the system was given thirty minutes to equilibrate before growth. Growth was initiated by either the application of a DC current across the substrate-solution interface or furnace ramp cooling in the following combinations:

    (1)   application of a growth current (+ polarity to substrate);

    (2)   furnace ramp cooling;

    (3)   furnace ramp cooling followed by superposition of a current of either polarity;

(4) furnace ramp cooling followed by isothermal

application of growth current.

Most experiments also involved pulsing for growth interface demarcation

(typically pulses of ~40 A/cm^2 x 0.2 sec at intervals of 5 minutes)

which was superimposed on temperature or current programming.

Growth was terminated by pulling the slider to isolate the solu-

tion, thus wiping the substrate free of solution. The substrates were

cooled to room temperature in either thirty minutes or ten hours.

After a visual inspection, the layer surface was cleaned in warm HCl

(50%) to remove any excess gallium, and stored for characterization.

4.2 Optical Characterization

Epitaxial layers were viewed under a microscope for the characterization of four effects: surface morphology, interface morphology, growth rate behavior and layer defect structure. All have been studied using Nomarski phase interference contrast microscopy. The microscopes used were a Reichert Zetopan F and a Zeiss Ultraphot II.

The substrate with epilayer was first cleaved along a (011) or (0$\bar{1}$1) plane perpendicular to the (100) sample surface. One cleaved piece was then etched in a fresh Abrahams-Biocchi etch (5 sec) obtained by dissolving 80 mgrams $AgNO_3$ in 20 ml H_2O, adding 10 g Cr_2O_3 and then 10 ml HF. After etching the sample was rinsed in distilled water, dried with nitrogen, and held in a slit in a flat piece of rubber with the cleaved face horizontal.

When viewed with interference contrast, the initial growth interface as well as interface demarcation lines (introduced during growth pulses) were visible. Linear dimensions were quantitatively obtained by a calibrated filar eyepiece. The layer thickness was measured at equally spaced intervals along the cleave. Layer thickness as a function of growth time (and hence the growth rate) were obtained from the distances between successive interface demarcation lines (and the interval between pulses corresponding to those lines). The interface demarcation lines also allowed for a cross-sectional examination of the interface morphology at different layer thicknesses.

4.3 Electrical Characterization

4.3.0 Introduction

Of many available techniques for electrical characterization of semiconductors, there are only a few that can give carrier concentrations on a microscopic scale for GaAs. The capacitance-voltage (C-V) technique was utilized in the present work for this purpose, to obtain doping profiles of layers grown under varying conditions. The CV technique, apparatus, and procedures are described in this section, along with the procedure used to obtain carrier mobilities as a measure of layer compensation.

4.3.1 CV technique and basic equations

The use of diode capacitance as a function of reverse bias voltage to obtain carrier concentration profiles was first reported by Hildebrand and Gold.[67] Refinements have since been made such as the use of Schottky diodes,[68] direct plotting of inverse profiles by monitoring harmonics of an AC signal,[69] direct plotting of profiles via pulses,[70] feedback,[71] or analog techniques,[72] and the use of a mercury contact for a Schottky diode.[73] The equations governing the measurement system used are basic to almost all C-V techniques, and are reviewed in each of the above references.

The capacitance-voltage technique is based on the abrupt junction depletion approximation which assumes that the depletion region consists entirely of ionized donors (and acceptors) (see Fig. 4.3). The expressions developed for the carrier concentration $n(x)$ and depth x are[74]
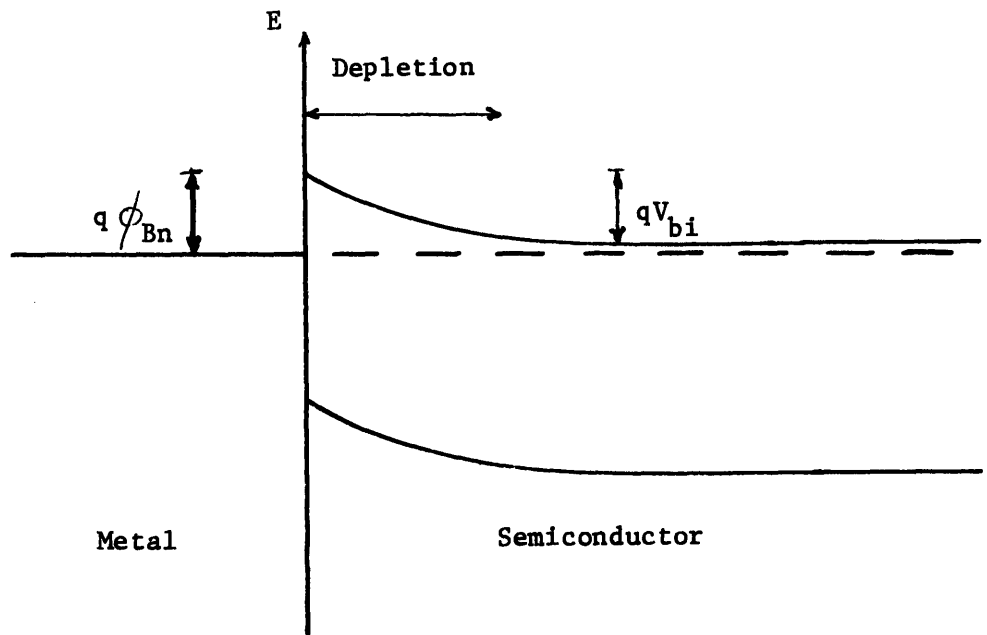
Figure 4.3: Energy diagram of a metal-semiconductor interface depicting the depletion region. ϕ_{Bn} is the schottky barrier height and V_{bi} is the built-in potential associated with band bending.

$$n(x) = \frac{C^3}{e \, \varepsilon \, A^2} \left(\frac{dC}{dV}\right)^{-1}$$

(4.1)

and

$$x = \frac{\varepsilon \, A}{C}$$

(4.2)

where C is the depletion layer capacitance, A the diode area, e the electronic charge, ε the dielectric constant of the material, and V the applied voltage. Corrections to these primary equations are discussed by Copeland[69] and Wu et al,[75] but apply to carrier concentrations obtained at non-zero voltage bias.

4.3.2 CV apparatus and procedures

The CV apparatus was comprised of a mercury probe coupled to CV instrumentation (figures 4.4 and 4.5). The probe was designed to make an ohmic contact to the rear of a sample, and a Schottky diode (with a column of mercury) to the front surface. The electronics measured the junction capacitance as a function of bias voltage, and converted it to carrier concentration vs. depth by analog methods.

The mercury probe was designed and built by R. McClelland at MIT Lincoln Laboratory, where the measurements reported in this work were taken. The probe basically consisted of a stage and mercury column mounted on a wheel that was able to rotate about a horizontal axis (see Fig. 4.4). The stage provided ohmic contact to the rear of the sample, which was held in place by a vacuum chuck. The mercury was contained in
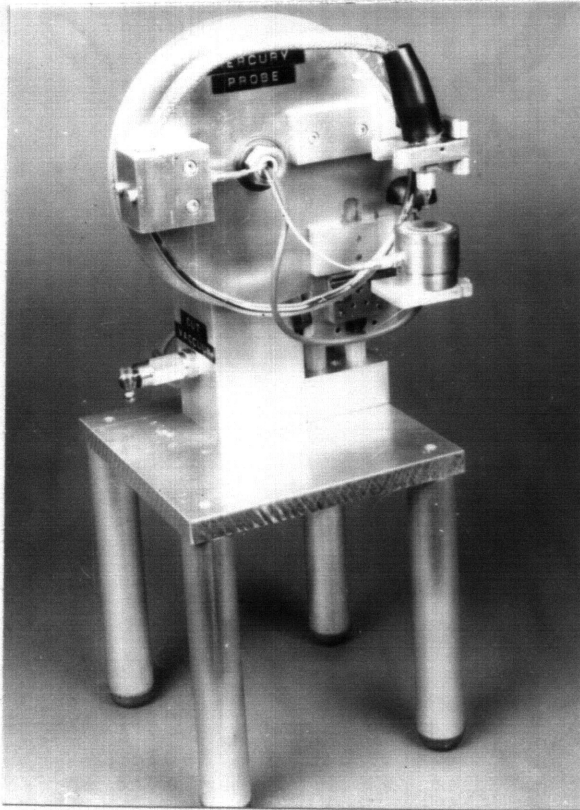
Figure 4.4: (a) Photograph of the mercury C-V probe. Various stage positions are shown schematically in (b) positioning the sample under the probe, (c) contacting the probe to the sample surface, and (d) establishment of the Schottky diode.
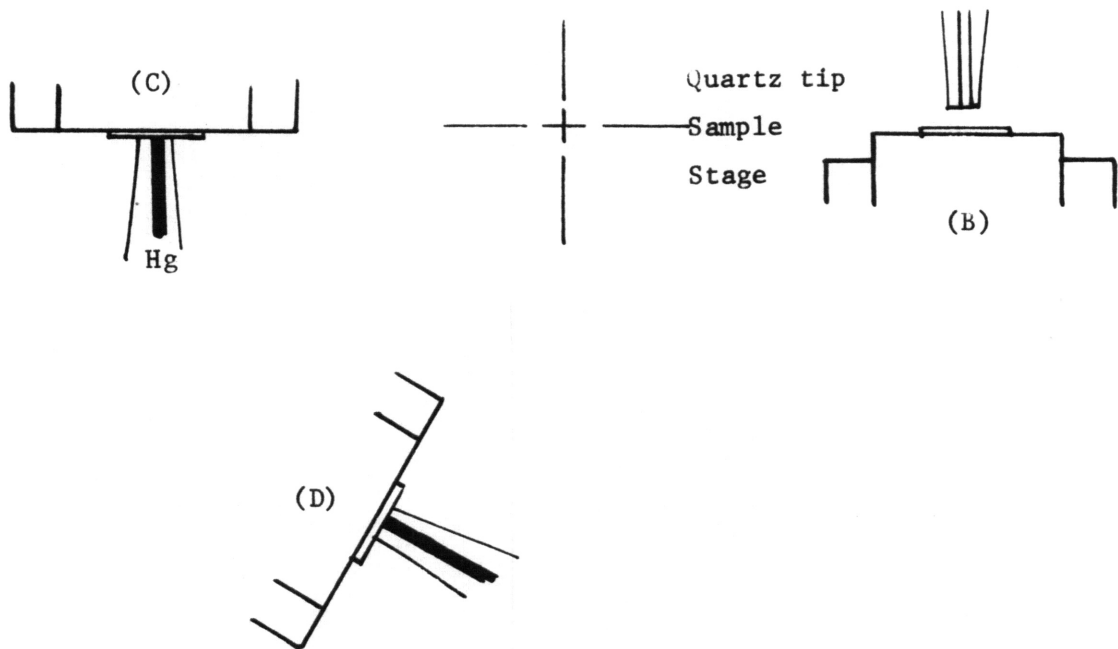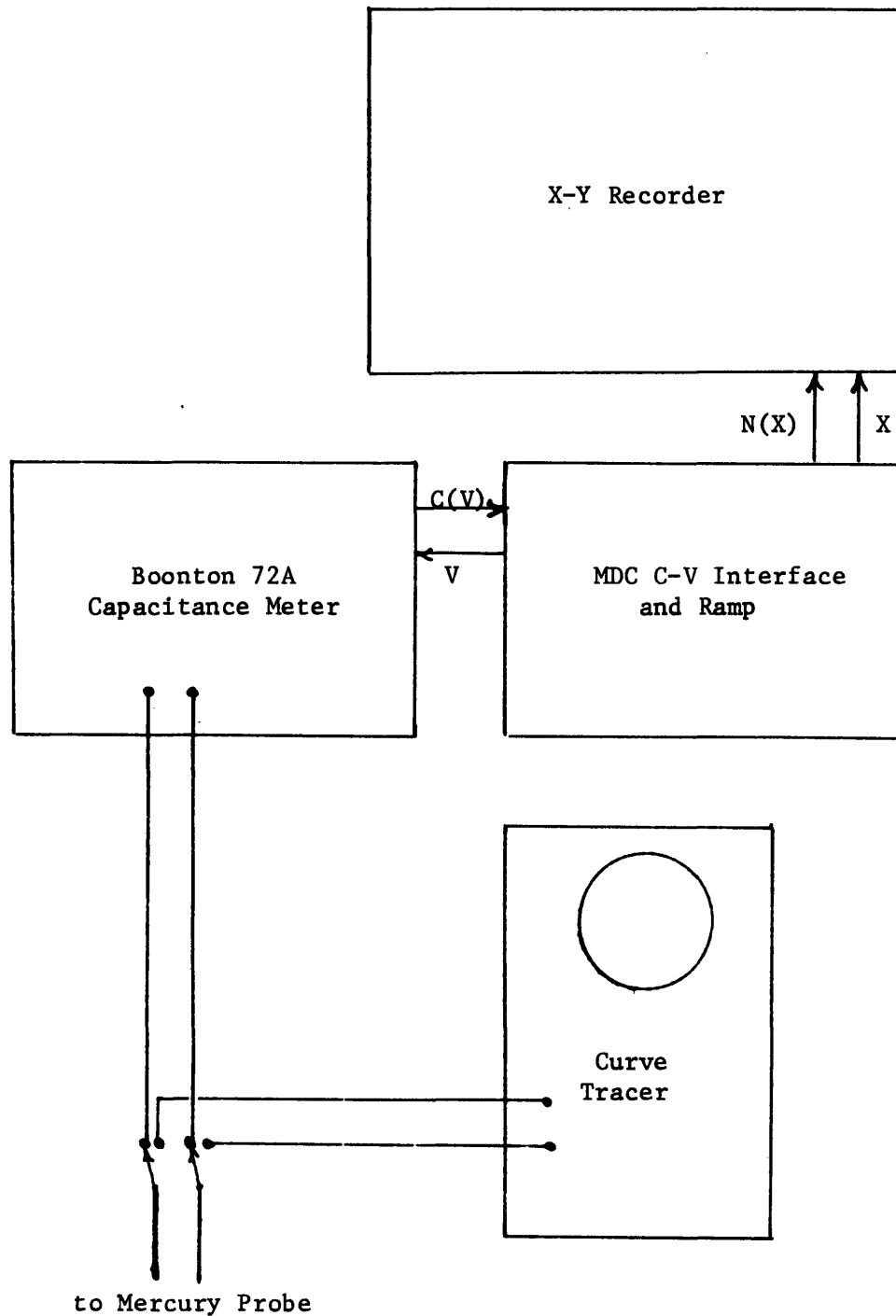
Figure 4.5: Schematic of the instrumentation associated with the
C-V measurement. All wiring is with high frequency
shielded cable.

the circular quartz tube, one end of which tapered into a capillary tip directly above the sample and stage. The rotating action served to shift the mercury in the tube in order to make Schottky contact to the sample surface in the following manner :

1. The sample was positioned such that the area to be profiled was directly below the capillary tip (Fig. 4.4b).

2. The assembly was then rotated 180°, inverting the sample and allowing the mercury present in the tube to approach the capillary tip. The stage was lowered until the sample surface contacted the capillary tip (Fig. 4.4c).

3. The assembly was rotated an additional 60°, forcing the mercury to fill the capillary tip and contact the sample (Fig. 4.4d).

The result was a constant and reproducible pressure of the mercury (approximately 20 psi) on an area 20 mils in diameter on the sample surface. The electrically measured Schottky diode diameter was 19.4 mils.

The instrumentation used with the mercury probe is shown schematically in Fig. 4.5. Two high frequency shielded cables connect the mercury probe (at the stage and in the mercury column) to a switching box. In the first position the diode I-V characteristics were displayed on a curve tracer's CRT. Forward voltage drop and reverse current were used to check the ohmic and Schottky contacts. The second position of the switch allowed carrier concentration profiles to be taken by an automatic

profiler system supplied by Materials Development Corporation. It consists of a Boonton 72A Capacitance Meter, an MDC C-V Interface unit and ramp generator and an H-P 7035B X-Y Recorder. The meter continuously sampled the capacitance as the bias voltage was swept from zero to reverse breakdown. Both the bias voltage and the capacitance were inputs to the profiler, which transformed these signals to depth and carrier concentration (see equations 4.1 and 4.2) and displayed them on the X-Y recorder. The result was a log-log plot of $n(x)$ vs. x for one area of the sample.

Since the layers were doped from 10^{16} to 10^{17} cm^{-3}, the maximum depletion depth varied from 2.0 to 0.3 microns. To profile layers of greater thicknesses, an etch was used to remove material.

The CV measurements were taken in such a way as to minimize the absolute and relative errors in the carrier concentrations. An n-type sample (G 106) with a layer of known concentration and thickness was used to calibrate the profiler and to check the calibration several times during each set of measurements. The concentration at zero bias was set to 6.2×10^{16} cm^{-3}, and the depth at 2×10^{17} cm^{-3} was set to 0.30 microns. Six different regions on this sample have been treated in sequence, and the variation in carrier concentration at low bias levels has been less than the recorder pen width ($\sim 3\%$). As a further test of the system's stability, measurements on other samples were repeated at random.

4.3.3 CV sample preparation

A central slice of each layer was cleaved to dimensions of approximately 1-2 mm by 12 mm. Ohmic contacts were made to the rear of the Si-

and Te-doped substrates by heating two Au/Sn preforms to a temperature of 400°C for a two second duration. Contacts to layers on semi-insulating substrates were made with the same preforms on the top surface of the layer near one edge of growth. A one mil diameter platinum wire was pressed on these contacts with a small piece of flattened indium. The sample was then mounted (layer up) on a section of a glass slide with black wax (Apiezon W), heated to 150°C. All indium electrical and ohmic contacts were completely coated with wax, while the free end of the plat-inum wire was allowed to bend around the glass edge. The sample was cooled and then cleaned in a soap solution and rinsed in deionized water.

4.3.4 Depth determination

In order to profile layers greater than ten microns a procedure was developed to obtain accurate concentration profiles after successive etches. After a CV measurement, the sample was rinsed in deionized water to remove any trace of mercury on the surface. The sample was dried in nitrogen and etched in twenty milliliters of free etch: 5:1:1 H_2SO_4: H_2O_2:H_2O at 15°C. The etching time varied from thirty seconds to twelve minutes, depending on the amount of material to be removed. The etch was quenched and the sample rinsed with deionized water and subsequently dried in nitrogen, ready for another CV measurement. If a delay was present, the sample was rewashed and rinsed just prior to the next measurement.

The etch rate was calibrated using a double-beam interferometer to determine the amount of material removed for different etch durations. The effects of dopants and dopant levels were determined, in addition to

temperature and etch volume. Thickness etched as a function of time is plotted in Fig.4.6 for several etch volumes at 16°C. The etch rates doubled when the temperature was raised to 30°C.

The thicknesses of the epilayers were thus determined by the number of successive etches and measurements until the substrate was detected $(n > 10^{18} \text{ cm}^{-3})$. The agreement between thicknesses determined by etches and by the standard cleave and stain techniques was excellent. Therefore the thickness determined by the number of etches was used in all profiles measured.

4.3.5 Determination of carrier mobility

To obtain the degree of compensation present in epitaxial layers, the resistivity and Hall mobility of layers grown on semi-insulating substrates were determined from Hall[76] and Van der Pauw[77] measurements. A review of the measurements' procedures and theory is presented by Sze,[74] and only the sample preparation and a brief outline of the measurements will be described here.

Hall samples were made by cleaving layers into squares 1-2 mm on a side. Thickness was determined by the procedure outlined in the previous section. The surface was cleaned in the following solutions: soap and water, warm HCl (50%), and warm HF (50%). After rinsing and drying, a small film of Indalloy flux (Electro-Rosin) was placed on the surface in the center of the four edges, and small pieces of tin or tin alloy (50% In) were placed on the flux films. The sample was heated to 500°C in a hydrogen furnace for 15 minutes to alloy the contacts. The contacts were
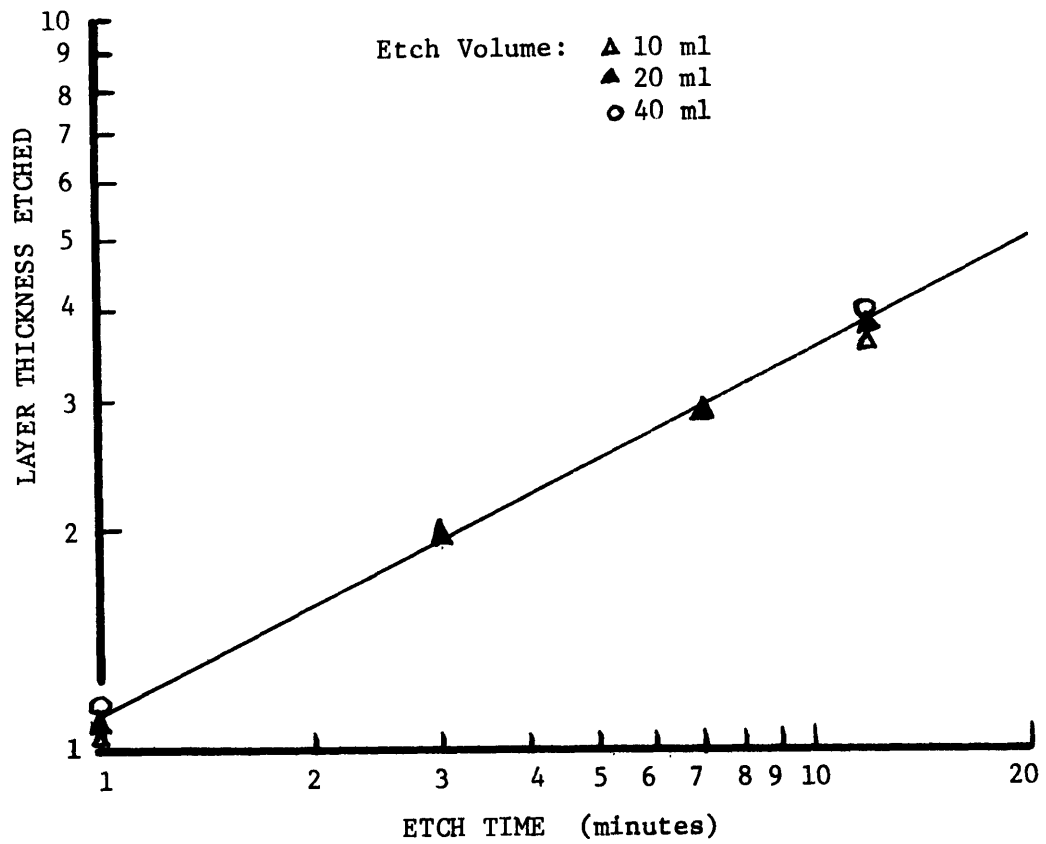
Figure 4.6: Thickness of GaAs removed as a function of etch time
for free etch (5:1:1 H_2SO_4:H_2O_2:H_2O) of several
volumes at 15°C.

subsequently checked for linear I-V characteristics, and bonded to one mil gold wires.

Conductivities of layers were calculated[77] from the layer thickness and the average of four "resistances", each obtained by measuring the voltage between two consecutive contacts and dividing by a known current (10 mA) passed through the remaining two contacts. Hall mobilities were determined with a 10 k Gauss magnetic field applied normal to the layer surface, a current (10 mA) applied through diagonally opposite contacts, and a voltage measured between the remaining two contacts. Both measurements were made at room temperature, and all combinations of similar measurements were made and averaged for each sample.

4.4 Defect Characterization

4.4.1 X-ray topography

Most of the X-ray topography was carried out on a Jarrell-Ash 80-000 Microfocus X-ray generator with either a copper or molybdenum target. The X-rays were generated in a spot size of 1.0 mm x 0.1 mm on the target with a take-off angle of 6°, effectively reducing the spot size to 0.1 mm x 0.1 mm. The beam was collimated by a set of slits (width: 150 μm) at a distance of 42 cm from the target. This corresponds to a maximum horizontal beam divergence of 150 seconds of arc.

The sample was mounted with transparent tape to a ring atop a goniometer on a Lang camera. The goniometer allowed two angular degrees of freedom, and the camera a third, as well as translation. A 1" x 1.5" film holder could be positioned on the camera stage within a centimeter of the sample while still allowing a pair of adjustable slits to be set between them. Topographs were recorded on either Ilford G Industrial film, G.5 nuclear plates, or L.4 nuclear plates with an emulsion thickness of 25 μm. Both plates and film were developed by the same procedure:

(1) 10 to 15 minutes (soak) in distilled water;

(2) 45 minutes in 3:1 Kodak D19 (developer);

(3) 10 minutes in 3% acetic acid (stop);

(4) 30-60 minutes in standard X-ray fixer without
     hardener (fix).

All of the above steps were carried out at 0°C. The plates were washed in filtered tap water for 90 to 120 minutes, rinsed in distilled water, and allowed to dry.

Once mounted, the sample was first alligned for the (004) diffraction peak in the reflection mode. The detector consisted of a scintillating crystal optically coupled to a photomultiplier tube with a pre-amplifier attached. The detection electronics include an amplifier, discriminator, and ratemeter. The (004) reflection is a strong one, relatively easy to find because the planes are parallel to the sample surface. Once the signal is found and maximized, the tilt of the sample is fixed and the stage and detector positions can be calibrated.

Three different configurations for X-ray topography were utilized in the work. Transmission topographs[78,79] used the (220) and ($\bar{2}$20) diffracting planes for the minimum distortion and maximum signal; reflection topographs[80,81] were taken with the (004), (115), (117) or (026) planes; cleavage-face X-ray topography[82] used the (333) planes, and unlike the other two modes, was not translated with respect to the beam. Becuase the Lang camera was unnecessary for this mode, cleavage-face XRT was also carried out using a double crystal X-ray spectrometer[83] with an effective beam divergence of less than thirty seconds of arc. Rocking curves were taken at different locations on samples mounted on the double crystal spectrometer.

Plates were viewed under a transmission microscope described in Section 4.2. Micrographs were thus obtained from the topograph at similar magnifications as micrographs of the samples themselves.

4.4.2 Dislocation etching

Dislocations were revealed on (001) GaAs surfaces by etching polished samples. Layers and substrates were mounted on polishing blocks and polished as described in Section 4.1.4 for times from one to ten minutes. After quenching, rinsing, and drying, the sample was inverted and suspended in a magnetically stirred A-B etch,[84] at room temperature, for etching times from two to ten minutes. An etch of the latter duration removed approximately 20 µm of material. After rinsing and drying the surface was viewed under interference constrast.

4.5 Electromigration Experiments

A series of experiments were conducted which were designed to pro-
vide information on the magnitude of the electromigration (EM) mobility
of As independent of growth. Basically, the experimental arrangement
consisted of two graphite reservoirs or wells[47] connected with a quartz
capillary of 2 mm diameter and 29 mm length (refer to Fig. 4.7). By
keeping the amount of solution in the reservoirs large, it was possible
to achieve with an applied potential a significant arsenic transport
through the capillary without substantially altering the concentrations
in the reservoirs ($\frac{\Delta C}{C} \leq 10\%$). A capillary of small diameter-to-length
ratio was intended to prevent any convective mass transport between bulk
solutions.

In preparation for an EM experiment, liquid gallium (4-5 g) was
poured into one reservoir. By means of a graphite plunger part of this
gallium was forced through the capillary into the other well. The amount
of gallium used for each experiment filled the two reservoirs to a height
in excess of the position of the connecting capillary. To achieve the
desired As-Ga solution, weighed amounts of GaAs were added to each well.
The wells were subsequently capped with graphite plugs to reduce the
evaporative loss of arsenic during the experiment. The apparatus was
inserted into the furnace tube of the growth system (described in
Section 4.1), and an inert atmosphere established by flushing with N_2 for
several hours. The system was brought to temperature (850°C) and allowed
to equilibrate for three to four hours. The temperature of the apparatus
was monitored by one thermocouple located below the left-hand well (see
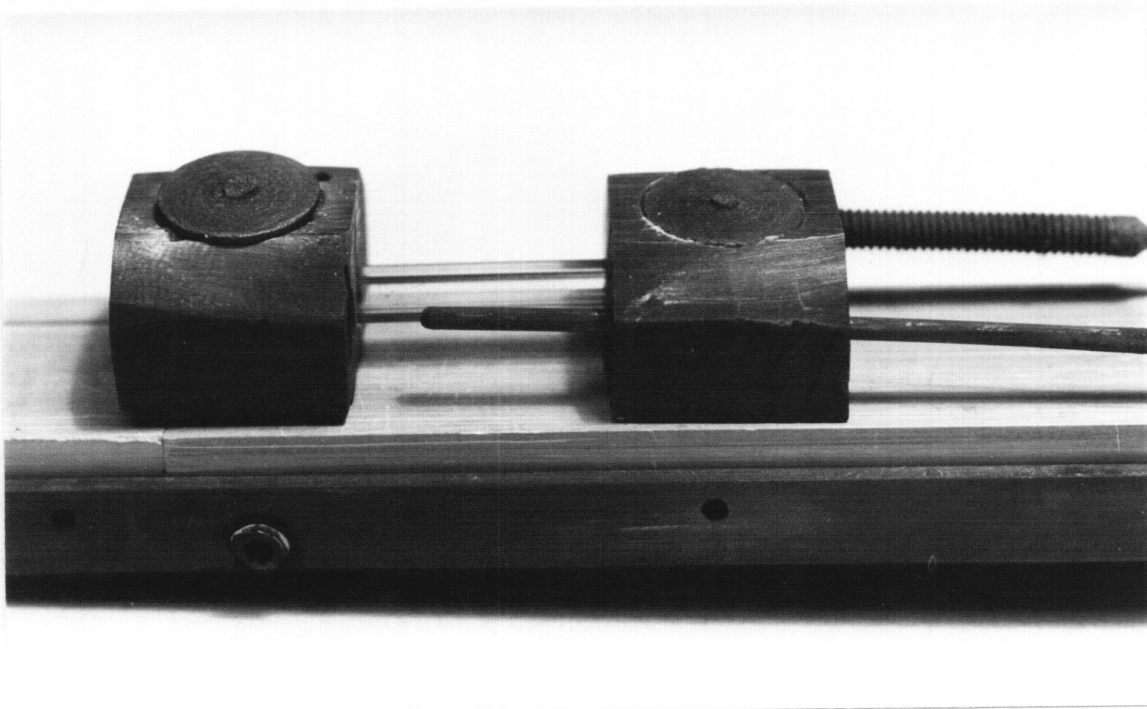
Figure 4.7: Photograph and schematic of the electromigration experimental
apparatus. The photograph shows the system without the BN
space (shown in the schematic as the cross-hatched region
around the quartz capillary). The lower thermocouple posi-
tion is depicted by a "T", while the upper thermocouple ("TC")
can be translated between the two graphite wells. The
schematic is twice actual size.
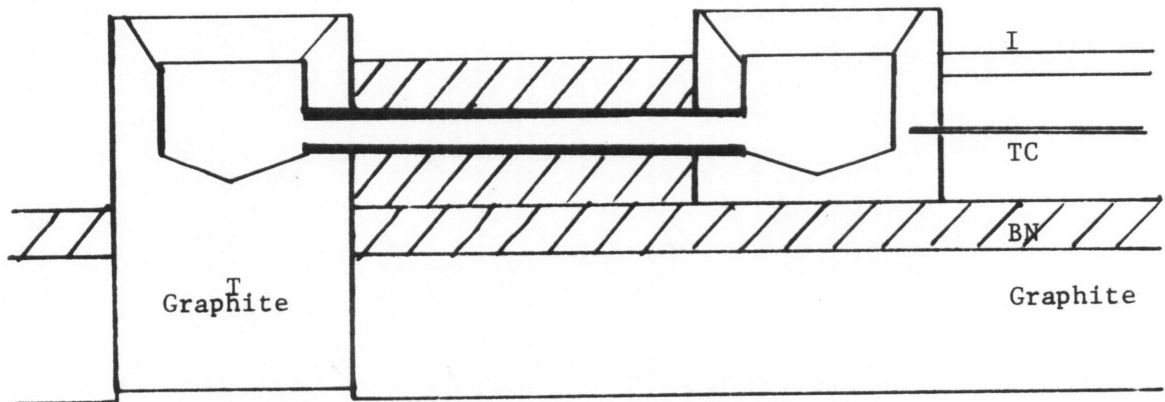
Fig. 4.7) and by another thermocouple position in the wall of the right-hand well, 0.5 mm from the solution. The use of a boron nitride spacer over the capillary was found to eliminate the thermal gradient along the capillary, and maintain identical temperatures in the two reservoirs (to within 0.03°C) that did not vary with the application of a potential across the capillary. An electric potential was applied across the capillary which maintained a constant current flow of 0.628 A (20 A/cm^2 in the capillary) for the duration of each 12.5 hour experiment.

The experiments were terminated by repositioning the system within the furnace tube to a location outside the high temperature region while maintaining the nitrogen flow and the current. In the first ten minutes after relocating the system the temperature dropped from 850°C to about 300°C, where the solubility of As in Ga is approximately 10^{-5} mole fraction. The system was subsequently removed from the furnace tube and the current flow terminated as the reservoirs were separated from the capillary.

The total mass of Ga plus GaAs was determined for each reservoir and the connecting tube, and the solutions placed in beakers of warm ($\sim$50°C) HCl (50%) to dissolve the gallium. The solutions were subsequently diluted and filtered and after the filter paper had dried the small GaAs crystals were collected and weighed. The initial and final amounts of free Ga and GaAs were compared for each experiment as an additional check.

To determine the electric field E present in solution during the experiments for the analysis of the EM data, the apparatus was modified to measure the resistivity of the gallium solution. For this experiment,

platinum wires were dipped into each Ga reservoir in order to monitor the potential across the capillary for a constant current flow. Resistivities of the solution at various temperatures up to 800°C were calculated by multiplying the resistance measured by the ratio of capillary cross-sectional area to length.

5. Growth Behavior and Morphology

5.0 Introduction

This chapter presents theoretical and experimental aspects of the growth behavior associated with conventional and current-controlled LPE of GaAs. Background information and theory are provided on the Ga-As equilibrium phase diagram, convection in solution, and interface demarcation. Models are presented for conventional and current-controlled LPE which are subsequently used to analyze experimental growth rate behavior. Other experimental data is classified under either temperature effects or an analysis of non-uniform growth. The last section in this chapter is a discussion of the results and conclusions, and their relationship to past and present work in this field.

5.1 Background

5.1.1 Ga/GaAs liquidus

In both conventional and current-controlled LPE the rate of growth is at all times related to the arsenic concentration in a gallium solution and its changes with temperature. Thus, any theoretical analyses of the growth behavior require knowledge of the characteristics of the Ga-As phase diagram over the temperature range of concern. Arsenic solubilities in Ga at temperatures from 500°C to the melting point of GaAs have been experimentally determined and reported,[85,86] and were reviewed by Thurmond.[87] The present work makes use of the data by Hall[85] which are in agreement with both earlier and later work. He found that a regular solution approximation

$$-\ell n \ [4C_{As} \ (1 - C_{As})] = \frac{\Delta S^{f*}}{R} \ (\frac{T_m}{T} \ 1) - \frac{w}{4RT} \ (1 - 2C_{As})^2 \qquad (5.1)$$

was in excellent agreement with his experimental data for the following values of these parameters:

ΔS^{f*} = 22.2 cal/°C-mole (effective entropy of fusion);

T_m = 1510°K (GaAs melting point);

w = 20.2 Kcal/mole (interaction parameter representing departure from ideal behavior);

R = gas constant;

T = absolute temperature;

C_{As} = solubility of As in Ga.

For dilute solutions (C_{As} << 0.5) which are presently of interest, equation 5.1 reduces to

$$-\ell n\ C_{As} = B/T + A \qquad (5.2)$$

where A and B are constants over a particular temperature range. A graphic representation of equation 5.2 with A = 1295 and B = 11750 (°K) is given in Fig. 5.1 together with data points from Hall[85] and Rubenstein.[86] Also given in Fig. 5.1 is a curve based on the assumption of a constant liquidus slope m = 2.89 x 10^3°C/at.frac.As at 850°C. The use of m is satisfactory for small temperature variations ($\Delta T \leq 10$°C) while the agreement of the data with equation 5.2 for this entire temperature region must be considered as excellent.

An analysis of theoretical and experimental results indicates that the solubility of As in Ga over the temperature range from 700 to 900°C presently investigated is given by equation 5.2 with the values for the constants A and B as indicated.

5.1.2 Theoretical analysis of growth behavior for conventional LPE of GaAs

There has been a great deal of work published on LPE growth models (see Section 2.2), using assumptions and methods of solutions of varying complexities. Most of the models in agreement with experimental results for GaAs are similar and assume diffusion-limited growth with equilibrium conditions at the interface. The models by Hsieh[17] are representative

Figure 5.1: Solubility of As in Ga, with data by Hall(85) [●] and Rubenstein(86) [▲].

$C_{As} = 1295 \exp[-11750/T]$

$m = 2.89 \times 10^3 \, (^\circ K / at.frac.)$
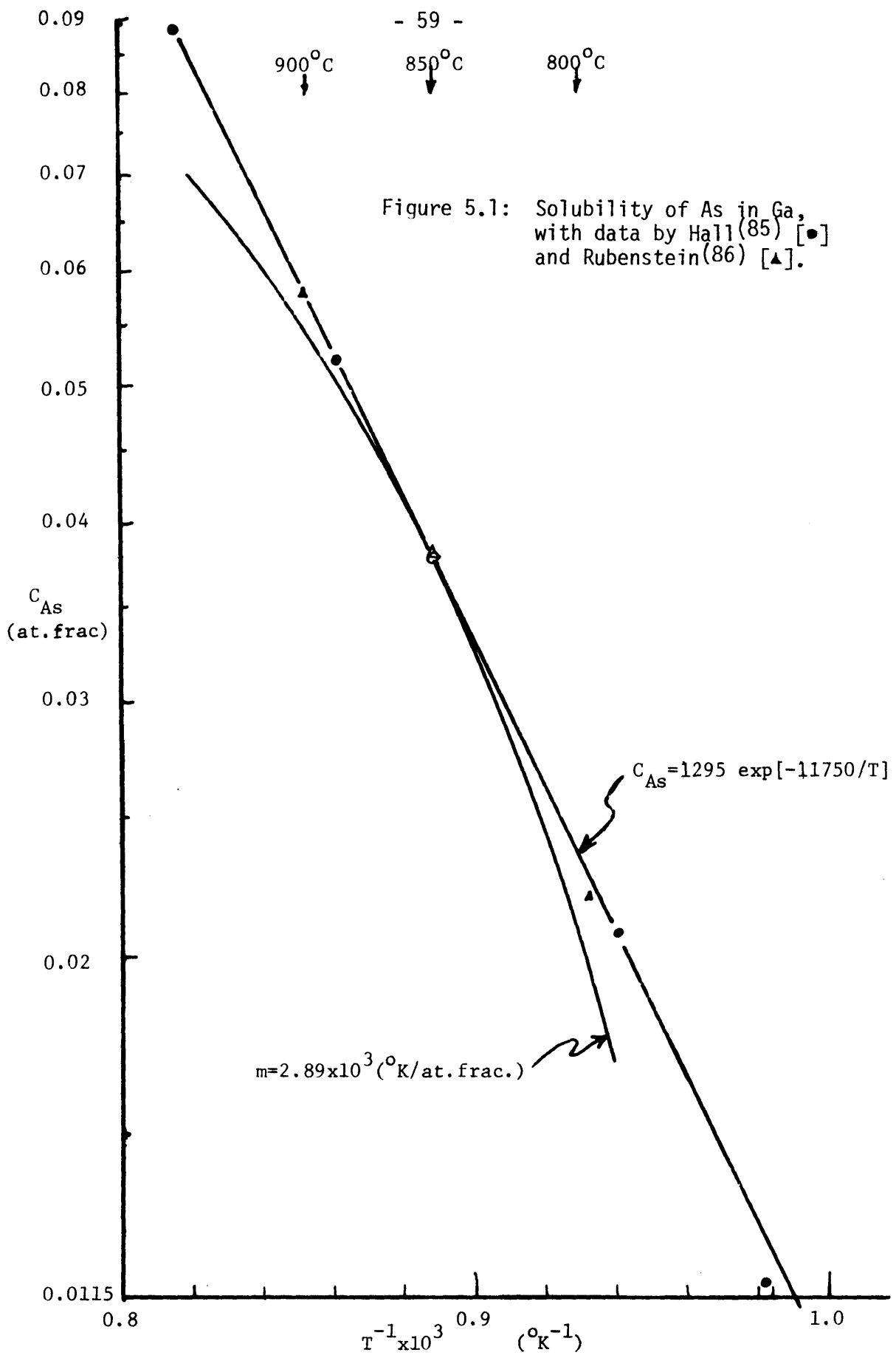
and relatively easy to work with because growth rate and layer thickness are in algebraic form. For growth induced by an abrupt temperature decrease (ΔT) of an equilibrated system, he obtained the layer thickness as a function of time,

$$d = 2\Delta T \ (1/mC_s) \ (D/\pi)^{1/2} \ t^{1/2} \tag{5.3}$$

and the growth rate

$$R = \Delta T \ (1/mC_s) \ (D/\pi)^{1/2} \ t^{-1/2} \tag{5.4}$$

where m is the liquidus slope, C_s is the arsenic concentration in the solid, and D is the diffusivity of As in Ga. For growth induced by continuous (ramp) cooling at a rate α (°C/min), the corresponding relationships are[17]

$$d = \frac{4}{3} \alpha \ (1/mC_s) \ (D/\pi)^{1/2} \ t^{3/2} \tag{5.5}$$

and

$$R = 2 \alpha \ (1/mC_s) \ (D/\pi)^{1/2} \ t^{1/2} \tag{5.6}$$

The difference in the growth behavior of these two types of cooling is evident: the ramp cooling leads to higher growth rates with time, while the step-cooling starts at an infinite growth rate that steadily

decreases. During actual growth these two conditions will be modified by nucleation in solution and the finite time to step-cool, respectively, but the functional dependencies have been verified for time,[14,17-19,25] liquidus slope,[20] temperature drop[17] or cooling rate,[18,19,21-23] and diffusion constant.[16,18] Hsieh also treated the superposition of step-cooling and ramp-cooling experimentally, finding that layer thickness was in agreement with the sum of equations 5.3 and 5.5 with the appropriate ΔT and α.

The presence of convection in solution during LPE growth has been reported to generally enhance the growth rate because of the additional solute mass transport.[5,7,29] Because fluid flow and its effect on growth are complex, models treating convection during LPE have been computer simulations of a diffusion boundary layer. Tiller and Kang[11] developed a model that used an exponential decaying form for the interface concentration that is inaccurate for large times. Crossley and Small[14] used the more accurate Arrhenius form for As solubilities (eq. 5.2), and included the effects of nucleation. However, their results are difficult to apply to arbitrary experimental conditions because they also include an initial undersaturation and omit any curves for growth rates. In order to compare experimental growth conditions to theory and estimate convective flow velocities present, a model similar to the ones above is presented.

LPE growth with convection is assumed diffusion-controlled through a stationary boundary layer thickness, δ, next to the interface with a completely mixed region beyond it. The arsenic concentration at the

interface is assumed in equilibrium with the solid and is given by the solubility (liquidus). The arsenic concentration in the mixed region is constant and is determined by conservation of mass (a function of the layer thickness). Algebraic solutions are derived first for a liquidus of constant slope in order to obtain functional dependencies of the growth parameters involved. A numerical solution is then derived with the exponential solubility (eq. 5.2), and a procedure presented to enable comparisons with experiment.

The boundary conditions for a linearly decreasing interface temperature are

$$C(o,t) = C_0 - \alpha t/m \tag{5.7a}$$

and in the mixed region $\delta < x < \ell$,

$$C(\delta,t) = C_0 - d\ C_s/\ell \tag{5.7b}$$

where α is cooling rate, m is the liquidus slope, t is the time, ℓ is the solution height, d is the layer thickness, C_s is the arsenic concentration in solution at height x above the substrate and at time t. The transport of As to the interface is given by Fick's first law:

$$J_{As}^D = - D\ \frac{\partial C}{\partial x}\bigg|_{x=0} \approx - D\ \frac{C(\delta,t) - C(o,t)}{\delta} \tag{5.8}$$

The diffusive flux J_{As}^D is proportional to the growth rate R of the layer,

$$R = - J_{As}^D / (C_s - C_i)$$ (5.9)

where C_i is the interface concentration of As in solution, approximated as C_0 for $C_i << C_s$. After substitution of the boundary conditions (eq. 5.7) for $C(o,t)$ and $C(\delta,t)$, the growth rate simplifies to:

$$R = \frac{\partial d}{\partial t} = \frac{D/\delta}{(C_s - C_0)} \left(\frac{\alpha t}{m} - \frac{d\ C_s}{\ell} \right).$$ (5.10)

Upon integration with respect to time, an equation is obtained for the layer thickness, d,

$$d = \frac{D\ \alpha\ t^2}{2\ \delta\ m\ C_s} - \frac{D}{\delta\ell} \int_0^t d\ \partial t$$ (5.11)

which is solved by iteration of d into an infinite series which reduces to an exponential in time:

$$d = \frac{\alpha\ \delta\ \ell^2}{D\ m\ C_s} \left(\frac{Dt}{\delta\ell} - 1 + e^{-Dt/\delta\ell} \right).$$ (5.12)

The growth rate is obtained by differentiation,

$$R = \frac{\alpha\ \ell}{m\ C_s} \left(1 - e^{-Dt/\delta\ell} \right)$$ (5.13)

which along with eq. 5.12 satisfies both (5.10) and (5.11) by direct substitution. The growth rate R from (5.13) is seen to approach a constant value of $\alpha\ell/mC_s$ independent of the diffusion constant and boundary layer thickness, which only determine the time necessary to reach "steady state". A concentration difference ΔC is established in time across the boundary layer such that flux $D\Delta C/\delta$ becomes constant and proportional to the driving force α/m,

$$D\Delta C/\delta = \frac{\alpha\ell}{m} \, (1 - e^{-Dt/\ell\delta}) \tag{5.14}$$

where a change in D of δ results in a different value of ΔC. A characteristic time τ can be defined as the transient time $\ell\delta/D$ which simplifies equations 5.12 to 5.14 and yields an expression for the ultimate supercooling ΔT_s in the region outside the boundary layer:

$$\Delta T_s = m \, \Delta C = \frac{\alpha\ell\delta}{D} = \alpha\tau \tag{5.15}$$

Using equations 5.14 and 5.7, a dimensionless concentration $(\alpha\tau/m)^{-1}C(x,t)$ is plotted versus x for several times t/τ in Fig. 5.2 that shows the boundary layer buildup.

Equations 5.12 through 5.15 represent an exact solution to an approximate model of growth under partial mixing conditions in the melt. They are useful insofar as they reveal the functional dependencies of layer characteristics on the various growth parameters. It is of interest to include the effect of a changing liquidus slope with temperature, which

Graphite Plug

Boron Nitride	MIXED REGION	Boron Nitride

BOUNDARY LAYER

Layer/Substrate
(GaAs)
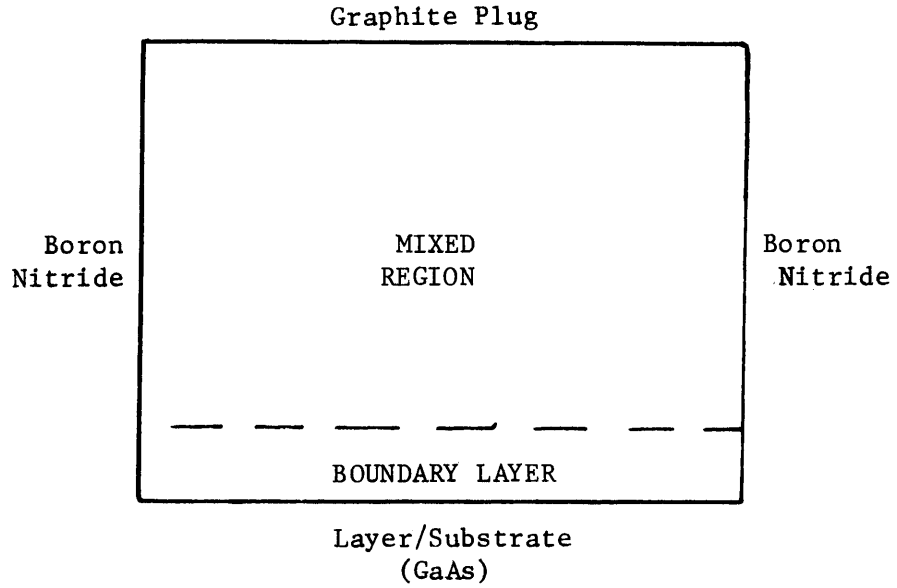
Figure 5.2a: Schematic of the growth solution with convection used in the conventional LPE model. Complete mixing is assumed for $\delta \leq x \leq \ell$, while no mixing is assumed for $0 \leq x \leq \delta$.

$$\text{DIMENSIONLESS CONCENTRATION} \quad (\alpha \mathcal{V}/m)^{-1}[\ c(x,t) - c_0\ ]$$

$t/\mathcal{V}$

0

1

2

3

4
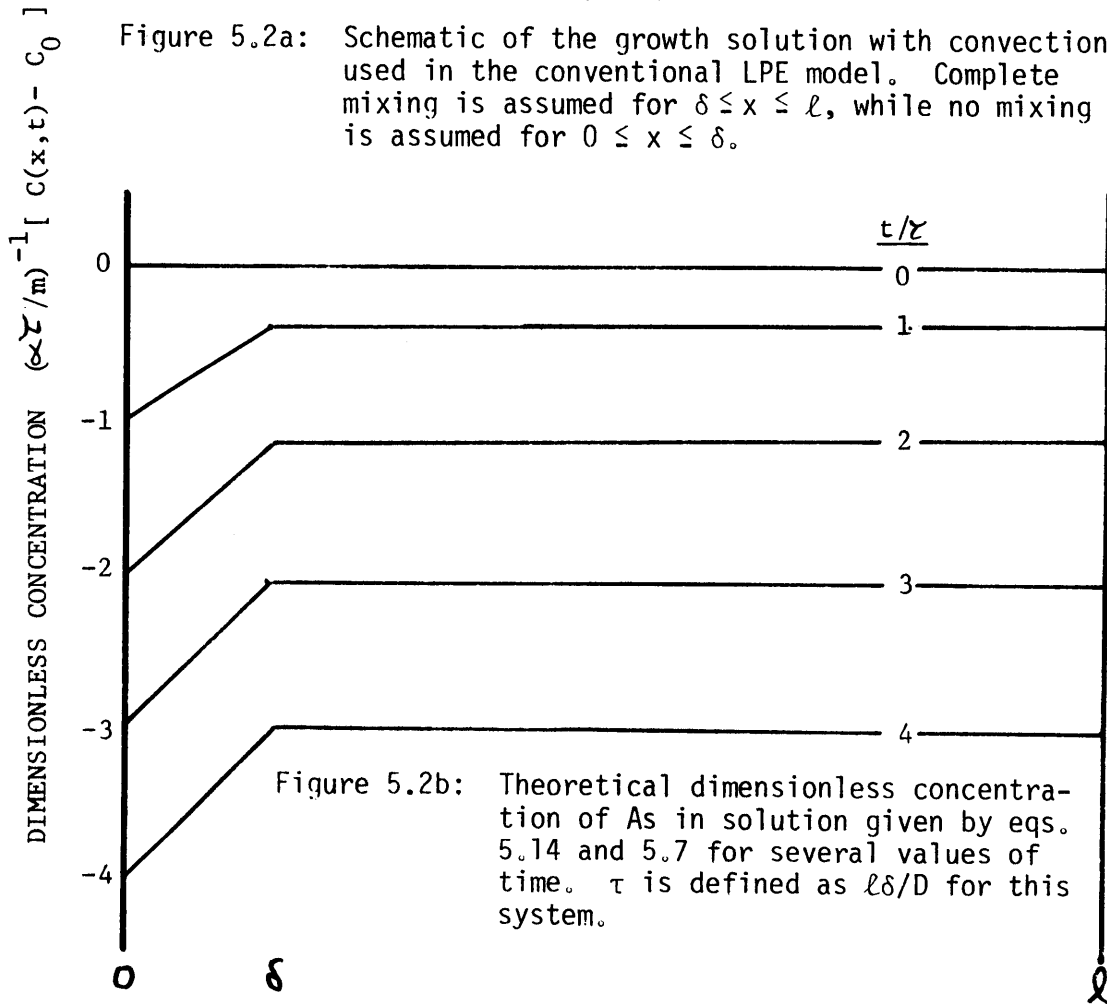
Figure 5.2b: Theoretical dimensionless concentration of As in solution given by eqs. 5.14 and 5.7 for several values of time. τ is defined as $\ell\delta/D$ for this system.

0   δ   ℓ

necessitated the use of numerical methods. The boundary condition (5.3a) was changed to :

$$C(o,t) = C^{eq \cdot} (T) = C^{eq \cdot} (T_o - \alpha t) \tag{5.16}$$

where $C^{eq \cdot}(T)$ represents the liquidus concentration of As in Ga at temperature T (given by eq. 5.2). Equation 5.11 is therefore modified and is used in an iterative program that calculates the microscopic growth rate R and layer thickness d in each time period Δt:

$$R_n = \frac{D}{\delta} \left[\frac{C_o - C^{eq \cdot} (T_o - \alpha n\Delta t)}{C_s} - \frac{d_{n-1}}{\ell} \right] \tag{5.17}$$

$$d_n = \sum_{i=1}^{n} R_i \, \Delta t \tag{5.18}$$

where $d_o \equiv 0$. Equations 5.17 and 5.18 were used to obtain values for R and d under experimental conditions. The results are plotted in Fig 5.3 for several values of solution height ℓ and diffusion-boundary layer thickness δ, along with growth rate for diffusion-limited growth (eq. 5.6).

Figure 5.3 indicates several important aspects of growth in the presence of convection. The magnitude of δ controls the time for the system to reach what essentially is equilibrium growth: complete deposition of excess arsenic as determined by the phase diagram. Once the maximum R is reached, the growth rates reflect the changing slope of the liquidus, and are proportional to the solution height. It is of interest
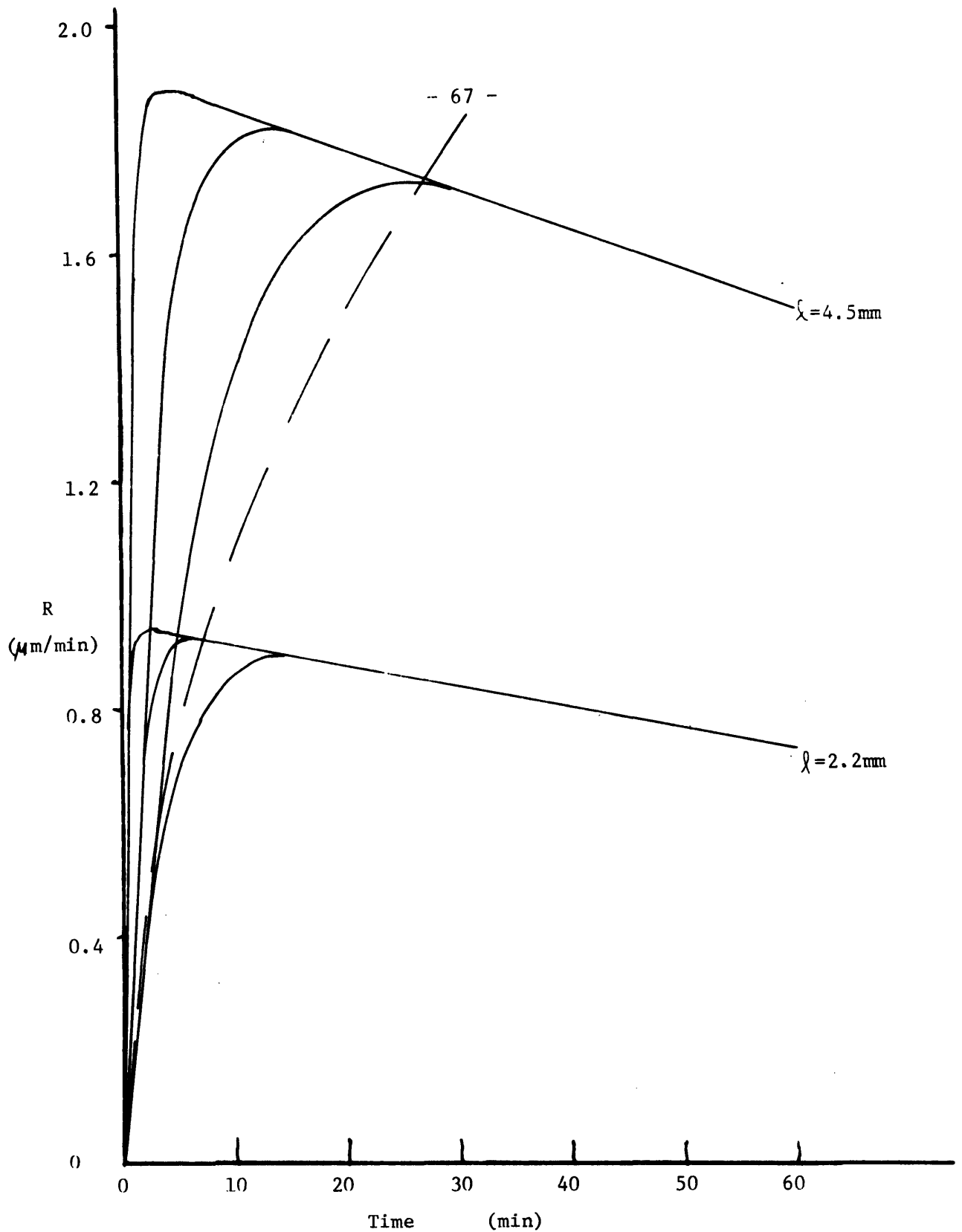
Figure 5.3: Theoretical growth rates for conventional LPE with convection calculated from equations 5.17 and 5.18 for solution heights of 4.5 and 2.2 mm, boundary layer thicknesses of 0.06, 0.24, and 0.6 mm, and a cooling rate of 0.5°C/min from 865°C initially. The dashed line represents diffusion-limited growth from a semi-infinite solution (eq. 5.6).

to point out that although nucleation has been neglected in these curves, the symmetry of the model allows growth on the solution's upper surface $(x = \ell)$ equal to growth for an effective $\ell/2$ solution height.

Experimentally determined growth rate transients cannot be adequately resolved to allow comparisons with curves such as Fig. 5.3. However, the layer thickness at a fixed time early during growth (within the transient times) is extremely sensitive to δ and can be obtained from the first interface demarcation in the epitaxially grown layer. Theoretical layer thickness after 10 and 20 minutes were calculated on the basis of equations 5.17 and 5.18 and are plotted in Fig. 5.4 as a function of transient time τ $(= \ell\delta/D)$ for two values of ℓ. Knowing the solution height ℓ, the layer thickness will determine a τ from which δ may be found.

A theoretical model for the growth behavior associated with conventional LPE in the presence of convection with a finite solution (equations 5.17 and 5.18) is developed. On the basis of this model, growth parameters and conditions during conventional LPE are determined making use of experimentally determined growth rates and layer thicknesses (Section 5.2.1).

5.1.3 Theoretical analysis of growth rate behavior for current-controlled LPE

The application of an electric current across an equilibrated solution and solution/substrate interface results in several simultaneous effects which may lead to epitaxial growth or substrate dissolution.
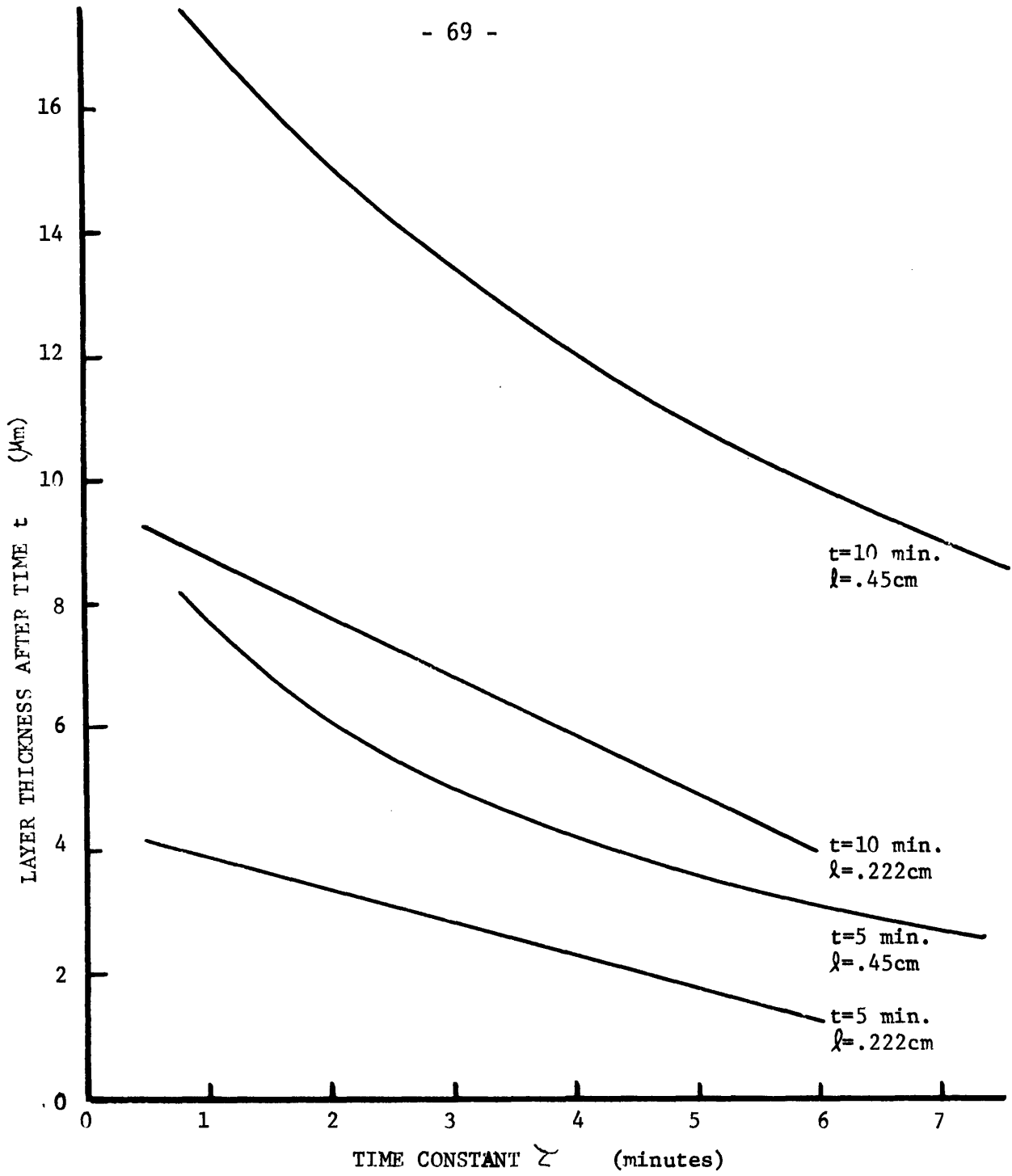
Figure 5.4:   Theoretical layer thicknesses calculated from eqs. 5.17 and 5.18 as a function of time constant τ given by $\delta\ell/D$.

(1) Depending on the current polarity, the Peltier
    effect leads to heat absorption or evolution
    at the interface, producing a localized tem-
    perature change and thermal gradients.

(2) Electromigration will tend to segregate the
    components of the solution, resulting in
    solute gradients.

(3) Joule heating will increase the overall system
    temperature.

(4) The electric field associated with the applied
    current will alter chemical activities of all
    species present.

The growth behavior reflects the influence of each of the above phenomena,
but in general the contributions of the individual effects cannot readily
be identified because of similar function dependencies. In particular,
the relative contributions of Peltier cooling and electromigration to
growth have not been readily obtainable from experimental data. A quanti-
tative model has recently been proposed by Jastrzebski and coworkers[88]
which predicts growth rates in the presence of both of these effects.
They treat the steady-state cases for a semi-infinite solution and a
source replenishing the solution, which do not yield individual contri-
butions of the different growth mechanisms.

In the context of the present work it is important to know the
effect of finite solution size on the rates of growth associated with
electromigration and Peltier cooling. A mathematical model was therefore

formulated that predicts growth rates and layer thicknesses for current-controlled growth under conditions of no mixing and mixing in solution (for the derivation, see Appendix 10.1). The model with no mixing in solution is an exact formulation of the growth behavior valid for all growth times. Both models are based on the following assumptions:

(1) The solute concentration at the growth interface remains constant once the current is applied, and is determined by the interface temperature.

(2) The applied field results in an electromigration flux proportional to solute concentration, as given by Verhoeven.[49]

The expressions for growth rate and layer thickness for the case of no mixing are summations (from eqs. 10.30 and 10.31, respectively):

$$R = \frac{D}{C_s - C_i} \sum_{n=1}^{\infty} \frac{\lambda_n e^{-k_n^2 Dt} [nC_0 e^{n\ell/2} \sin\lambda_n\ell + (C_0 - C_i)\lambda_n]}{k_n^2 (\ell/2 + \frac{n}{4\lambda_n^2} \sin^2\lambda_n\ell)} \tag{5.19}$$

and

$$d = \frac{1}{C_s - C_i} \sum_{n=1}^{\infty} \frac{\lambda_n [nC_0 e^{n\ell/2} \sin\lambda_n\ell + (C_0 - C_i)\lambda_n]}{k_n^4 (\ell/2 + \frac{n}{4\lambda_n^2} \sin^2\lambda_n\ell)} (1 - e^{-k_n^2 Dt}) \tag{5.20}$$

where t is the time, D is the solute diffusivity, ℓ is the solution height, and C refers to the solute (As) concentration with the subscripts

s, o and i for solid phase, initial and interfacial, respectively. The quantity η is defined as $\eta \equiv \mu E/D$ where μ is the differential electro-migration (EM) mobility, E is the applied electric field, and the product represents an EM drift velocity. λ_n is determined from equation 10.18,

$$\tan \lambda_n = - (\lambda_n \ell) / (\eta \ell/2) \tag{5.21}$$

and k_n^2 is obtained from equation 10.20,

$$K_n^2 = \eta^2/4 + \lambda_n^2 . \tag{5.22}$$

Growth rates and layer thicknesses calculated according to equations 5.19 and 5.20 are shown in Figs. 5.5 and 5.6, respectively, for values of $(C_0 - C_i)$ greater than, equal to, and less than zero. It is evident that the initial transients are determined by $(C_0 - C_i)$, while in all three instances the rate approaches zero exponentially with time constant $\tau = 4\ell^2/\pi^2 D$. The decreasing growth rates result from arsenic depletion in the finite solution. It is of interest to note that for increasing solution heights $(\ell \to \infty)$ the growth rates computed through equation 5.19 approach those by Jastrzebski et al[88] who used a semi-infinite melt. Maximum layer thicknesses obtained by equation 5.20 (as $t \to \infty$) are in excellent agreement with thicknesses obtained from the steady-state con-centration distribution (eq. 10.6). In the absence of electromigration $(\eta = 0)$, expressions 5.19 and 5.20 describe the growth behavior of a diffusion-limited step-cooled system[17] which for initial growth $(t \ll \tau)$ obeys equations 5.3 and 5.4.

Figure 5.5: Normalized theoretical growth rates as a function of normalized time for current-controlled LPE without a source. The upper, middle, and lower curves represent the effect of step-changes in the interface temperature of cooling, no change, and heating, respectively (the magnitude of the heating change was one-half of that of the cooling change). The quantity $\mathcal{T}$ is defined as $(k_1^2 D)^{-1}$ where k_1^2 is given by eqs. 5.22 and 5.21 for n=1.

NORMALIZED GROWTH RATE
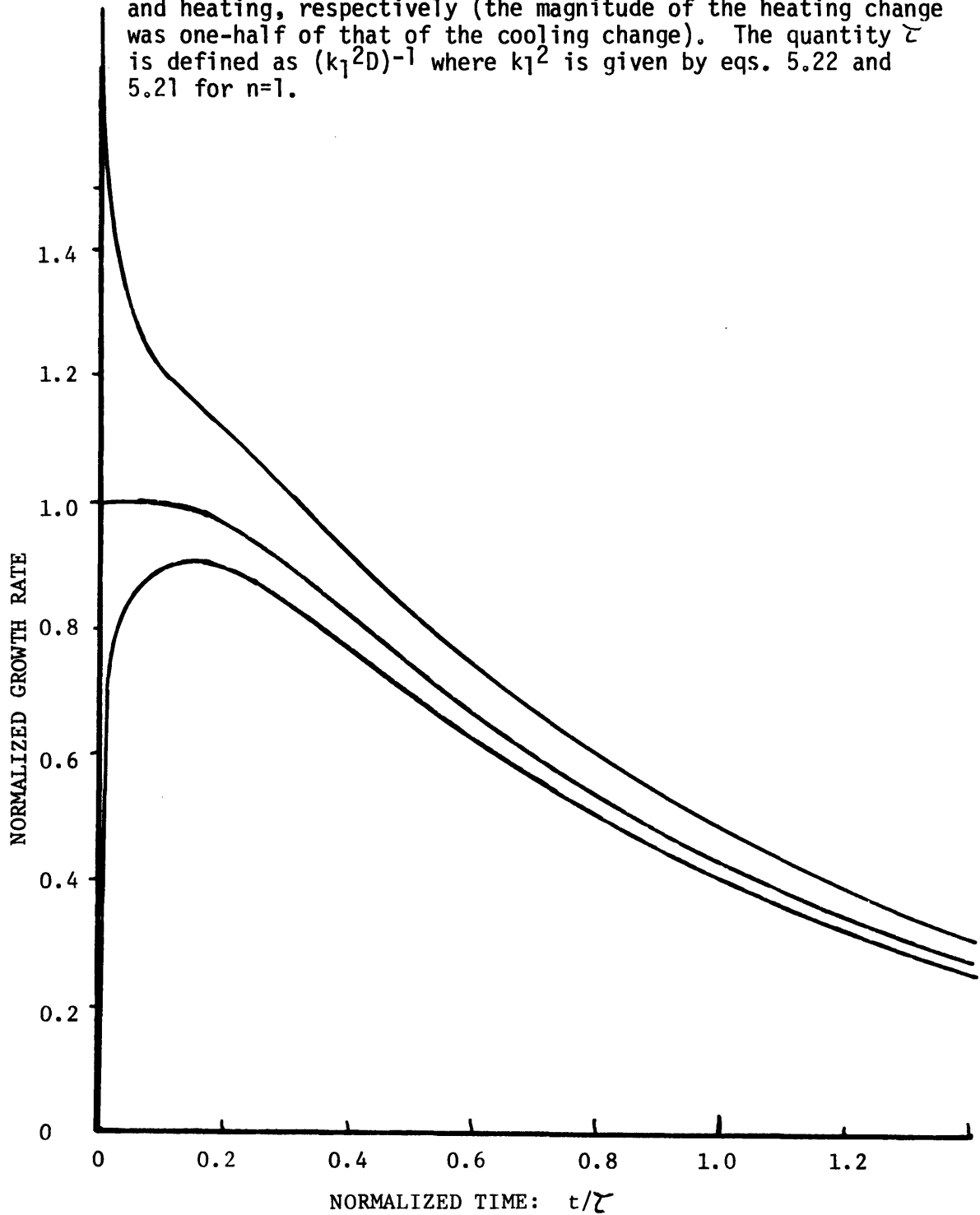
NORMALIZED TIME: $t/\mathcal{T}$

Figure 5.6: Normalized theoretical layer thickness as a function of normalized time for current-controlled LPE without a source. These curves correspond to the growth rate curves given in Fig. 5.5. The quantity d_{max} is the limiting value for the middle curve (constant interface temperature).
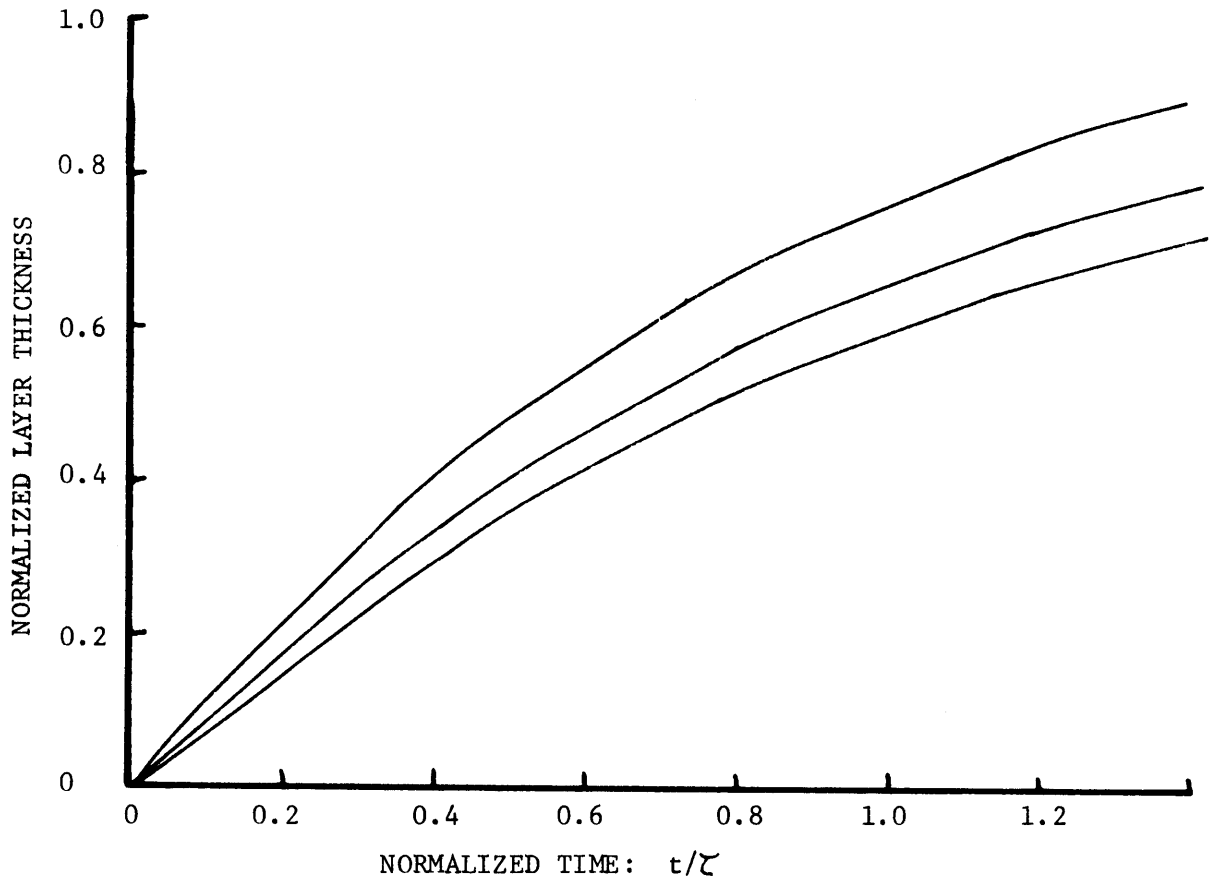
The model developed for current-controlled growth from a finite solution with convection (see Appendix 10.1.2) yields essentially the same relationships as (5.19) and (5.20) with the substitution of ℓ by an effective solution height ℓ_e which is a function of the actual solution height ℓ, the boundary layer thickness δ, and to a lesser extent $(C_o - C_i)$ (see eq. 10.44). The model is limited by the assumption of complete mixing in solution outside of the stationary boundary layer, but allows for boundary layer buildup and yields a maximum layer thickness consistent with this assumption.

In order to apply these models to current-controlled LPE growth, several simplifying assumptions must be made. Already incorporated into the models are the conditions of constant temperature (for $t > 0$) and growth or dissolution at the interface only. While the latter condition is satisfied by the experiments, there are, however, temperature effects associated with current flow. These are neglected except for their effect on the interface concentration C_i. Furthermore, to relate Peltier cooling to C_i, the interface must be assumed to be at equilibrium, such that C_i is determined from the liquidus at the interface temperature. Thus the Joule effect, the Peltier effect, and furnace thermal changes are treated together as an instantaneous temperature change at the interface. The quantity $(C_o - C_i)$ can then be replaced by $\Delta T/m$.

A theoretical model for growth associated with current-controlled LPE from a finite solution (with no source) is presented (eqs. 5.19 and 5.20). This model includes two basic driving forces for growth, each of which

has a different effect on growth rates: electromigration (proportional to an As mobility μ_{As}), and a temperature change at the growth interface, ΔT. The lack of a GaAs source in the solution enables all thermal effects (Peltier and Joule effects, and the existing gradients) to be incorporated into the change in the interface temperature, while precluding the separation of the contributions of each. For this reason no effort has been made to determine from first principles the effect of Peltier cooling on growth. The applicability and implications of this current-controlled LPE model are discussed in Section 5.3, after being used to analyze experimentally determined growth rates in Section 5.2.2.

5.1.4 Analysis of convective solution behavior

Compositional as well as thermal gradients constitute potential driving forces for the establishment of convection in a solution.[89-93] These density gradients may be either parallel or normal to the gravitational force, leading to different flow behavior. In addition, the magnitude of these driving forces determines the type of flow present: laminar (time-independent) flow, or turbulent (time-dependent) flow. Criteria for the onset of turbulent flow have been established,[90] and are used to show that the present system exhibits only laminar flow. The driving forces for convection are discussed in the context of the growth geometry and experimental conditions used, and estimates of time-independent fluid velocities are made. Where enough physical information is available, the fluid flow is used to calculate boundary layer thicknesses.

The usual approach to convection is through dimensionless analysis of the governing fluid- and heat-flow equations.[92,93] Parameters used include the Rayleigh number Ra, the Grashof number Gr, the Prandtl number Pr, and the aspect ratio A. The aspect ratio is the fluid height divided by its width. The Prandtl number is a ratio of mass flow to heat flow defined as

$$Pr = \nu/\kappa \qquad (5.23)$$

where ν is the kinematic viscosity and κ is the thermal diffusivity. The Grashof number represents the ratio of buoyancy to viscous forces, and as such has a different form for thermal or compositional density gradients. For thermal gradients $\partial T/\partial x$, the Grashof number is

$$Gr = \frac{\beta \, g \, (\partial T/\partial x) \, d^4}{\nu^2} \qquad (5.24)$$

while for compositional gradients $\partial C/\partial x$ it becomes

$$Gr = \phi \, g \, (\partial C/\partial x) \, \frac{d^4}{\nu^2} \qquad (5.25)$$

where g is the gravitational acceleration (980 cm/sec^2), β is the thermal coefficient of volume expansion, ϕ is the volumetric change with unit concentration change, and d is a characteristic length depending on the orientation of the gradients to gravity.

The Rayleigh number is the product of Gr and Pr and can be used as a basic criterion for the onset of turbulent flow. Lamillar flow is expected in a cylindrical system with an aspect ratio of 1 if

$$Ra = Gr \cdot Pr < 1000 \quad [91]$$

(5.26)

The Ga/GaAs system of present interest has stabilizing vertical thermal gradients (the solution upper surface is approximately 0.5°C warmer than the lower interface) but there are horizontal thermal gradients present from $\leq$ 0.1 to 0.8°C/cm. Using published values[7] of ν (10^{-3} cm^2/sec), κ (0.3 cm^2/sec), and β (10^{-4}/°C), Rayleigh numbers ranged from 115 to 1.2, indicating laminar flow only.

Fluid velocities (ν) can be estimated from the Grashof number, for Gr > 1 as[92]

$$U = (Gr)^{1/2} \nu/d$$

(5.27)

and for Gr < 1 as[92]

$$U = Gr \, \nu/d$$

(5.28)

A detailed description of fluid flow in rectangular confinement with lateral heat flow is given by Stewart and Weinberg.[94,95]

Vertical solute (arsenic) gradients are present and are stabilizing for conventional LPE of GaAs with the substrate below the solution (with

no source present), but may become destabilizing for current-controlled growth in the same configuration. Depletion of the solution due to electromigration will lead to a density inversion which may drive convective flow, particularly in the latter stages of growth.

With the lack of sufficient data on As in solution, a quantitative approach to solute-driven convection is not possible. Batchelor[91] devised an expression for ϕ, the volumetric change with unit concentration change, involving densities and atomic weights for a binary system. Use of these physical constants for Ga and As in this formula yields a ϕ, and thus Ra (from eqs. 5.25 and 5.26), predicting that the Ga-As LPE system is unstable for the substrate below the solution, contrary to experimental observations.[7,96] Long and coworkers,[7] concerned with this problem, calculated from experiment an upper limit for the arsenic density in solution as 5.4 g/cm^3 as compared to 5.6 g/cm^3 for Ga at 700 to 800°C. A lower limit for the effective density of As in Ga may be obtained by assuming that bonding takes place in solution and thus using ρ_{GaAs} = 5.16 g/cm^3 (960°C). The volumetric coefficient ϕ therefore ranges from 0.036 to 0.08 /at.frac. As after substitution of the above limiting values into Batchelor's expression.[91] A critical vertical concentration difference of 0.5 at.% As, above which turbulent convection is expected, was calculated from equations 5.25 and 5.26 with ϕ = 0.08 /at.frac. As. It is therefore concluded that convection due to composition-induced density variations is time-independent.

Although no work known to the author has specifically treated thermally-driven convection in a cylindrical system of aspect ratio 0.5 and Prandtl number 3×10^{-3}, the streamline function of Batchelor[91] may be used as an approximation to other systems,[89] such as the one presently concerned. The fluid velocity at the center of the layer, distance X above the growth interface, is

$$U = \frac{\kappa \ Gr \ Pr}{3\omega} \ (0.5)^3 \ (\frac{X}{\omega}) \ (1 - \frac{X}{\omega}) \ (1 - \frac{2X}{\omega}) \tag{5.29}$$

valid for lamillar flow. Using Carruthers' definition of δ,[89] at $X = \delta$ the diffusive flux to the interface is one-tenth the magnitude of the convective flux (Cv). For conventional LPE the former is given by equation 5.11, and is independent of:

$$J_D = \frac{\alpha \ell}{m} = \frac{1}{10} \ C_\ell \ U \ (\delta) \tag{5.30}$$

where C_ℓ is the solute concentration in the mixed region and α is the furnace cooling rate. Substituting equation 5.29 in 5.30, δ is solved for (assuming $\frac{2\delta}{\omega} \ll 1$):

$$\delta = \frac{24 \ \alpha \ \ell \ \omega^2}{m \ Gr \ Pr \ \kappa} = \frac{240 \ \alpha \ \nu}{m \ C_\ell \ g \ \beta \ \Delta T \ A^3} \tag{5.31}$$

where $A = \ell/\omega$ the aspect ratio. δ is plotted as a function of ΔT in Fig. 5.7 for values of the constants in (5.31) previously given.

Figure 5.7: Theoretical dependence of the momentum boundary layer thickness δ on the horizontal temperature difference across the solution (eq. 5.31).
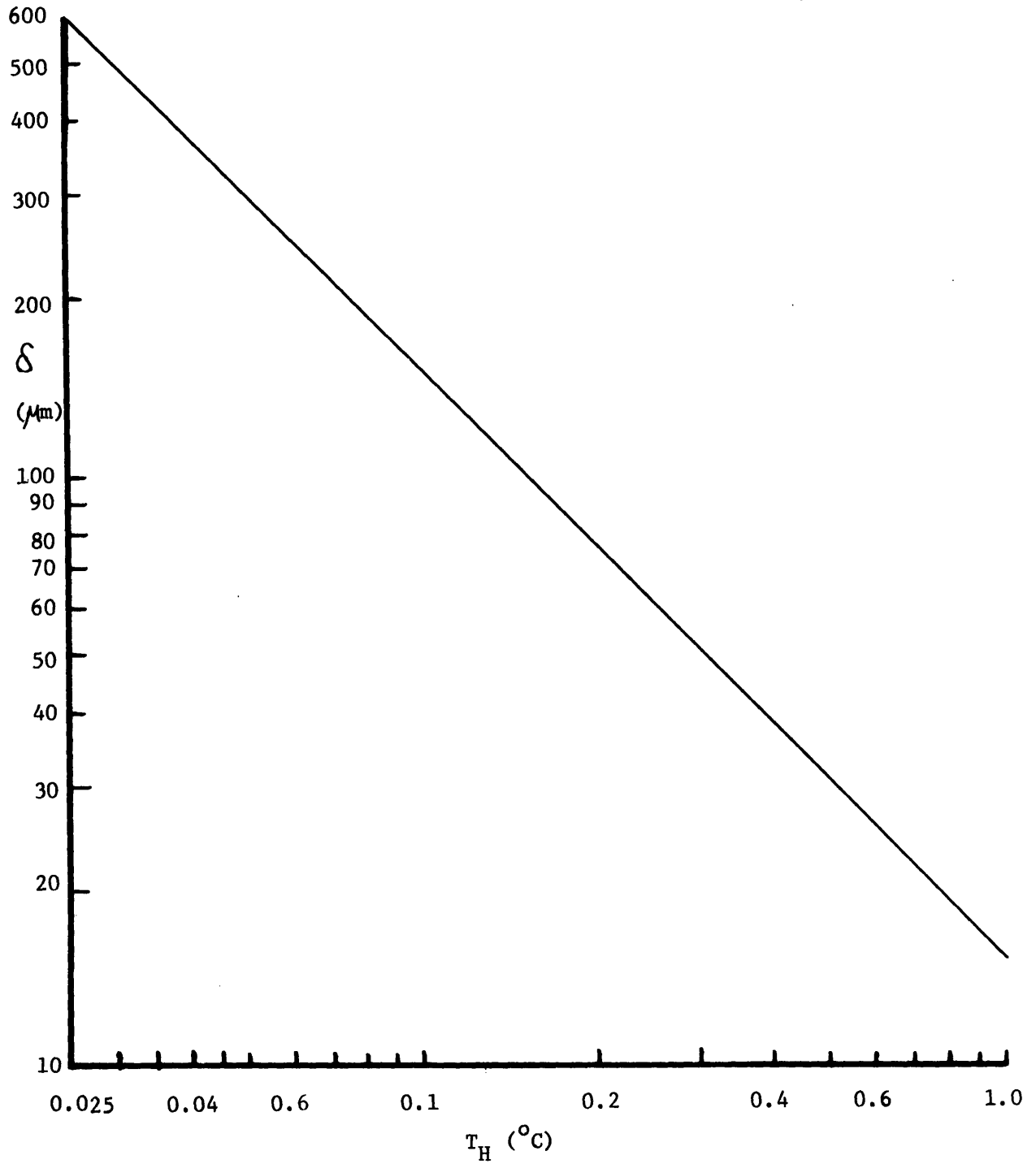
The above analysis indicates that for the thermal and compositional conditions normally encountered during LPE growth, convection, if present, is time-independent (i.e., laminar flow). In addition, momentum boundary layer thicknesses associated with laminar flow are related to the magnitude of an applied horizontal temperature gradient in an affort to characterize the effect of convection on growth.

5.1.5 Interface demarcation

Interface demarcation involves the application of a current pulse across an advancing solid-melt interface. Due to a change in the microscopic growth rate during the pulse, segregation is affected along the entire plane of the interface. This compositional difference can be detected under interference microscopy after selective etching of a crystal cross-section.

The fundamental nature of the segregation effect upon pulsing is not clearly understood. After extensive work on segregation associated with electromigration in liquid alloys,[47,49-52,97-101] growth rate changes due to the Peltier effect at the growth interface were studied with Ge[53] and InSb.[1] It was concluded[54,55] that dopant segregation phenomena associated with the observed values of growth rates resulted from changes in the interface distribution coefficient and were not diffusion controlled. Larger growth rate changes in LPE of InSb[1] upon pulsing were described as "freezing-in" a region of high dopant concentration, followed by a depleted region. Blom and coworkers,[56] using heating pulses during LPE of GaAs, explained the demarcation lines as

regions of rapid regrowth following dissolution brought on by the pulses. The one conclusion reached by all of these workers was that the pulsing did not affect the overall crystal growth process.

The particular problem of pulsing in a dilute solution of Ga and As is that the growth rate is diffusion controlled with characteristic transport times that far exceed typical pulse durations (t < 2 secs). Thus only instantaneous changes in the interface liquid concentration of As (or Ga) will lead to large growth (or dissolution) rates from the large concentration gradients created at the interface, and these will fall off rapidly as transport occurs. A change in the interface concentration can be due to a change in the interface temperature while assuming local equilibrium conditions at the interface, or to a departure from equilibrium caused by the pulse itself. The latter possibility is discussed in Chapter Six, while the former is presently treated with respect to Peltier heating or cooling at the interface.

The application of a current pulse across a solution and solution/ substrate interface leads to growth rate behavior which is initially similar to continuous current-controlled growth and is modeled by equations 5.19 and 5.20 for times $t \leq 6$ seconds. Figure 5.8 is a simulation of the growth rate at the onset of a cooling pulse approximately 50 A/cm^2 across a saturated solution at 850°C for four values of interface cooling due to the Peltier effect. It is evident that the growth rates are dominated by temperature changes at the interface for times smaller than one second. The thickness of GaAs deposited was calculated after 0.5 seconds to be 250 Å from the electromigration (EM) effect alone, and
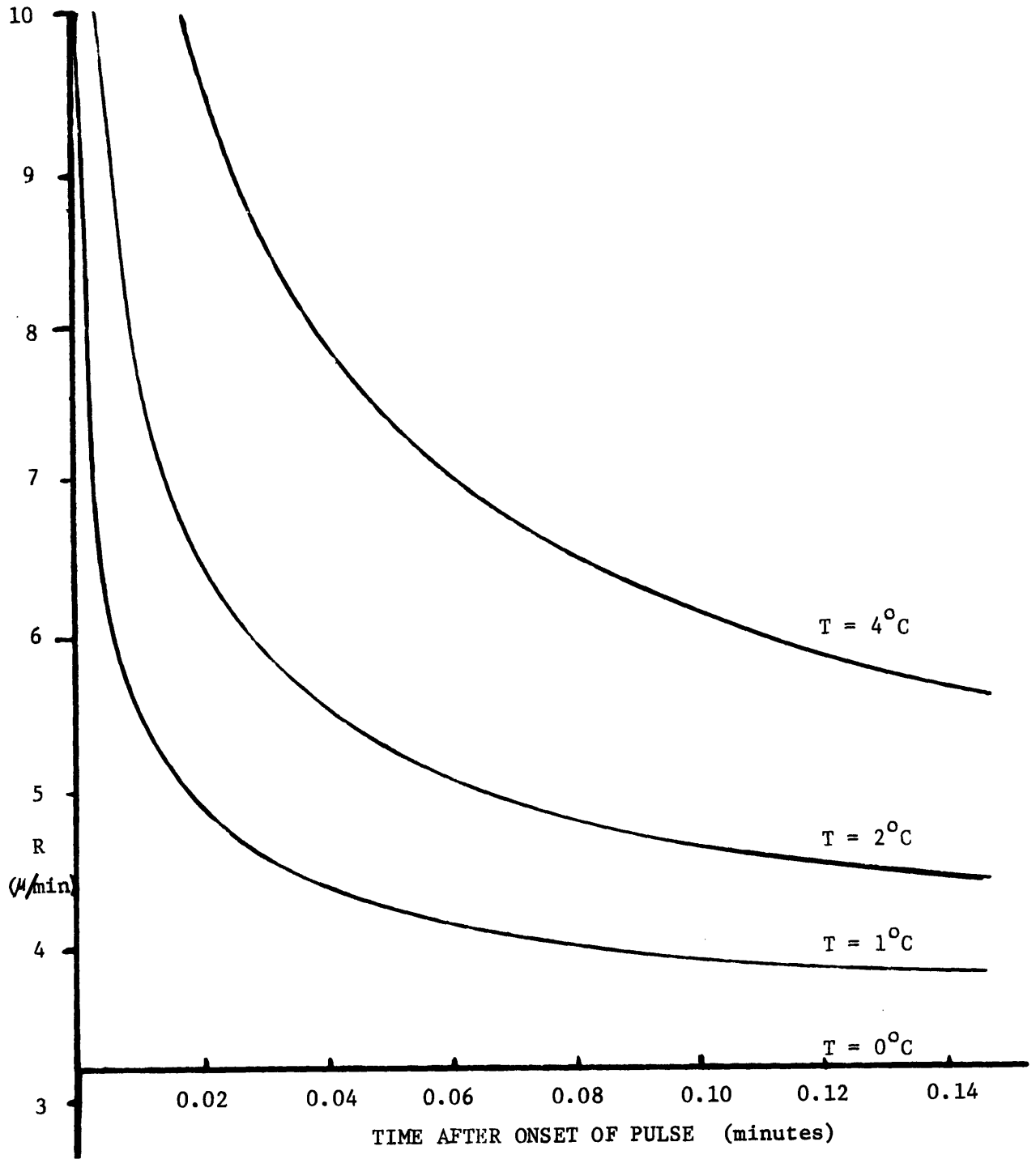
Figure 5.8: Theoretical growth rates at the onset of a current pulse for
four values of interface cooling (ΔT) and a high estimate of
an electromigration flux ($\mu E = 42$ µm/min).

650, 1050 and 1800 Å for EM with cooling of 1, 2 and 4°C respectively (the last being the closest estimate of actual cooling). The electromigration effect is therefore neglected for simplicity. Results obtained for a heating pulse are essentially the same, with dissolution rates equal to the above growth rates with respect to time.

When a pulse is terminated and no external driving forces are applied to the system, there is a relaxation of temperature and composition to the pre-pulse conditions. Thus, a cooling pulse will normally be followed by dissolution, a heating pulse by deposition. The thermal relaxation time can be estimated from the thermal diffusivities of GaAs and Ga ($\kappa \backsim 0.8$ and 0.3 cm^2/sec respectively) as $\tau = r^2/\kappa$ where r is a distance of interest. Taking r as the substrate thickness (0.04 cm), τ is on the order of milliseconds, and the thermal response for leading and falling edges of the pulse is assumed instantaneous. The major effect of including thermal response times would be limiting the initial rates from infinite to some large but finite values.

The compositional relaxation at pulse termination is simply diffusion-limited growth or dissolution which can also be treated by the growth model of Appendix 10.1 with one change in the initial condition. Instead of being constant, the initial As concentration profile in the solution is a result of the applied pulse, and is given by equation 10.28 for $t = t_o$, the pulse duration. Epitaxial growth rates and thicknesses in the Ga/GaAs system at 850°C (0.45 cm solution height) have been calculated for a 4°C step-heating lasting 0.008 min, and are plotted in Fig. 5.9. It should be pointed out that these curves apply to both heating and
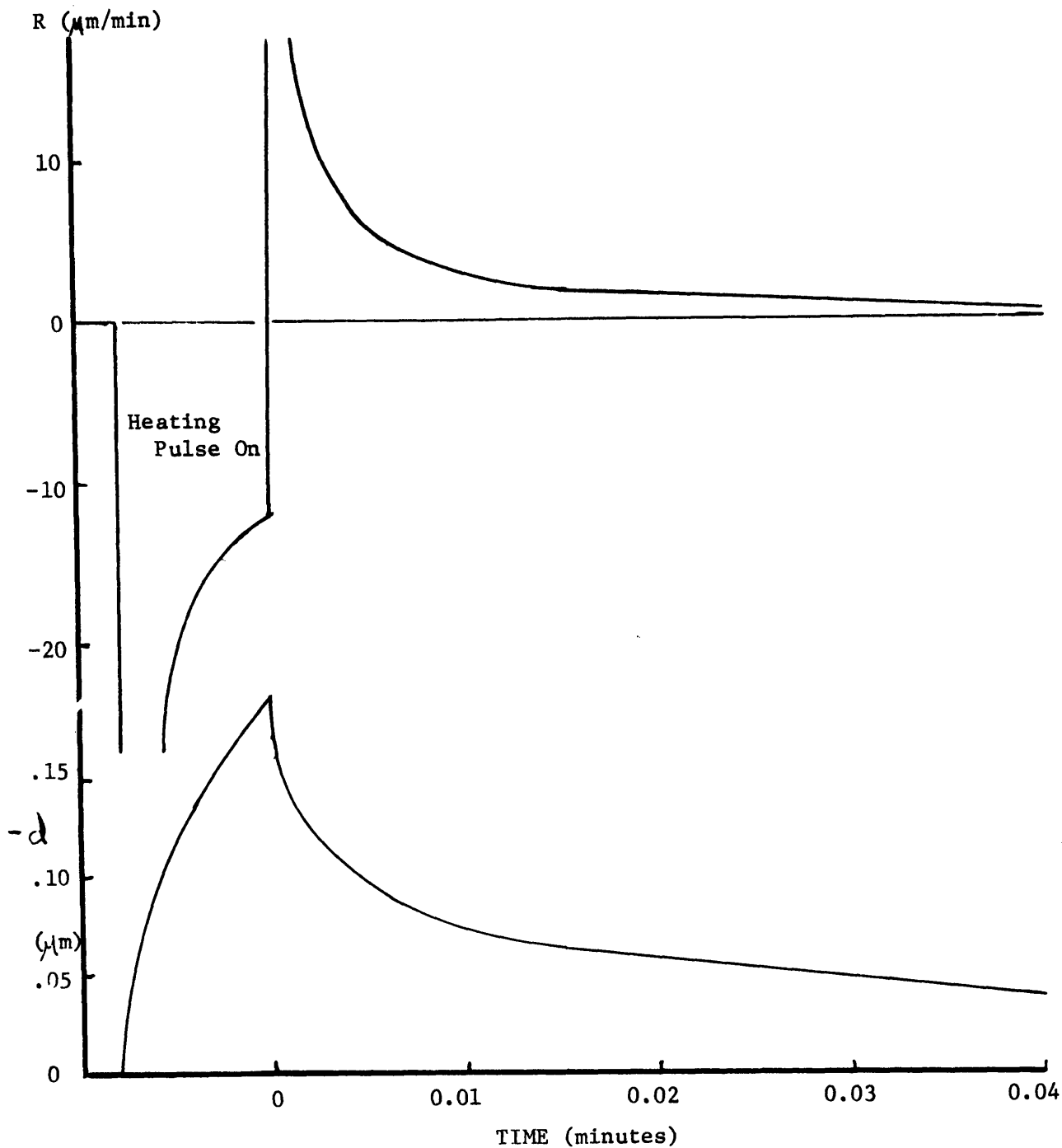
Figure 5.9: Calculated recovery of the growth rate and layer thickness after the application of a heating pulse ($\Delta T = -4°C$) of 0.008 minute duration from equilibrium conditions at 850°C. Dissolution occurs for 0.008 min until pulse termination at t = 0 when regrowth begins.

cooling pulses, the only difference being growth or dissolution taking place. In Fig. 5.9a the growth rate approaches negative infinity and stays negative (dissolution) while the pulse is applied. Upon termination of the pulse, the growth rate approaches plus infinity but falls more rapidly to smaller rates making the recovery extend well past the original pulse duration. The amount of dissolution plotted in Fig. 5.9b shows the initial effect of the heating pulse and the regrowth during recovery. In this particular example it takes approximately 10 seconds for the system to reach 90% of its equilibrium position after the 0.5 second pulse. However, after five minutes (the normal pulsing period), there is 98% recovery with a net change in layer thickness of only 0.004 μ, indicating no net measurable effect on the growth process.

Because of the extremely high growth rates and the short time involved, a pulse superimposed on normal growth due to continuous current or cooling should exhibit growth behavior similar to the one just discussed. The heating pulse behavior will appear as in Fig. 5.9 with the growth rates shifted an amount R_o toward the positive R direction, and the maximum amount of dissolution reduced less than 5% for $R_o = 1$ μ/min. What will remain in the epitaxial layer is the region of rapid regrowth assymptotically approaching the steady-state growth rate (see Fig. 5.10). The cooling pulse will thus result in a region of rapid growth whose width depends on the dissolution time which in turn is determined by the steady-state growth rate. However, the region grown next will start at zero growth rate and approach R_o from below. These regions are depicted in Fig. 5.10 for heating and cooling pulses on a steady-state
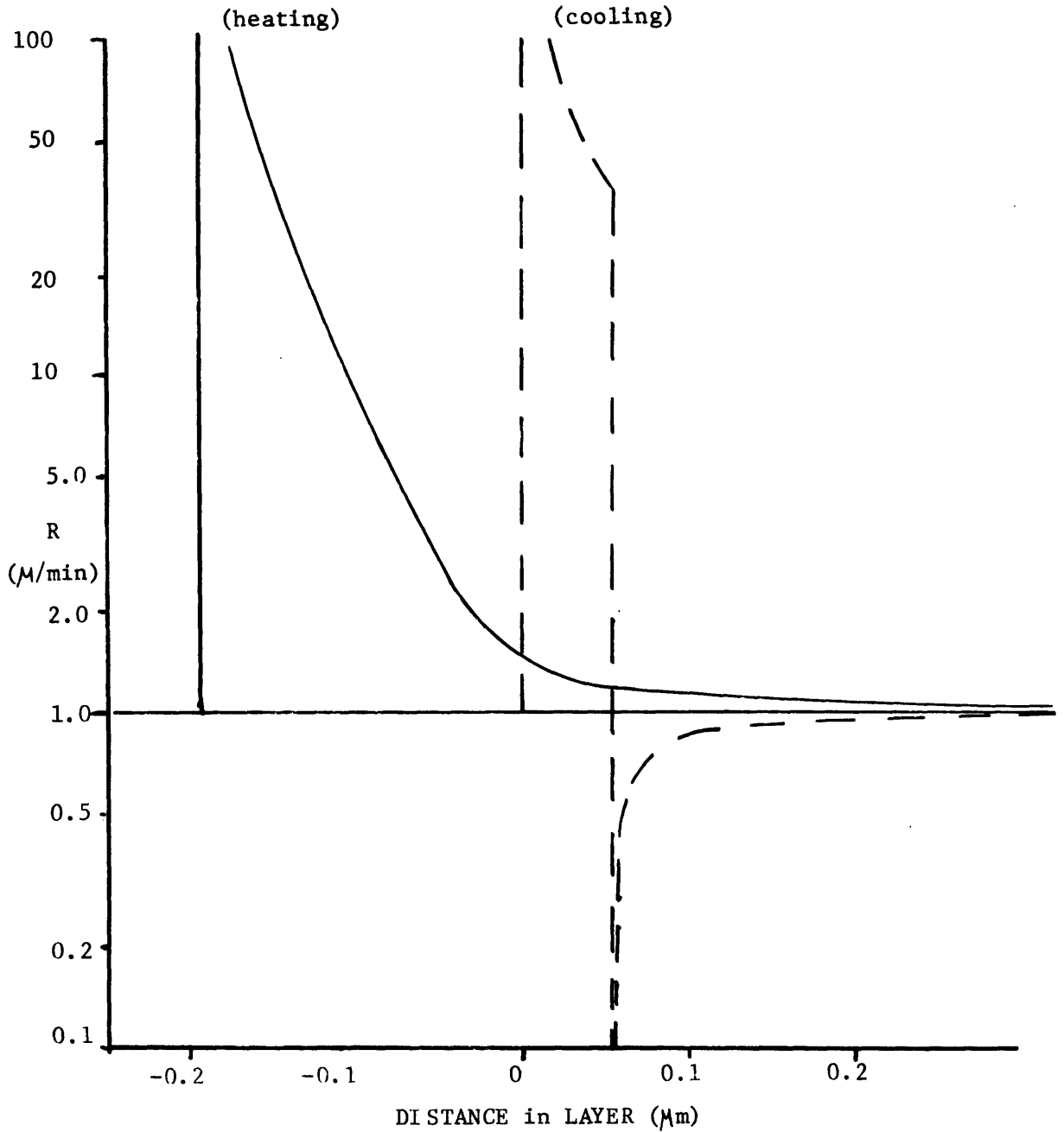
Figure 5.10: Calculated growth rates versus distance grown for heating ($\Delta T = -4°C$, solid line) and cooling ($\Delta T = 4°C$, dashed line) pulses of 0.008 min duration applied at d = 0 is a layer with an average growth rate of 1 μm/min at 850°C. The heating pulse results in layer dissolution of 0.2 μm followed by growth. The cooling pulse results in growth of 0.2 μm followed by dissolution of 0.15 μm.

growth of 1.0 μ/min. The width of the high growth rate region is clearly defined by dissolution after a cooling pulse, but is arbitrary for a heating pulse. Using $R = 2R_0$ as the boundary in this latter case, the region width for both pulses was calculated and is plotted in Fig. 5.11 as a function of the background growth rate. The width of the high growth rate region grown into the layer by the heating pulse is larger than for a cooling pulse for any given average growth rate-related segregation effect, then heating pulses should result in thicker demarcation lines in the layer than for cooling pulses.

The effect of interface demarcation pulses on growth is analyzed with the current-controlled LPE model of Section 5.1.3. It was shown that the dominant effect of an electric pulse on the growth rate is due to Peltier cooling or heating with the associated change in interface temperature and composition. Since interface demarcation is basically a segregation effect, it is discussed further in Chapter Six.

5.1.6 Application of interface demarcation to the determination of growth conditions reflected in the layer morphology

The determination of microscopic growth rates through periodic interface demarcation is actually a by-product of their primary function: to delineate the entire solid-solution interface at a specified instant in time. The demarcation lines are presently used to establish the growth interface shape and its changes with time, which yields information on substrate dissolution, thickness variations, faceting, and corresponding

Figure 5.11: Calculated thickness of the high growth rate region ($R \geq 2R_0$) introduced into the layer by applied pulses as a function of the steady-state (background) growth rate (R_0). The growth parameters used are for GaAs at 850°C with $\Delta T = \pm4°C$, and neglecting electromigration.

HEATING PULSE

COOLING PULSE

GROWTH RATE (μm/min)
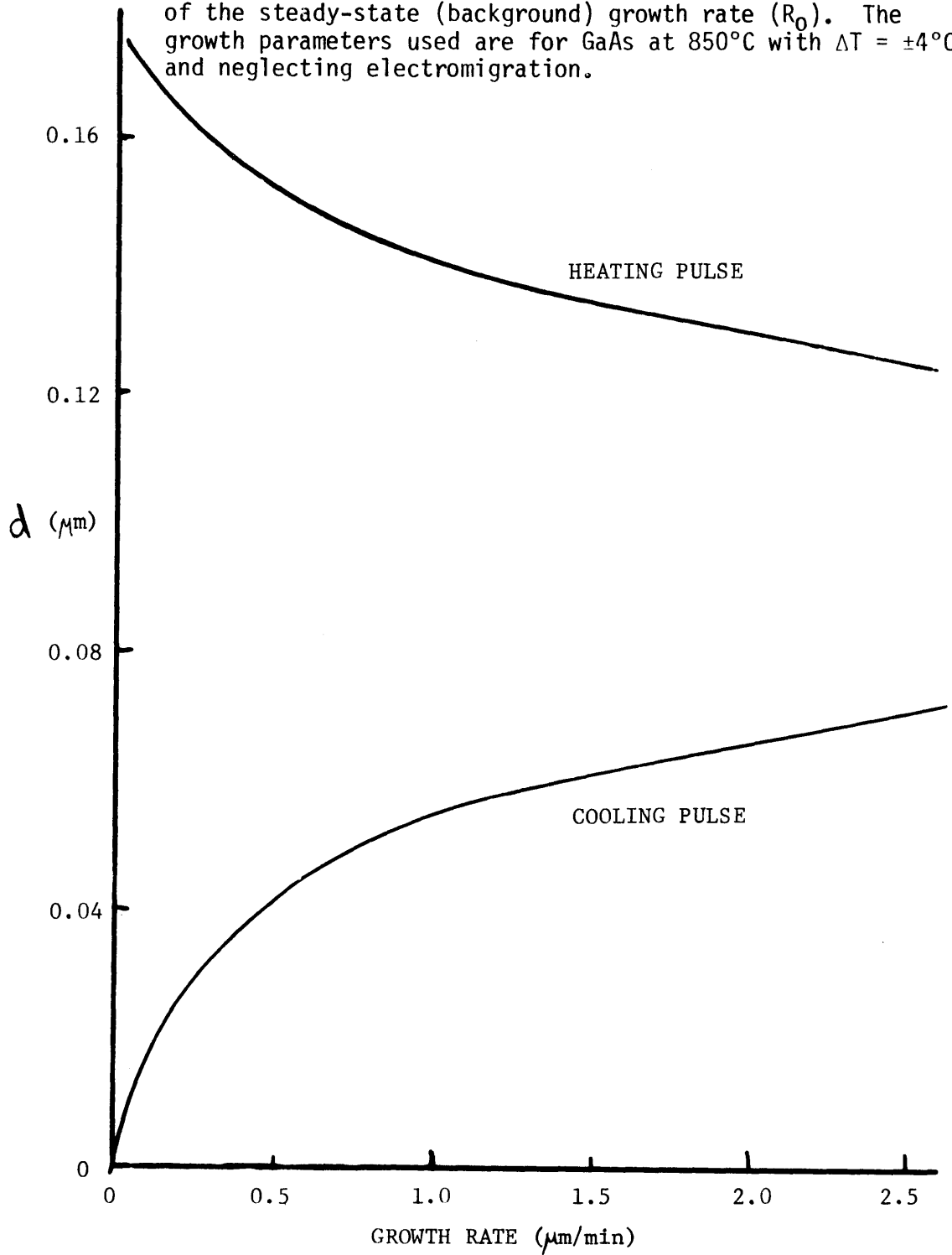
surface morphologies. This section discusses the application of interface demarcation to the study of the interface morphology during the initial, middle, and final stages of growth.

The conditions at the substrate-solution interface during the onset of growth (initial stage) are controlled by the substrate preparation (surface treatment), solution preparation (degree of saturation), establishment of substrate-solution contact, and by the manner in which growth is initiated and sustained. A typical substrate dissolution associated with an increase of 5°C in the furnace temperature while the substrate was in contact with the solution is presented in Fig. 5.12 for two regions of the layer subsequently grown. It can be seen that the dissolution process is uniform over a limited region (400 μ long in Fig. 5.12a), but is detectable near the layer (solution) edge. A similar substrate dissolution process is expected to take place if the solution is unsaturated prior to the establishment of the solution-substrate contact, although no experiments were performed with initially unsaturated solutions. Intentional dissolution is also caused from Joule heating associated with an AC signal applied across the substrate-solution interface (see Section 4.1.1 for procedure). Because Joule heating is dependent on current density, non-uniform current flow results in irregular dissolution. Interface demarcation was also used to establish the extent of wetting contact between substrate and solution, as seen in Fig. 5.13. Local non-wetting conditions impeded substrate dissolution as the furnace temperature was increased, and later retarded growth as the temperature was lowered (0.5°C/min). Deposition occured over most of the non-wetting
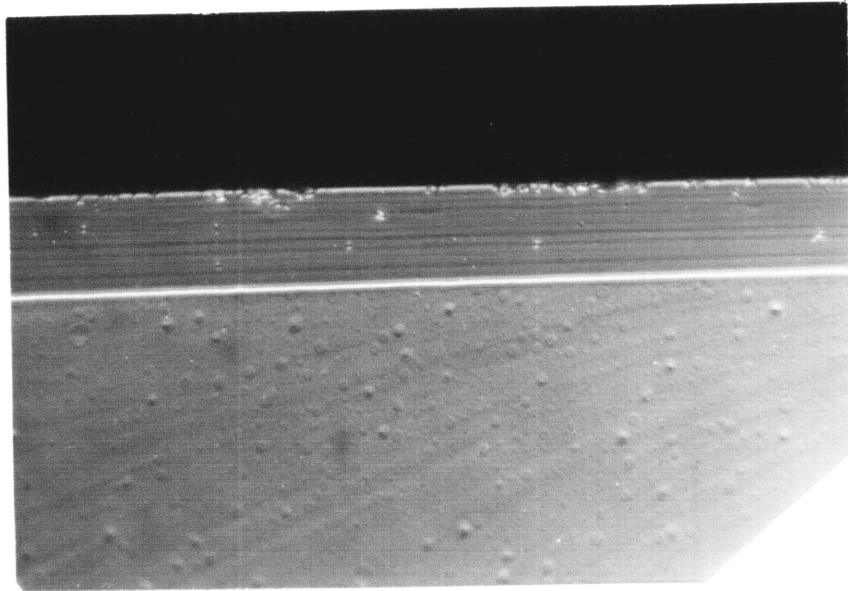
Figure 5.12: The effect of substrate dissolution on a layer grown first
by conventional and then by current-controlled LPE (at
850°C). Dissolution is detectable only near the layer
periphery. (Layer thickness in upper photo: 45 μm.)
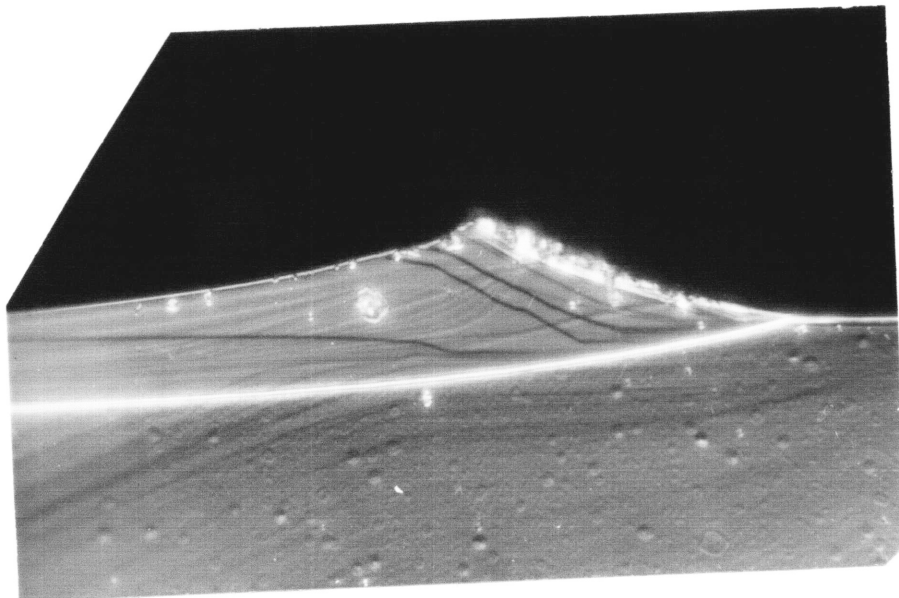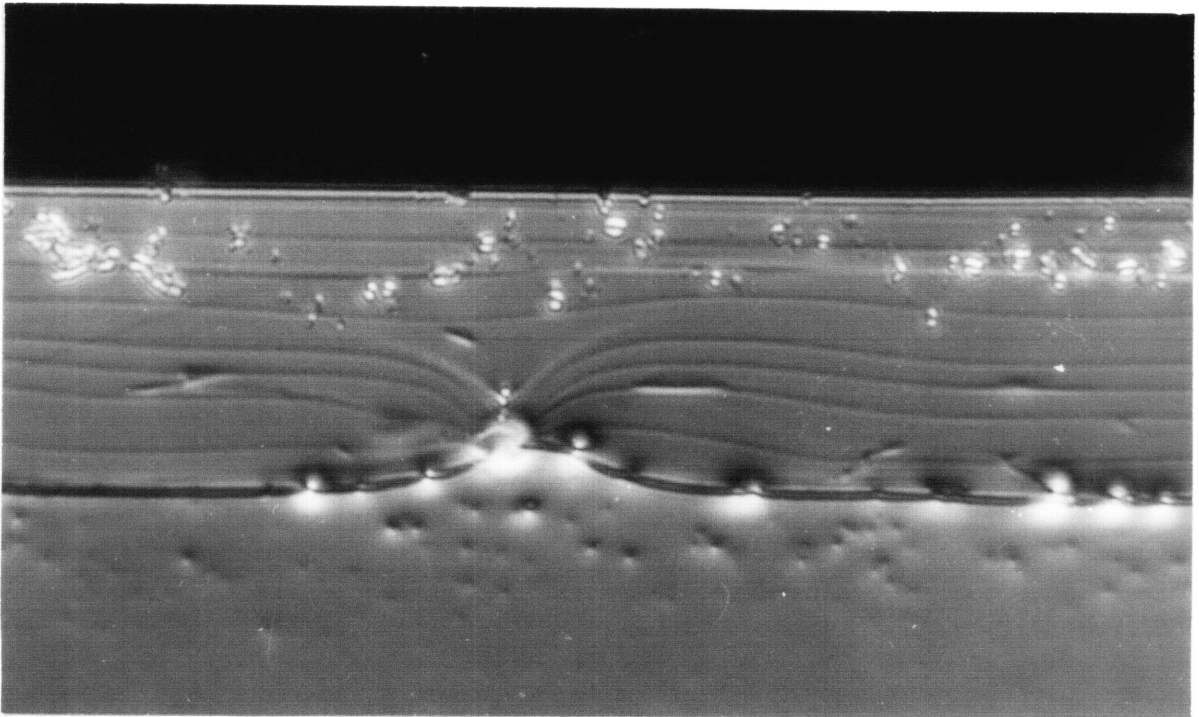
Figure 5.13: The effect of solution non-wetting on substrate dissolution and subsequent layer growth. The layer (thickness: 54 μm maximum) with 0.4°C/min cooling after intentional dissolution.

area within the first ten minutes of growth, but did not cover the inclusion site (probably an oxide or a BN particle) for thirty minutes (the time of the fourth demarcation lines). Final recovery occurred within another ten minutes with the microscopic growth rate reaching twice the average value of the surrounding regions. It should be noted that without interface demarcation, only the original interface, defect, and surface would be visible for analysis.

The presently used experimental approach can also be applied directly to the determination of thickness variations as they occur during the middle stages of growth. The layer discussed above (in Fig. 5.13) shows dramatic thickness variations during growth that are not reflected by the surface or by the original interface. The layer morphology usually tends to become flat with time as perturbations are eliminated by lateral forces that accompany them. In Fig. 5.13 the furnace cooling was interrupted for 60 minutes, during which the interface adjusted itself by growth and dissolution to the flat morphology reflected by the last two demarcation lines and the isolated surface. By comparison of distances between demarcation lines in two different regions of a layer, the origins of thickness variations can thus be determined. Another example is shown in Fig. 5.14 where the micrographs are taken from regions 6 mm apart on a layer grown by cooling $0.5°C/min$ from $853°C$. The difference in final layer thickness can be attributed to the initial segments of growth. This example is analyzed in greater detail in Section 5.2.4, where information on convection is obtained from the interface demarcation lines. Another perturbation that may lead to thickness variations is the facet effect on (001)

(a)

(b)
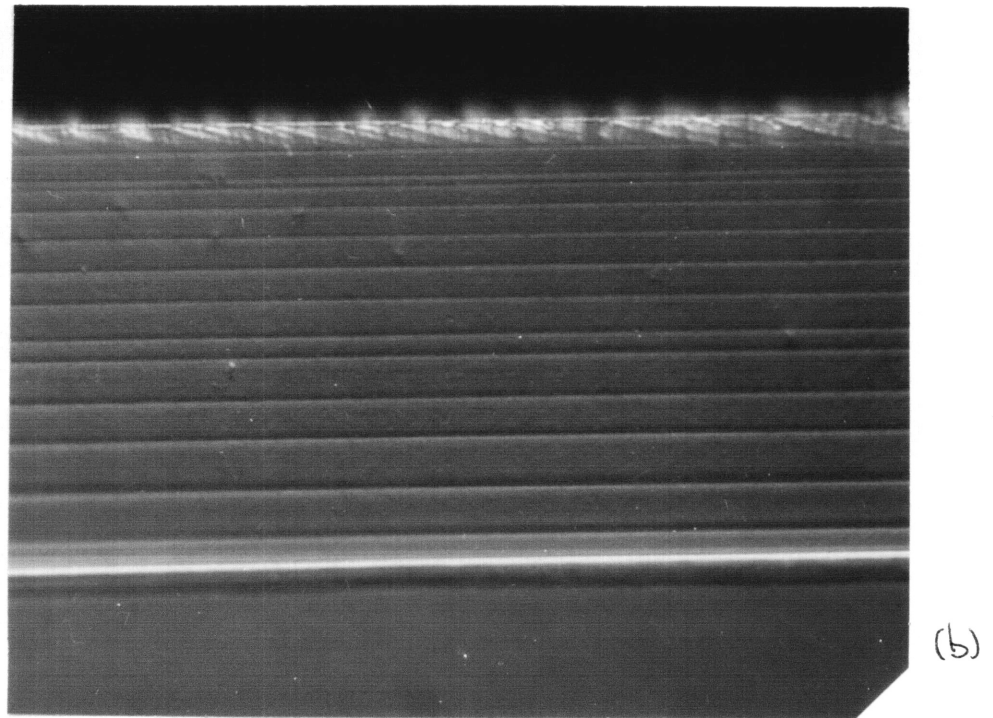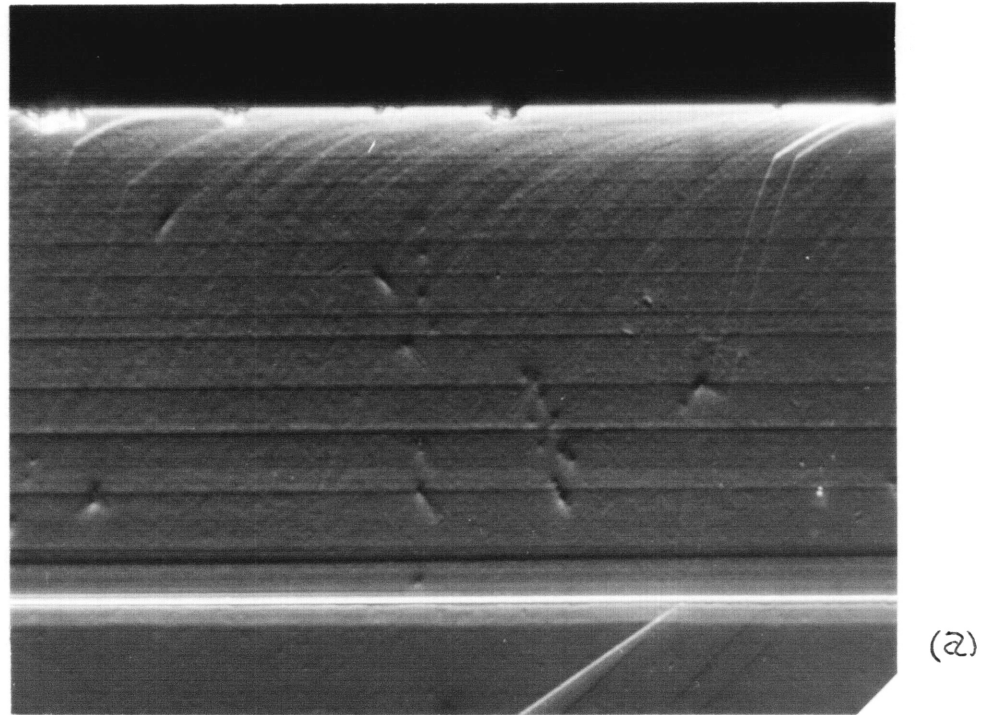
Figure 5.14: Layer thickness variations as revealed by interface demarcation. The micrographs are from two regions 6 mm apart in a conventional LPE layer [thicknesses: (a) 110 µm; (b) 102 µm].

planes in GaAs. The faceted regions in Fig. 5.15, revealed by preferential etching of the on-facet/off-facet boundaries, ahve flat interface morphology with growth rates more constant and slightly larger ($\sim$5%) than in the surrounding areas.

The surface morphology of the isolated epitaxial layer, when viewed in conjunction with interface demarcation, yields significant information on conditions during the final stage of growth and on the isolation procedure.

It is shown in previous examples that the surface may reflect the recovery of a flat interface. In contrast, Fig. 5.16 shows surface breakdown of a current-grown layer (+20 A/cm^2, 850°C), where the surface effect is demonstrated in Fig. 5.17, a layer grown by simultaneous furnace cooling (0.4°C/min) and current heating (-10 A/cm^2) after equilibration by the AC method (10 A/cm^2 rms; refer to Section 4.1.4). The thin region of the layer corresponds to an area on the substrate's lower surface that was wet by the gallium contact. The expected high current density over this region resulted first in more dissolution (greater Joule heating), and second in less growth (greater Peltier heating) than in the adjacent regions.

The above are but a few examples of the effects on layer morphology that may be encountered in the various stages of LPE growth. Throughout this discussion it is assumed that the measurement technique, interface demarcation, has a negligible effect on growth rate and morphology, but the last example raises an interesting question: can it? If local variations exist in the current density, then the application of a heating
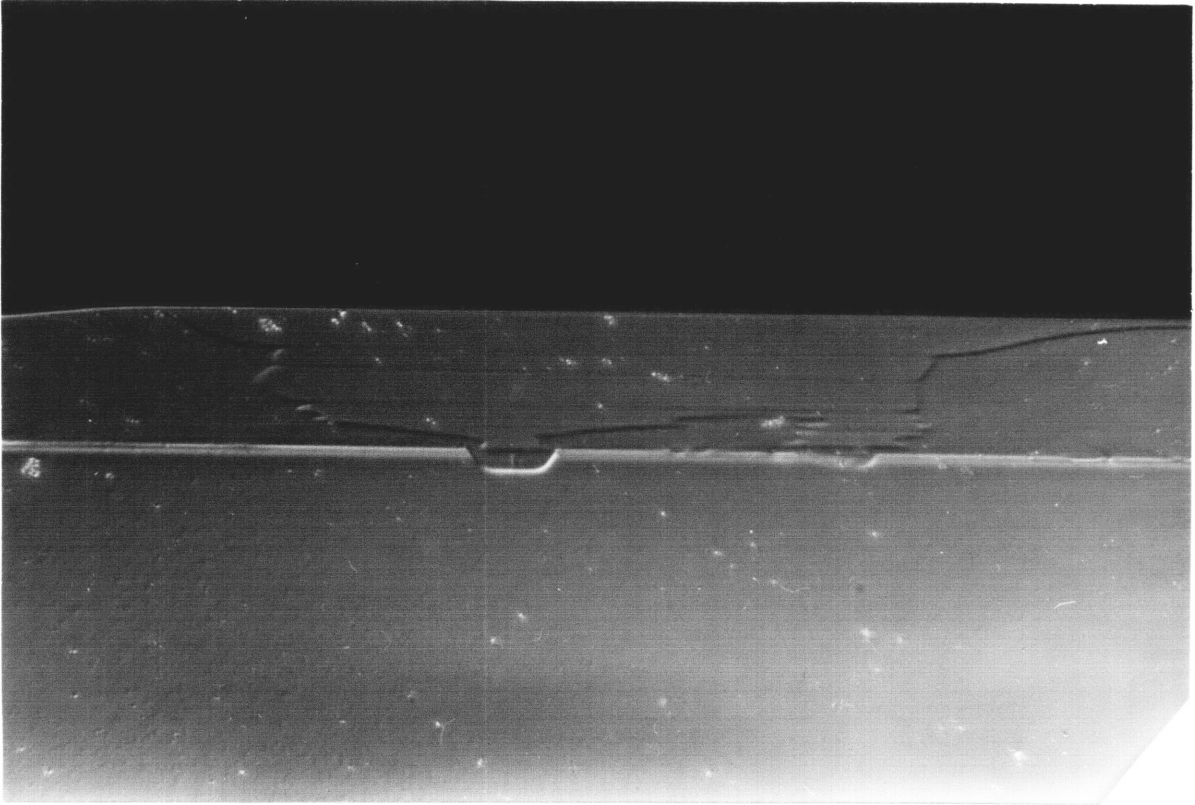
Figure 5.15: Facet (100) in a layer grown by current-controlled LPE at 850°C (thickness on facet: 45 μm).
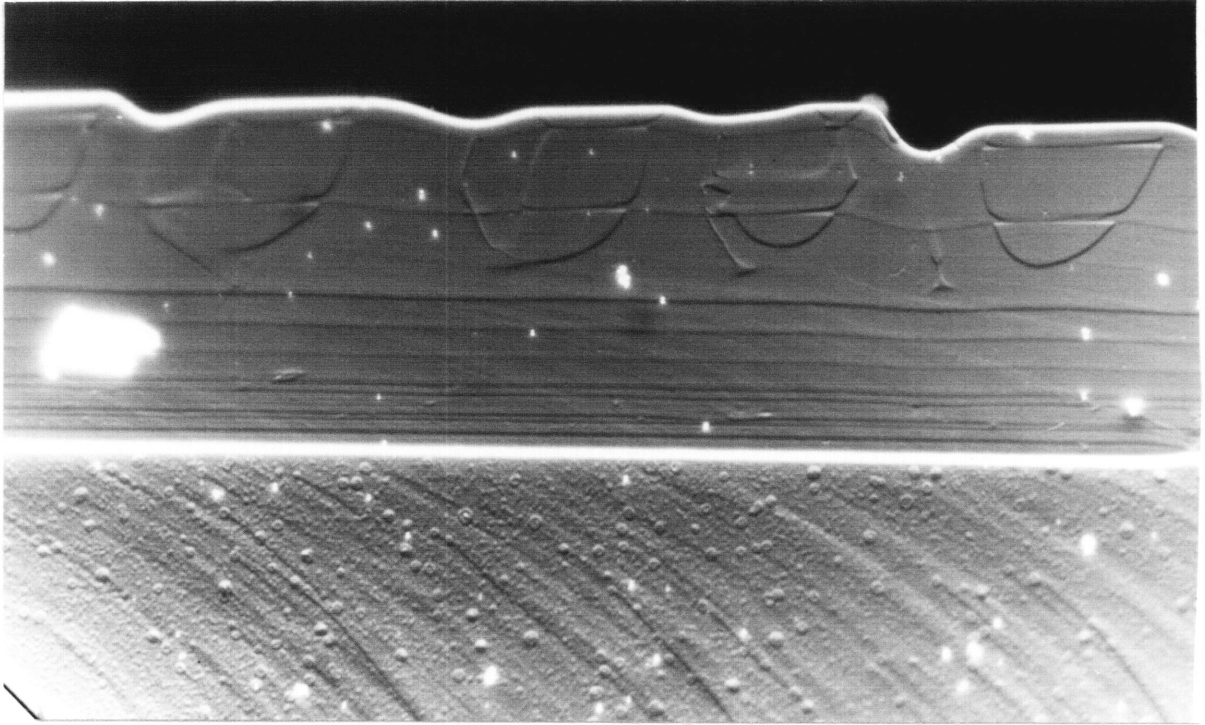
Figure 5.16: Faceting due to surface breakdown. The layer was grown at 850°C by current densities of 5, 10, and 20 A/cm^2 (thickness: 55 μm).
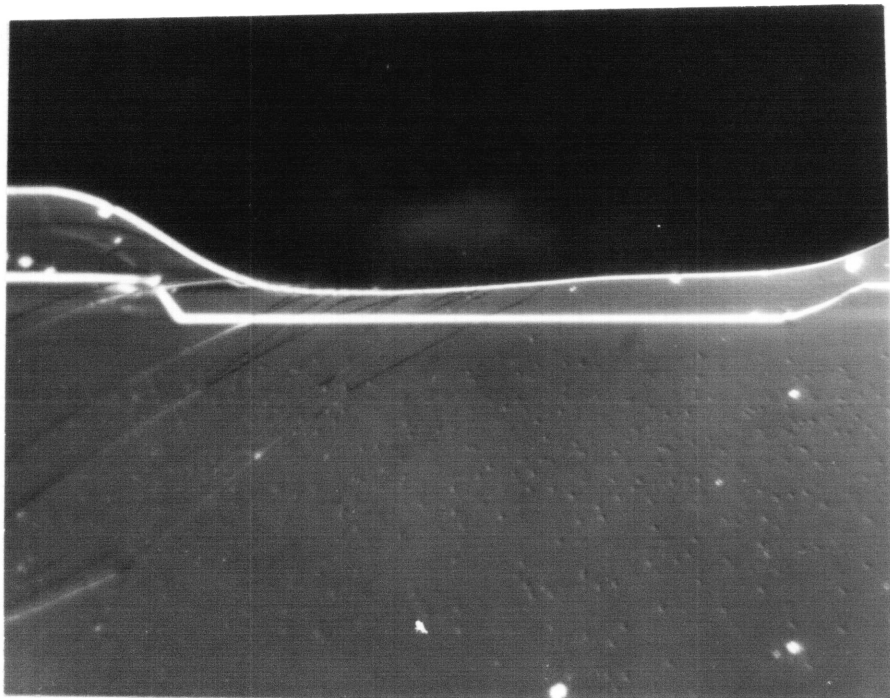
Figure 5.17: The effect on epitaxial growth of non-uniform current flow through the interface. Substrate dissolution was induced by an AC signal (10 A/cm^2 rms) which was followed by combined cooling at 0.4°C/min and a direct heating current of -10 A/cm^2. (Magnification: 700X)

pulse will result in varying amounts of dissolution. The resulting demarcation line will indicate the interface shape after the dissolution occurs which, if non-uniform, will not represent the true interface morphology. In order to obtain an estimate of the magnitude of these variations, the amount of heat evolved per unit volume and time (Q_J) from an applied current is derived in Appendix 10.2 as

$$Q_J = Q_o \, (\rho_o/\rho) \qquad\qquad (5.32)$$

where ρ is the resistivity of a volume in the layer and ρ_o and Q_o are the average resistivity and heat evolved over the layer, respectively. Dissolution from a 40 A/cm^2 heating pulse (0.5 sec duration) at 850°C is approximately 0.2 μm from the previous section, which would indicate that the ratio of ρ_o/ρ needs to exceed a value of 6 for a variation in thickness of 1 μ due to the pulse. In most instances the current density is uniform over the layer, as determined by current-controlled growth rates, and does not approach the estimated magnitude required for the morphology changes discussed. Unless noted to the contrary, interface demarcation is therefore assumed to have no effect on interface morphology.

The use of interface demarcation is demonstrated to be a significant tool in the determination of the interface morphology of epitaxial layers.

5.2 Experimental Results

5.2.1 Growth rate behavior of conventional LPE

Growth experiments with continuous cooling (i.e., conventional LPE) were carried out with interface demarcation in the system described in Section 4.1. The cooling rates studied ranged from 0.03°C/min to 2°C/min and involved temperature drops of 5 to 50°C from initial temperatures at or near 865°C. Gallium solutions with heights ranging from 3.6 to 8.4 mm and doped with tin or tellurium were saturated from an undoped GaAs source prior to contact with the substrate.

Two "base line" experiments were carried out at 850°C in order to identify any departure from solution equilibrium arising from use of standard procedures (Section 4.1.4). A solution (assumed saturated) was allowed to contact the substrate in the absence of furnace cooling or growth current. After three minutes in one experiment and 100 minutes in another, the solution was isolated from the substrate by wiping. The surfaces and cross-sections of the substrates were analyzed from which it was found that neither growth nor dissolution could be identified.

In preliminary growth experiments it was found that layer thicknesses exhibited a near-linear time dependence, in contrast to the $t^{3/2}$ dependence predicted for diffusion-limited growth (see eq. 5.5). Consequently, experiments were performed which were designed to identify for given solutions their departure from diffusion-limited growth and from equilibrium during growth. Solutions were cooled from initial equilibrium conditions at a constant rate for 60 minutes and then the cooling stopped to allow the re-establishment of equilibrium. Thus, any growth occuring

isothermally after the system had reached its final temperature could be identified by interface demarcation and be related to the type of growth process involved. At the end of 60 minutes at constant temperature a buffer layer was grown to isolate the original layer from wipe-off effects. The results of two of these experiments are presented in Figs. 5.18 and 5.19. The micrographs are of etched (110) cleavage faces perpendicular to the growth direction [001] under Nomarski interference, showing from bottom to top: the substrate/layer interface, interface demarcation lines, and the layer surface. The third demarcation line in each sample is used as an internal time reference, inserted half-way through the normal pulsing period, in order to unambiguously identify each line. In Fig. 5.19, the experimental layer thickness as a function of time for these two samples is compared to was initiated at 870°C by cooling the system 0.035°C/min, with demarcation every 40 minutes. At 865.4°C the cooling rate was increased to 0.36°C/min with demarcation spaced at 4 minute intervals, and at 862°C the cooling rate was raised to 1.7°C/min with demarcation every minute. The photomicrograph in Fig. 5.20a shows the demarcation lines having approximately equal spacing from which growth rates were obtained averaging 0.034, 0.34 and 1.60 μ/min, respectively, for the three different cooling rates. The growth temperature is plotted versus the layer thickness in Fig. 5.20b, showing the theoretical dependence assuming 52% efficient deposition (solid line), and the measured data points (with different symbols used in each cooling region). In view of these results, the deposition efficiency is concluded to be independent of cooling rates for the present experimental conditions.

K

I
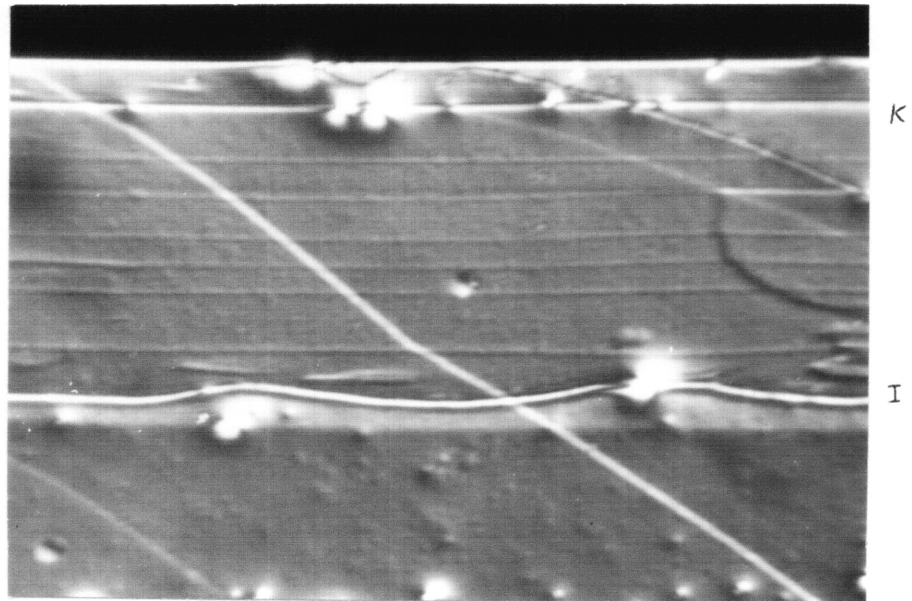
Figure 5.18: Micrographs of layers 34 and 35 (magnification: 1000X). The initial portion of the layers, between the original interface (I) and the intermediate interface (K), is analyzed in figure 5.19.

K

I
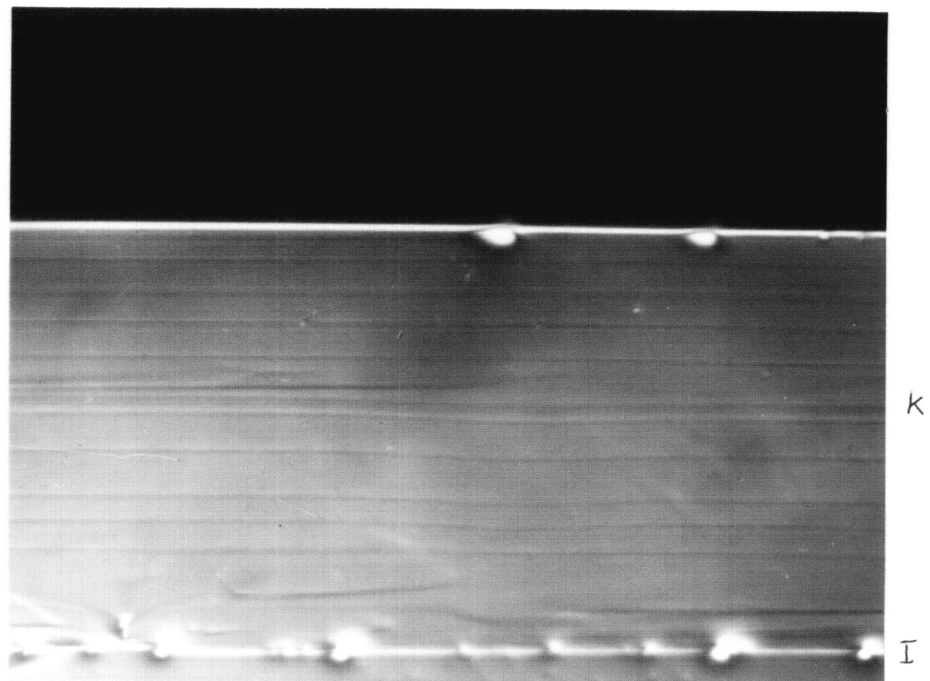
Figure 5.19: Experimental and theoretical thicknesses of two conventional
LPE layers as a function of growth time. The calculated
curves represent the growth expected for 100% and 50% of the
arsenic determined from the solubility to precipitate out of
solution onto the substrate. The experimental points were
determined from interface demarcation.
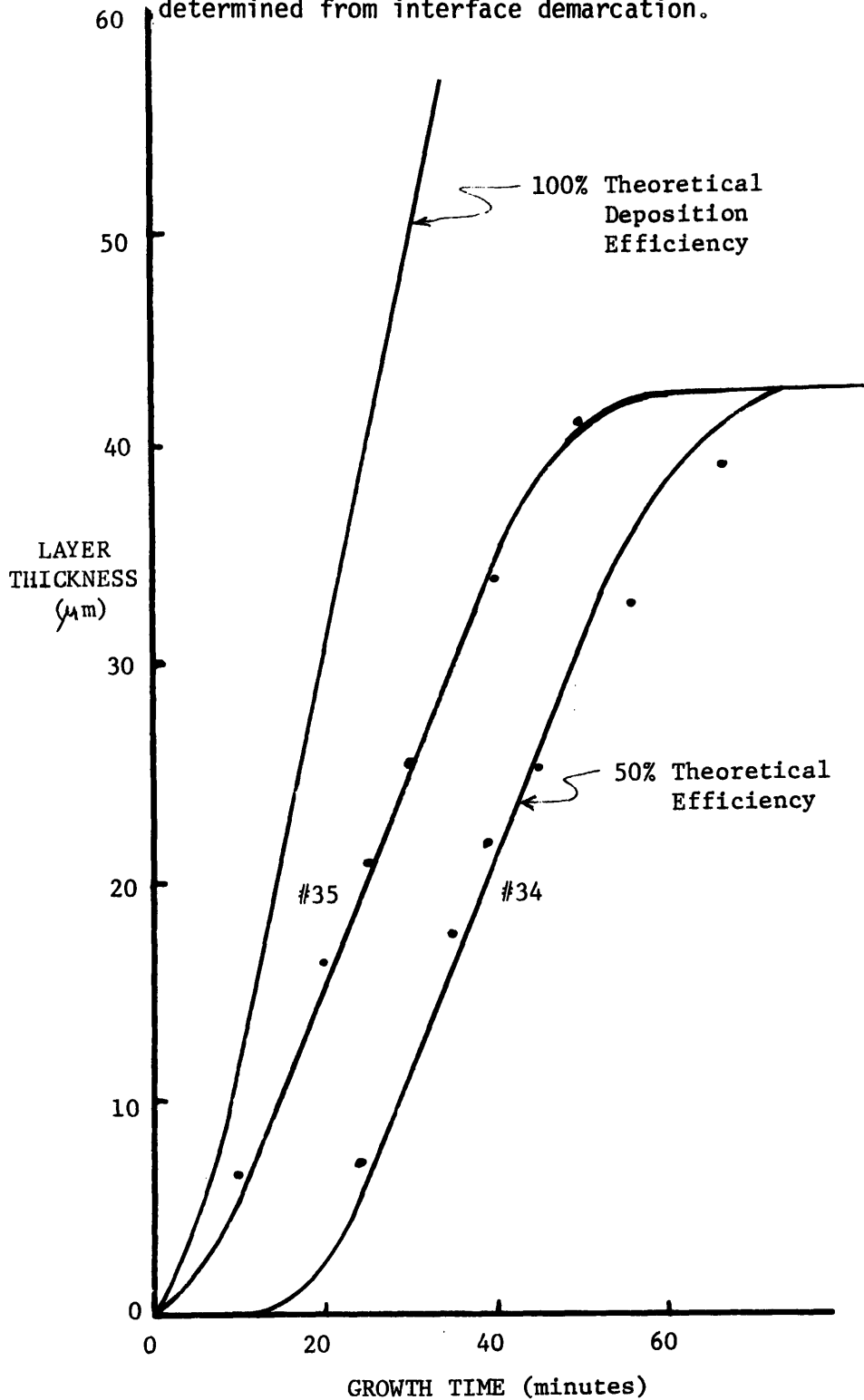
Figure 5.20: Growth temperature plotted as a function of layer thickness taken from the micrograph in the insert. The layer was grown by conventional LPE with cooling rates of 0.035, 0.36, and 1.7°C/min for the three sections shown. The solid line represents equilibrium growth with 50% deposition calculated from arsenic solubilities and the cooling curve. After the last demarcation line, growth occurred which is not analyzed.

$\overline{R} = 0.034 \; \mu/min$

$0.34 \; \mu/min$

$1.60 \; \mu/min$
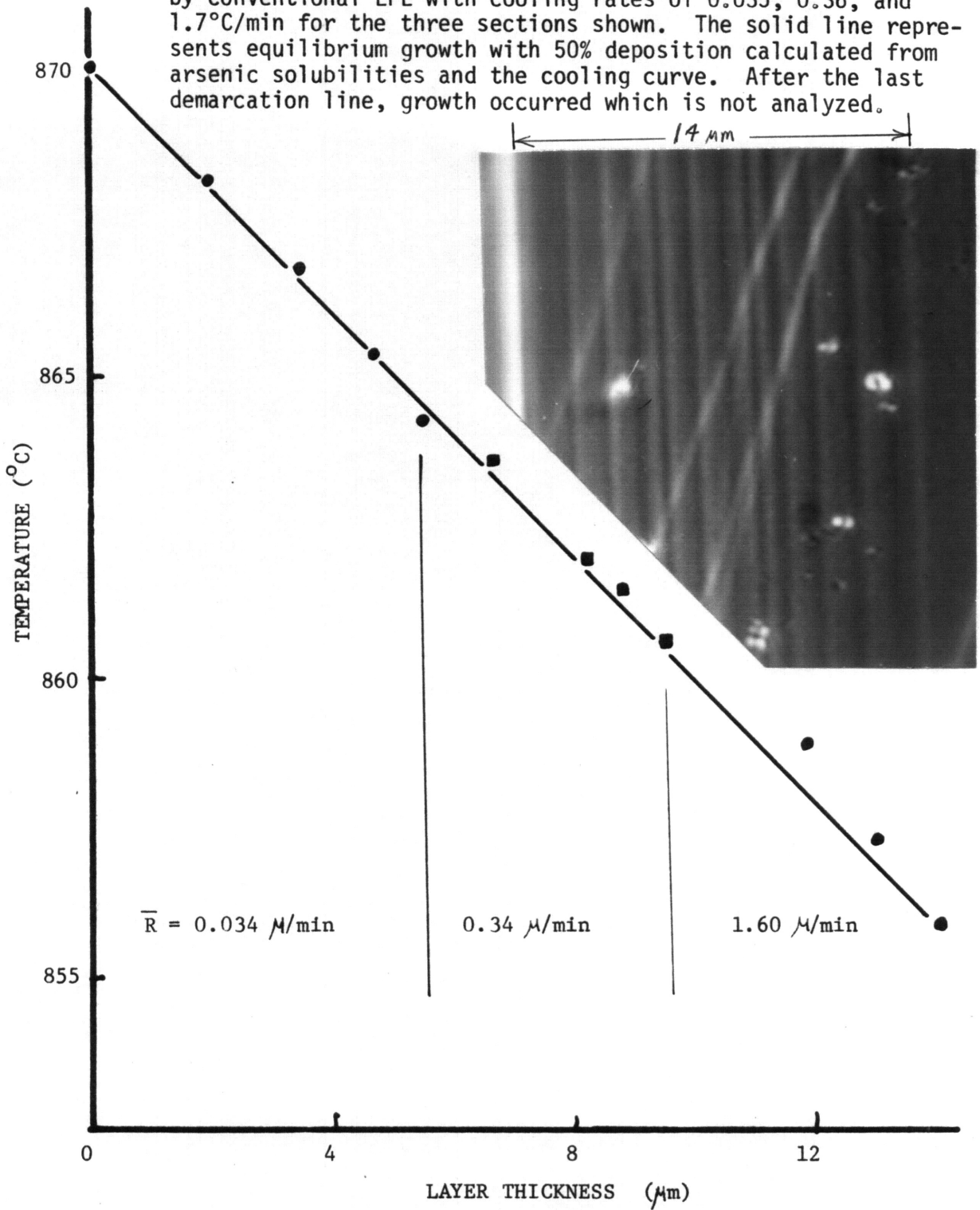
The observed 50% deposition efficiency is several times greater than that expected from diffusion-controlled LPE.[17] This additional mass transport cannot be explained except in terms of fluid flow, i.e., convection in solution. To identify the experimental parameters that determine the growth behavior, layers grown by constant cooling from equilibrium were analyzed with respect to the growth-convection model developed in Section 5.1.2. Growth rates obtained as interval averages from successive demarcation lines for times greater than twenty minutes uniquely determined the value of ℓ_c (effective solution height) in equation 5.13. The layer thickness at 10 or 20 minutes, known precisely from demarcation, was then used to determine the boundary layer thickness δ from Fig. 5.3. The results of three of these comparisons are presented in Fig. 5.21. The agreement between the theoretical behavior from equations 5.14 and 5.15 plotted as solid lines and the experimental data plotted as points is excellent. The apparent disagreement of the first data points is due to the data being an average while the line gives the instantaneous growth rate. The values of ℓ_c obtained from the curve fitting process range from 53 to 62% of the experimental solution heights of these three samples, consistent with the earlier results. The values of δ obtained vary from 0.33 to 0.69 mm, which are within the expected range (see Section 5.1.4).

Experimental and theoretical parameters from these and other samples are presented in Table 5.1. For cooling rates ranging from 0.035 to 0.49°C/min and solution heights from 3.6 to 8.4 mm, the ratios of the effective to experimental solution height are fairly constant from 0.52
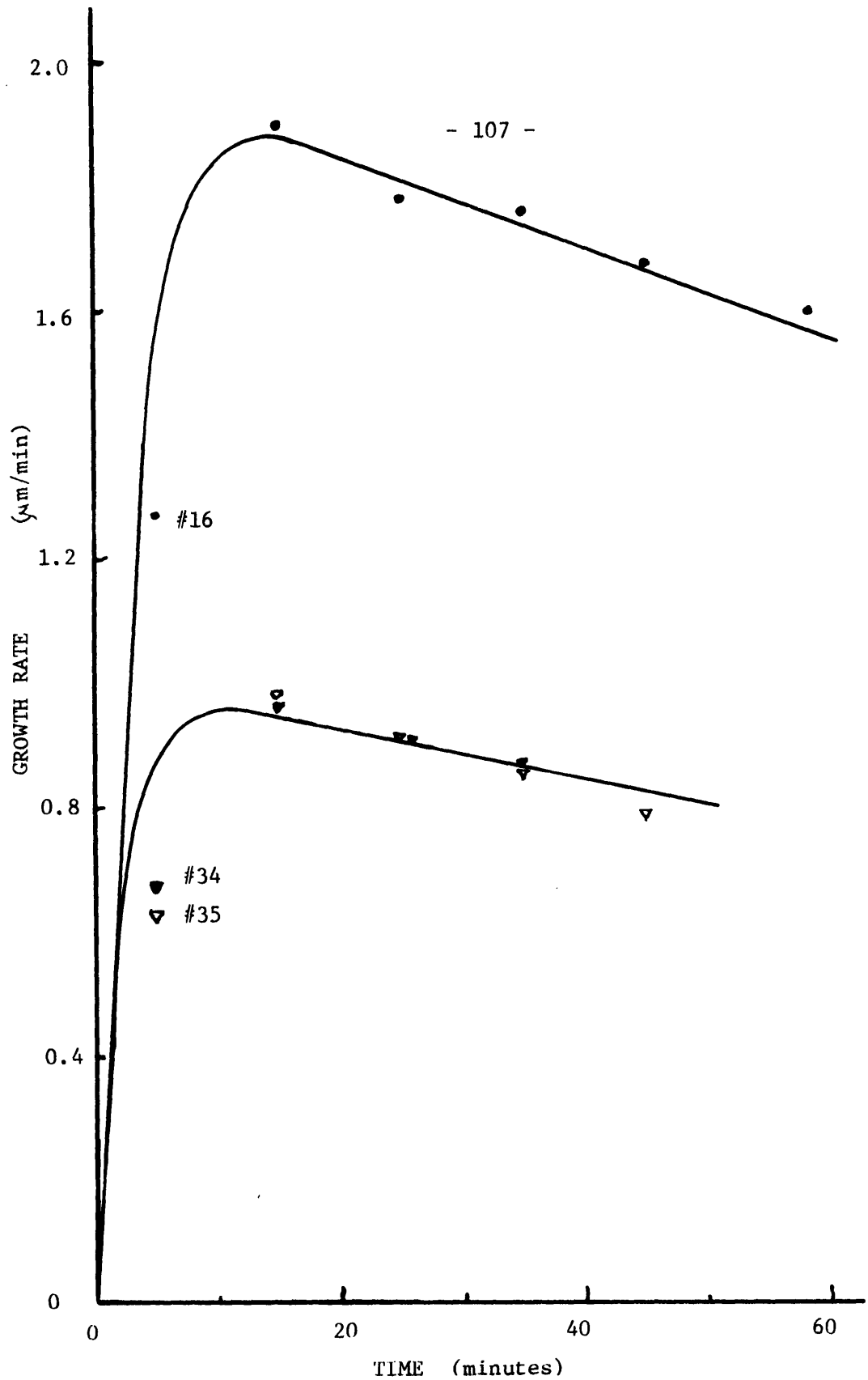
Figure 5.21: Experimental and theoretical growth rates versus time for three conventional LPE layers. The solution heights were, for sample #16, 8.4 mm and for samples #34 and 35, 4.5 mm. The solid lines were calculated from eqs. 5.17 and 5.18 using a 53% deposition efficiency and the experimental parameters given in Table 5.1 (page 108).

TABLE 5.1

Summary of conventional LPE experiments with a comparison to theory (Section 5.1.2).

Sample	Cooling Rate (°C/min)	Solution Height ℓ(exp) (mm)	Solution Height ℓ(eff) (mm)	Ratio of ℓ(eff) to ℓ(exp)	Momentum Boundary Thickness (mm)	Horiz. Thermal Gradient (°C/cm)	Initial Growth temp. (°C)	Grashoff Number
16	0.49	8.4	5.2	0.62	0.33	0.69	853.5	34400
37	0.144	7.3	4.2	0.58	0.15	0.52	863	14800
34	0.47	4.5	2.4	0.53	0.42	0.52	863	2130
35	0.48	4.5	2.4	0.53	0.69	0.52	864	2130
149	0.30	4.0	2.2	0.56	≥ 1.0	0.20	864	512
150	0.44	4.0	2.1	0.53	≥ 1.0	0.20	867	512
124	0.37	3.6	2.1	0.58	≥ 1.0	0.22	864	370
125	0.37	3.6	1.9	0.52	≥ 1.0	0.22	864	370

to 0.62. The boundary layer thickness δ, however, increases with decreasing solution height and with decreasing horizontal thermal gradients. The solution Grashof number, calculated from equation 5.24, is a measure of the fluid velocities present (see Section 5.1.4), and as such will help determine the boundary layer thickness. Larger Grashof numbers will lead to smaller δ's, which is observed experimentally.

From this qualitative agreement with fluid dynamics and the quantitative agreement in magnitude and behavior of growth rates, the growth-convection model of 5.1.2 is seen to apply to conventional LPE with convection. In addition, the experimental results support the basic assumption behind the model: the solution is in local equilibrium with the solid at the interface. Thus interface kinetics are considered infinitely fast and there is no significant undercooling of the solution at the interface for the experimental conditions discussed.

5.2.2 Growth behavior of current-controlled LPE

Current-controlled LPE of GaAs was carried out in two different experimental configurations involving growth with and without a GaAs source present in solution. In both cases, experiments were performed isothermally at growth temperatures ranging from 700 to 850°C by the procedures described in Section 4.1. Growth currents were +10 A/cm^2 except where noted otherwise, with positive polarity applied to the n-type substrate (Peltier cooling). Saturated gallium solutions doped with tin or tellurium were used with solution heights ranging from 4.5 to 7.0 mm.

The growth behavior as evidenced from interface demarcation is the result of a complex interaction of solute transport and thermal effects, which include diffusion, convection, electromigration, Peltier cooling, and Joule heating. In order to analyze this behavior and, in particular, to identify the relative contributions of electromigration and Peltier cooling to current-controlled growth, growth rates were compared to theoretical curves derived from the current-controlled growth model developed in Section 10.1 and presented in Section 5.1.3. Theoretical R(t) curves (such as Fig. 5.4) were calculated for each layer from equation 5.19 using the experimental solution height, and calculated liquidus concentrations (from Section 5.1.1). Values of ΔT, μE, and D were obtained from a curve fitting process using the initial, middle, and final transients of growth, respectively. These regions can be identified in Fig. 5.22, showing experimental points and several theoretical curves for the growth rate of a layer deposited at 850°C with 20 A/cm^2 current. The experimental points are average growth rates over time intervals defined by two consecutive interface demarcation lines. The solid and dashed lines are theoretical curves (from eq. 5.19) calculated with the values of ΔT, μE, and D as indicated. The experimental rate determination of the initial transient (t $\lesssim$ 5 min) is difficult because of the limited resolution of interface demarcation; thus interface cooling, ΔT (as determined from the model) may vary from zero to 1.5°C and still agree with experimental data. In spite of this uncertainty in ΔT, μE can be determined by the remainder of the curves as 27.5 μ/min for $\Delta T = 0$ and 30.0 μ/min for $\Delta T = 1.5$°C. It is seen that the difference in these two

Figure 5.22: Experimental and theoretical growth rates versus time for a layer grown at 850°C by current-controlled LPE without a GaAs source. The theoretical curves were calculated from eq. 5.19 with values for μE of 30.0 and 27.5 $\mu m/min$ for upper and two lower curves, respectively, and with data in Table 5.2 (p. 121).
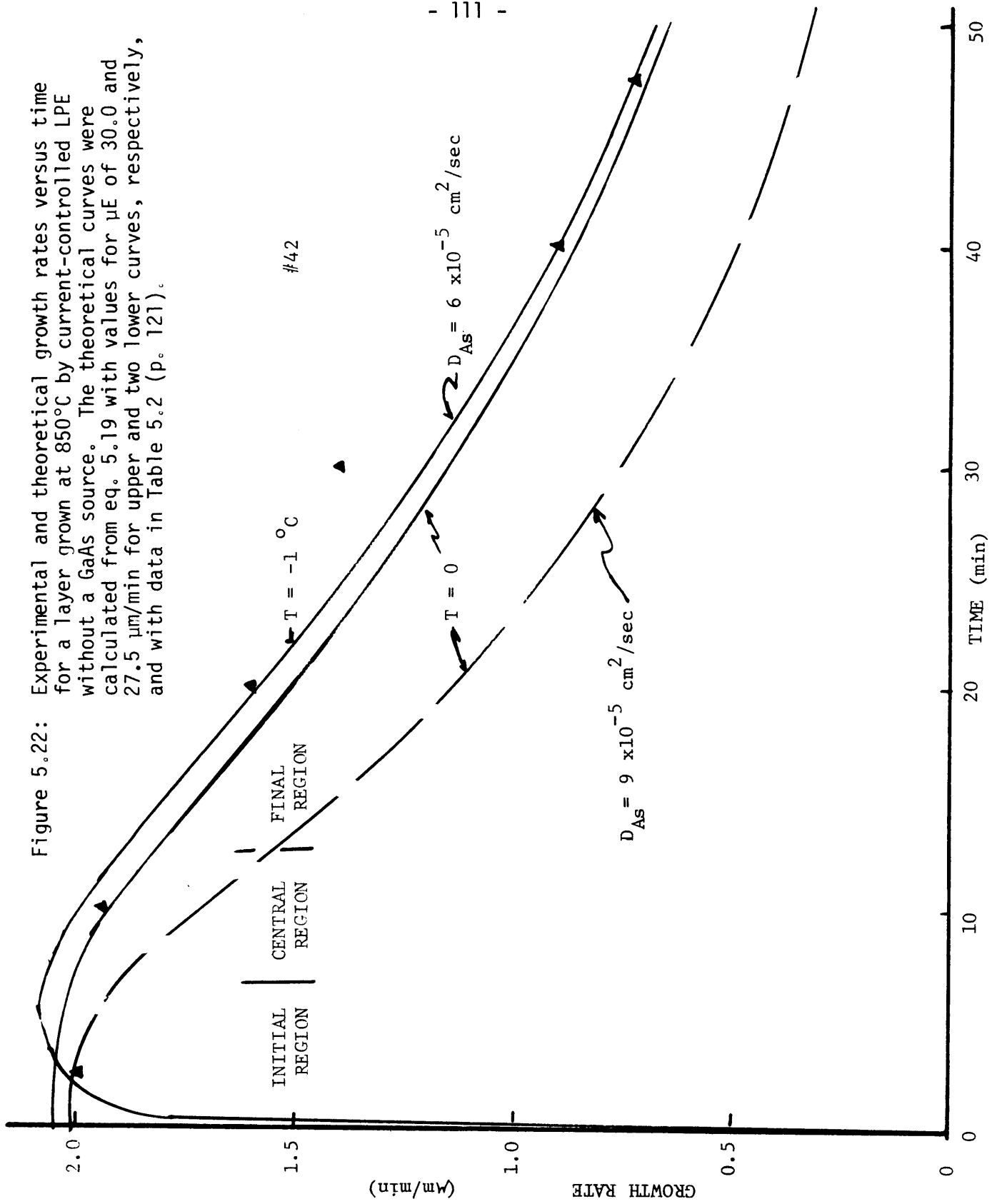
limiting values is only 10%, while the error introduced to μE by thickness nonuniformities of the layers can be several times larger. The final transient (the region of decreasing R values) in Fig. 5.17 has a characteristic fall-off time which, through a comparison of the two theoretical curves with the same value of μE and ΔT, is found to be sensitive to D. Although the effects of these three parameters on the growth rate behavior are interrelated, the region of influence of each of these can thus be identified: the diffusion constant, D, controls the fall-off time and thereby the shape of R(t); the EM drift velocity, μE, determines the magnitude of R(t), and the interface undercooling, ΔT, is responsible for the initial transient characteristics and, to a lesser extent, for the magnitude of R(t).

The effect of convection on the growth behavior is accounted for in the current-controlled growth model through the effective solution height ℓ_c (given by eq. 10.44); it tends to decrease the fall-off time of the growth rate and limit the maximum theoretical layer thickness. The applicability of the term ℓ_c to the given growth conditions is determined by the value of the diffusion constant as obtained by the above approach. If the computed D value is less than or equal to the "true" value of D, then $\ell_c = \ell$ and convection may be neglected. A value of D greater than the true value indicates, on the other hand, the presence of a momentum boundary layer; $\ell_c < \ell$ in the curve fitting process. For example, the dashed line in Fig. 5.22 represents growth for the above conditions with a diffusivity of 9×10^{-5} cm^2/sec. If the "true" value of D is 6×10^{-5} cm^2/sec, the dashed line would be consistent with growth in the presence

of a boundary layer of thickness $\delta = 3.5$, or 60% of the experimental

solution height (from eq. 11.44). The presently obtained value of

D (6 x 10^{-5} cm^2/sec) at 850°C is within the lower range of reported

diffusion constants. On the basis of the present analysis it can there-

fore be concluded that convection was absent during the growth of the

layer depicted in Fig. 5.22.

It is of interest to analyze the current-controlled growth behavior

at temperatures lower than 850°C. Experiments were conducted at temper-

atures ranging from 850°C to 700°C with identical current densities

(10 A/cm^2) and solution heights. To simultaneously obtain information of

the effect of Peltier cooling on the growth behavior, each of these exper-

iments was conducted in two sets involving different rear electrical sub-

strate contacts. One type of contact used was an alloy of Ga and In

ultrasonically spread over the substrate's lower surface and on the upper

surface of the graphite pedestal (Section 4.1). The other type of contact

had a germanium pedestal (10^{17} n-type 1.5 mm thick) inserted between the

substrate and graphite with all surfaces wet by gallium. (In some

experiments tantalum foil (25 mm thick) was inserted between the substrate

and Ge to prevent alloying.) This type of contact has been reportedly

used to increase the amount of Peltier cooling at the growth interface.[57]

Growth rates of the layers grown at decreasing temperatures are

presented in Figs. 5.23 through 5.26. The experimental data are given as

points representing the average rate between interface demarcation times,

while the solid lines are theoretical growth rates calculated as indicated

above from equation 5.19 on the basis of known experimental data. The

Figure 5.23: Experimental and theoretical growth rates versus time for a layer grown at 841°C by current-controlled LPE (10 A/cm^2) without a GaAs source. The theoretical curve (solid line) was calculated from eq. 5.19 with the parameters given in Table 5.2 (p. 121).

#53

TIME (minutes)

GROWTH RATE (μm/min)
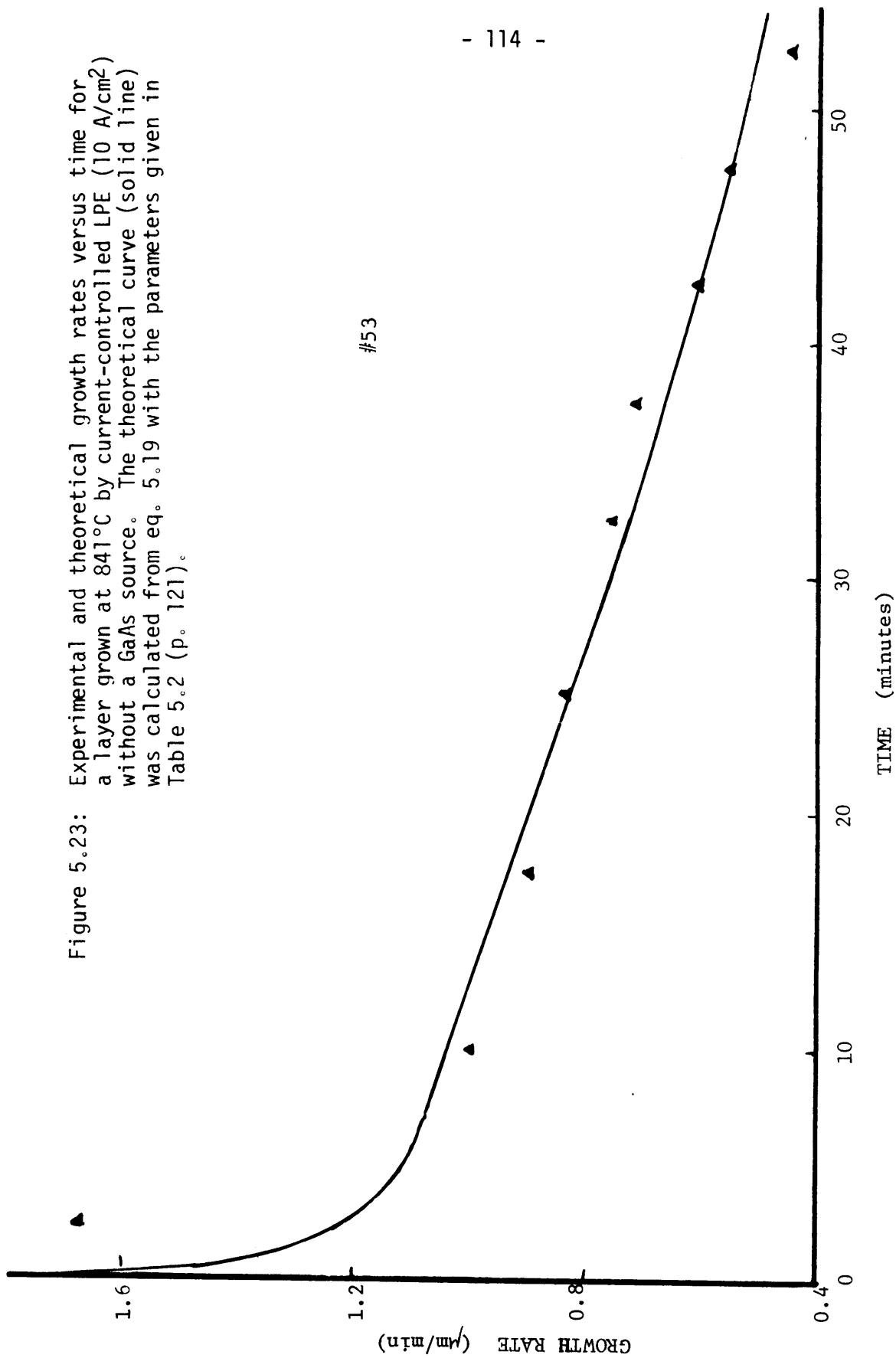
Figure 5.24: Experimental and theoretical growth rates versus time for a layer grown at 803°C by current-controlled LPE (10 A/cm^2) without a GaAs source. The theoretical curve (solid line) was calculated from eq. 5.19 with the parameters given in Table 5.2 (p. 121).

#54

GROWTH RATE (μm/min)

0.6   0.4   0.2   0

TIME (minutes)

0   10   20   30
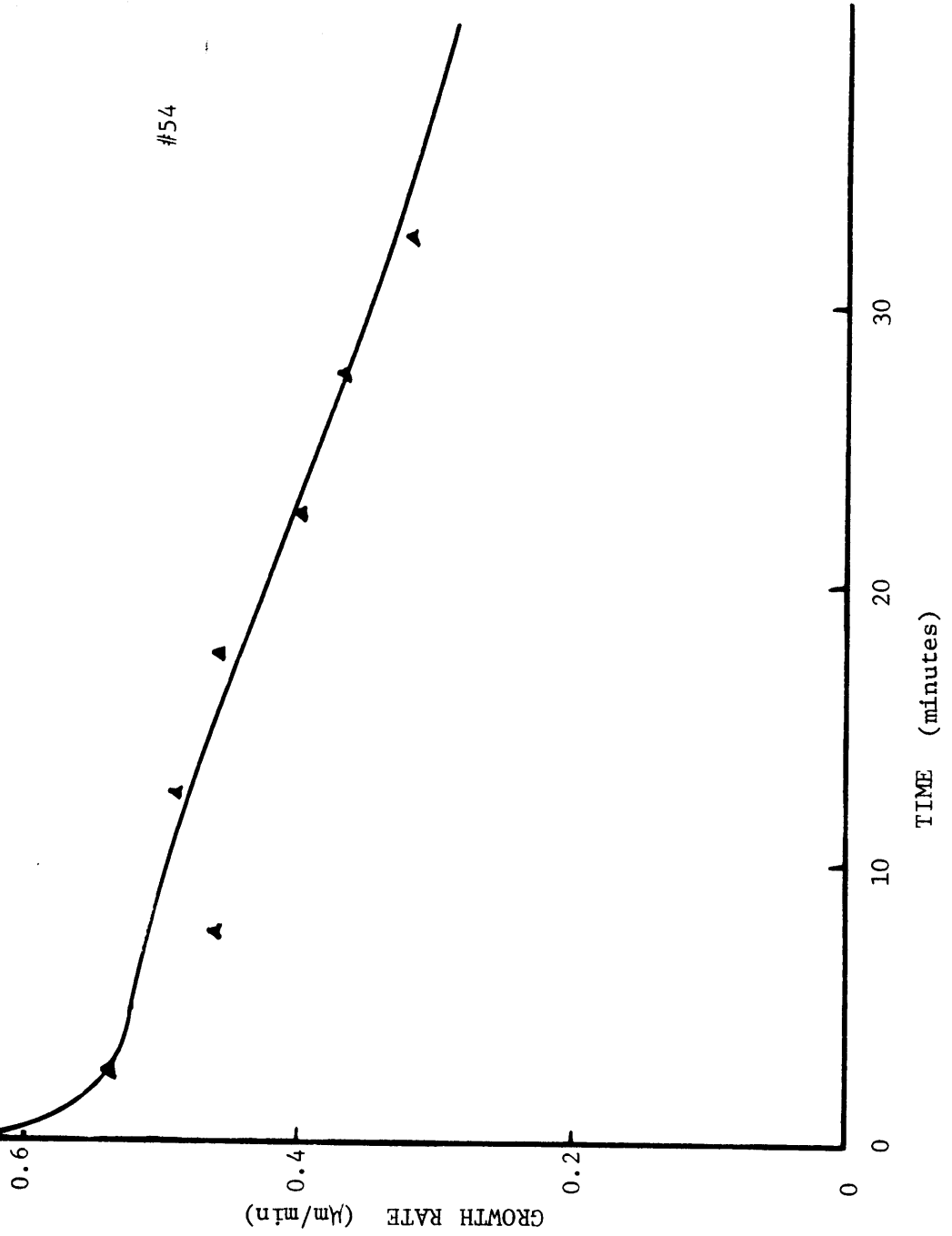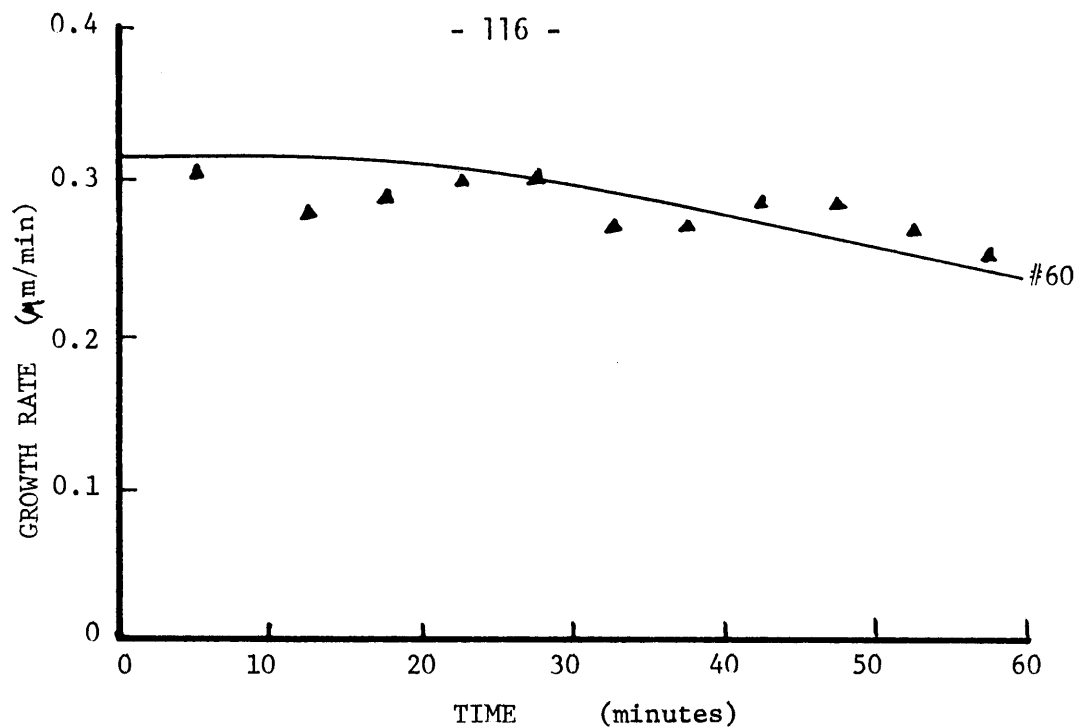
Figure 5.25: Experimental and theoretical growth rates versus time for a layer grown at 755°C by current-controlled LPE (10 A/cm²) without a GaAs source. The theoretical curve (solid line) was calculated from eq. 5.19 with the parameters given in Table 5.2 (p. 121).
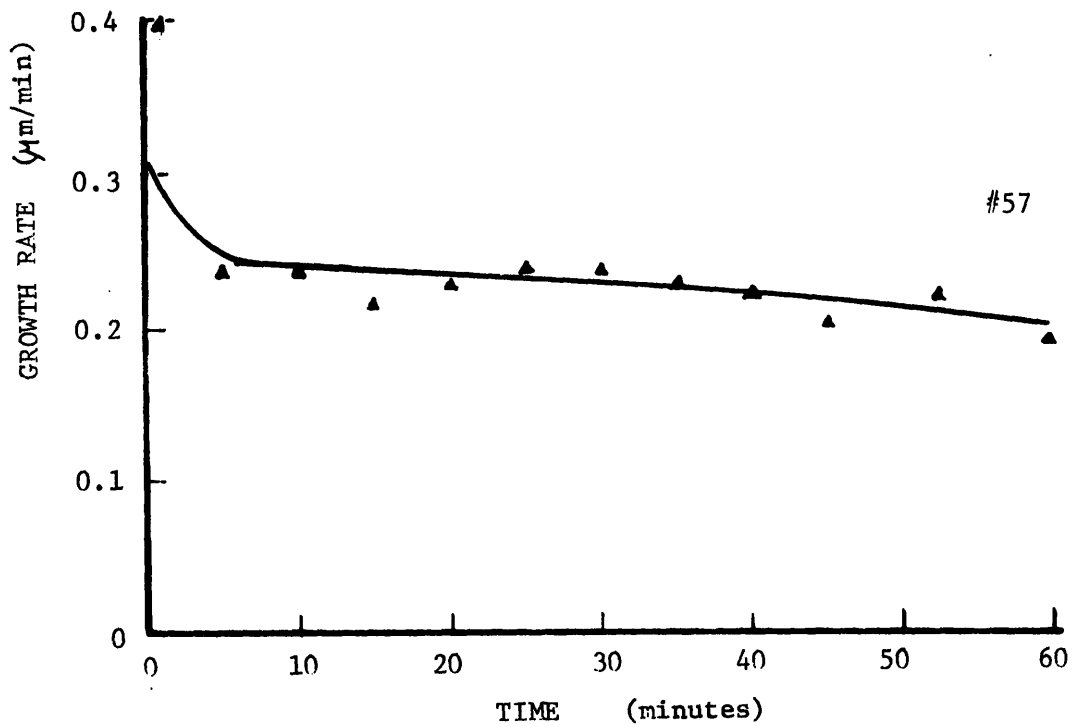
Figure 5.26:   Experimental and theoretical growth rates versus time
for a layer grown at 703°C by current-controlled LPE
(10 A/cm^2) without a GaAs source. The theoretical
curve (solid line) was calculated from eq. 5.19 with
the parameters given in Table 5.2 (p. 121).

data in Figs. 5.23, 5.24 and 5.26 are for layers deposited on substrates where the rear electrical contact was a germanium pedestal, while the layers of Figs. 5.22 and 5.25 were obtained with only gallium contacts. The growth behavior indicates noticeable trends with decreasing temperatures:

(1) the average growth rate decreases;

(2) the growth rates stay constant for a longer period of time;

(3) the magnitude of the initial transient remains constant.

The observations are presently discussed in reverse order.

An experimental analysis of the initial transient, as previously stated, is limited by the resolution of the growth rates over that region. The data presented here show that the transient, as determined by the first demarcation interval, is a significant fraction of the background growth rate at all temperatures studied. This observation cannot be accounted for except as due to experimental errors averaging R and/or growth perturbations such as initial non-wetting of the substrates at lower temperatures. From a physical standpoint the initial transient is expected to decrease in width with decreasing T due to the decrease of D. It is also expected to decrease in magnitude because of a decreasing Peltier coefficient[61] and an increasing liquidus slope.[87] For the above mentioned reasons, the experimental data do not lend themselves to an exhaustive analysis of these thermal effects.

The apparent change in the shape of the R(t) plot at lower growth temperatures can be viewed as the same curve (Fig. 5.5) plotted with different time axes. It was shown previously that the different drop-off

times are dependent on the diffusion constant D. Thus, at lower temperatures the growth rate will remain constant longer. This behavior is taken into account for the model by the determination of D from the drop-off in R(t).

The overall growth rate decrease with temperature may be analyzed by restricting the data to R(t) in the second and third demarcation intervals so as to remove variations arising from the initial and final transients. Growth rates thus obtained are plotted as a function of 1/T in Fig. 5.27. This plot yields a straight line which has a best fit ($r^2 = 0.95$) of R = 16470 exp[-11118/T], very close to the temperature dependence of the arsenic solubility (exp[-11750/T], Section 5.1.1). This analysis indicates that the growth rate is, to a first approximation, proportional to the arsenic concentration in the solution (as indicated by eqs. 10.1 and 10.29).

A summary of the results of layers grown from solutions with no source is presented in Table 5.2. The listed values of D, μE, and ΔT were obtained through the current-controlled growth model (Section 5.1.3). The value of μ was calculated from μE using the applied current density and the solution resistivity presented in Section 7.2. The values for the diffusion constant (D) obtained from this analysis are all well within the limits of published data for the respective temperatures, and confirm the absence of convection in the system for these experiments. These values for D are plotted in Fig. 5.28 as a function of inverse temperature. The solid line is a best fit ($r^2 = 0.98$) given by D = 0.32 exp (-9700/T), but the uncertainty associated with the low temperature values for D introduce an unknown of ±20% in the activation energy.
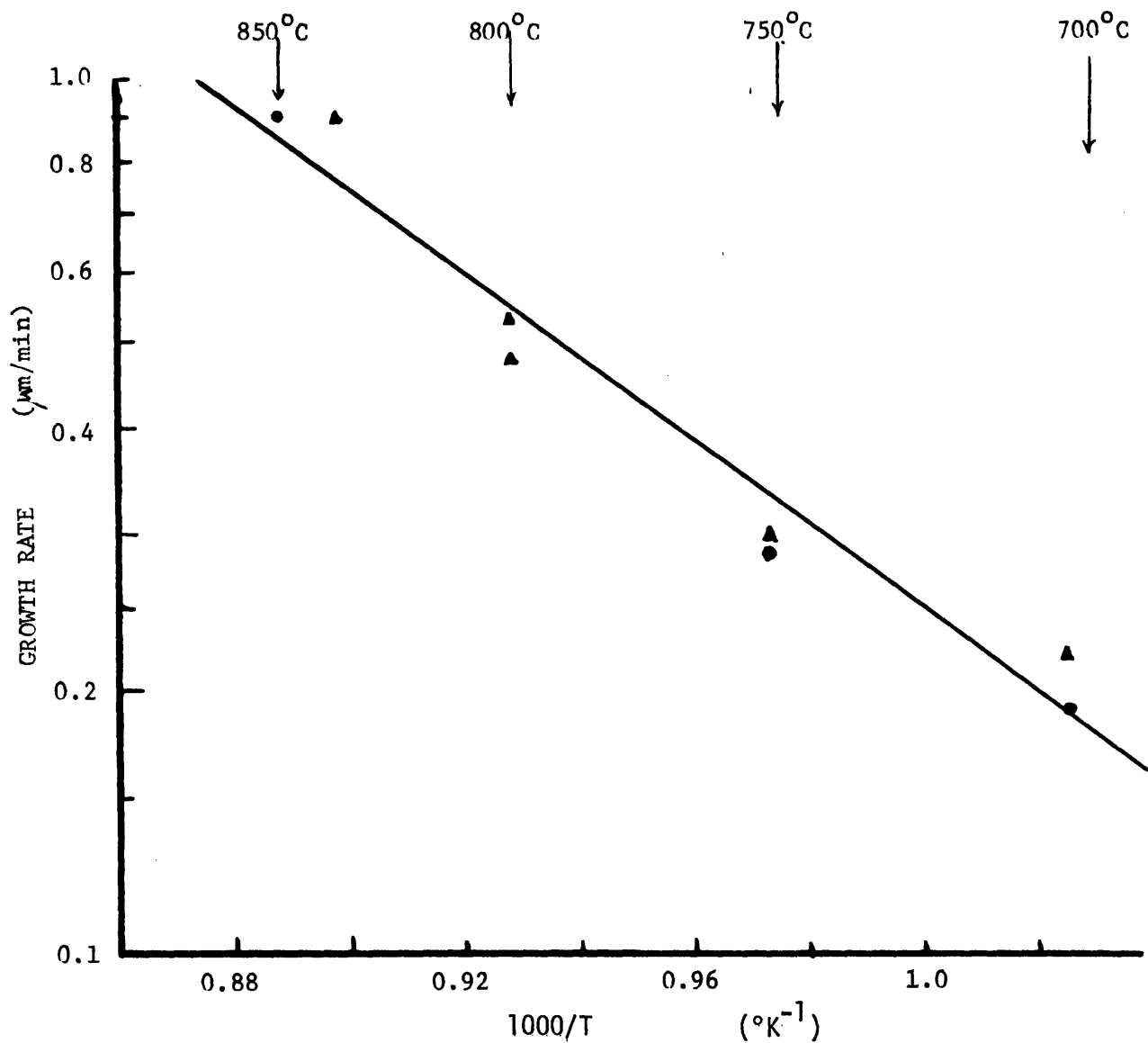
Figure 5.27: Experimental current-controlled LPE growth rates (obtained by neglecting the initial and final transients) plotted as a function of inverse temperature. The data is from layers grown isothermally on substrates contacted with (▲) or without (●) a germanium pedestal.

TABLE 5.2

Growth parameters determined by fitting the current-controlled growth model (of Section 5.1.3) to the experimentally determined growth rate behavior of layers deposited from solutions with no GaAs source.

Sample	Growth Temp. (°C)	Solution Height (mm)	$D(As) \times 10^5$ (cm²/sec)	As EM Mobility (cm²/V-sec)	Interface Temp. Drop (°C)	Rear Contact*	Notes
57	703	7	1.6	0.028	>1.7	Ge/Ta	
59	701	7	1.6	0.030	-0.8		
56	756	7	3.4	0.033	>1.8	Ge/Ta	
60	755	7	3.4	0.035	0		
54	803	7	4.2	0.037	1.0	Ge/Ta	
64	803	5	4.2	0.034	>2.2	Ge/Ta	
67	823	5	4.0	0.032	0	Ge	Cr-doped substrate
53	841	7	5.5	0.038	>2.2	Ge/Ta	
100	849	7	6.0	0.042	-1.0		
42	850	6	6.0	0.042	-0.4		20 A/cm²

*No entry indicates the use of Ga-In only; Ga was also used on Ta and Ge for wetting.
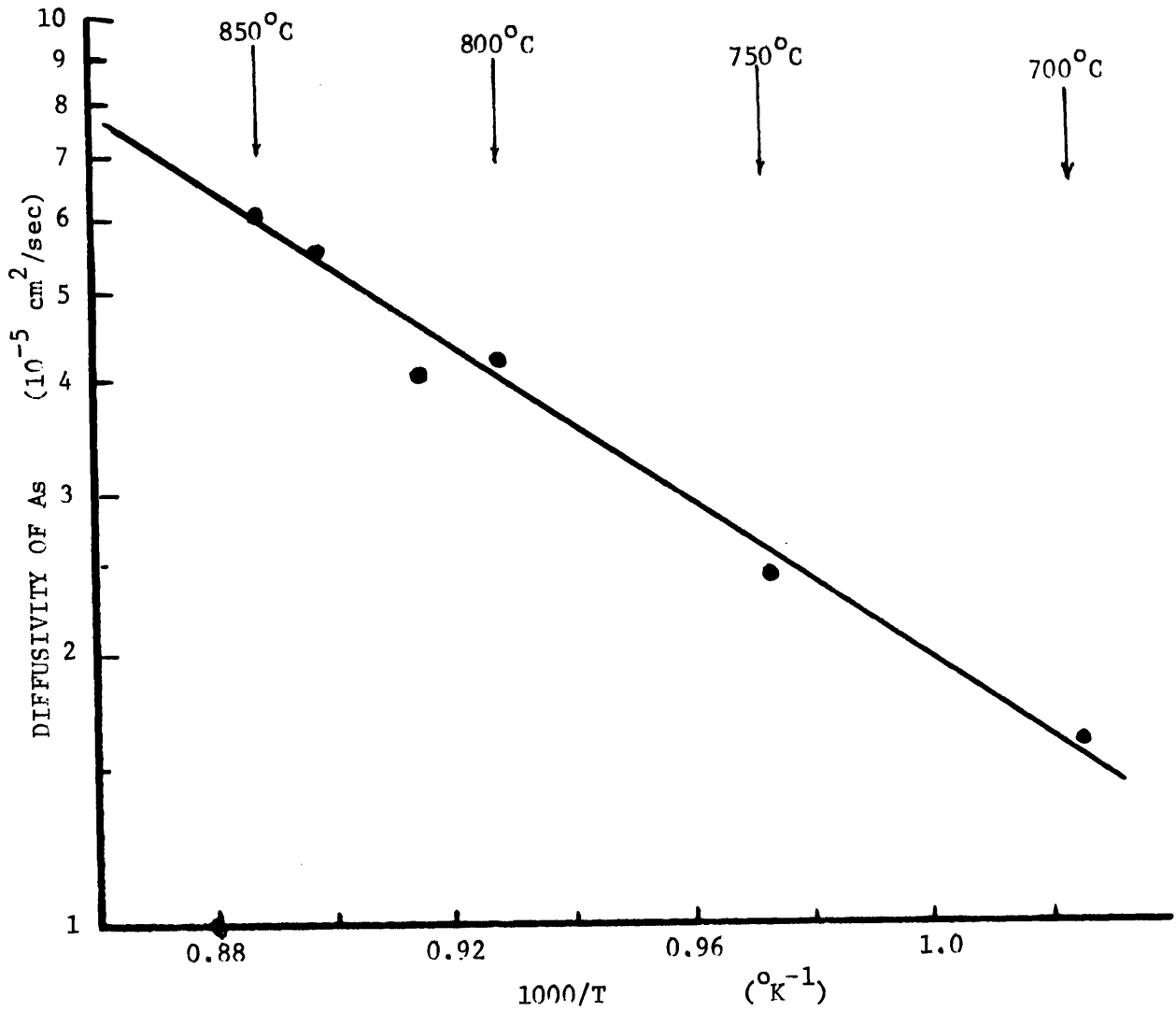
Figure 5.28: Diffusivity of As in Ga versus inverse temperature as deter-
mined (using the current-controlled LPE model) from an
analysis of growth rate behavior. The uncertainty in
values is ±20% for T ≥ 800°C, and ±100% for T ≤ 755°C. The
solid line, determined from regression analysis (r^2 = 0.98),
is given by D_{As} = 0.32 exp[-9700/T] cm^2/sec.

Interface heating or cooling (ΔT) at the onset of growth was found to be strongly dependent on the back contact of the substrates. In general, the layers grown on substrates contacted with a germanium pedestal exhibited rapid initial growth corresponding to interface cooling from 1.0°C to in excess of 2.2°C; the analysis of layers grown without the use of a Ge pedestal shows a heating effect present, between 0 and 1°C. It is of interest to note that the one instance presented where a Ge pedestal did not result in interface cooling was for a semi-insulating (Cr-doped) substrate. However, in all layers the contribution of these thermal effects to growth after the initial ten minutes was found to be small compared to the electromigration flux.

The differential electromigration coefficient of As in Ga, μ_{As}, was found to have values from 0.029 to 0.033 cm^2/V-sec in the temperature range from 700 to 850°C. These values are plotted in Fig. 5.29 as a function of inverse temperature. The straight line represents the results of a regression analysis for the Arrhenius law, although the data can be fit equally well to an expression linear with temperature. The uncertainty in these values ($\pm 20\%$) also allows μ_{As} to be independent of temperature. This behavior is consistent with the analysis of Fig. 5.22, which demonstrated that the growth rate due to electromigration has a temperature dependence similar to the arsenic solubility. Thus μ_{As}, on which R is also proportional, was not expected to have a significant temperature dependence.
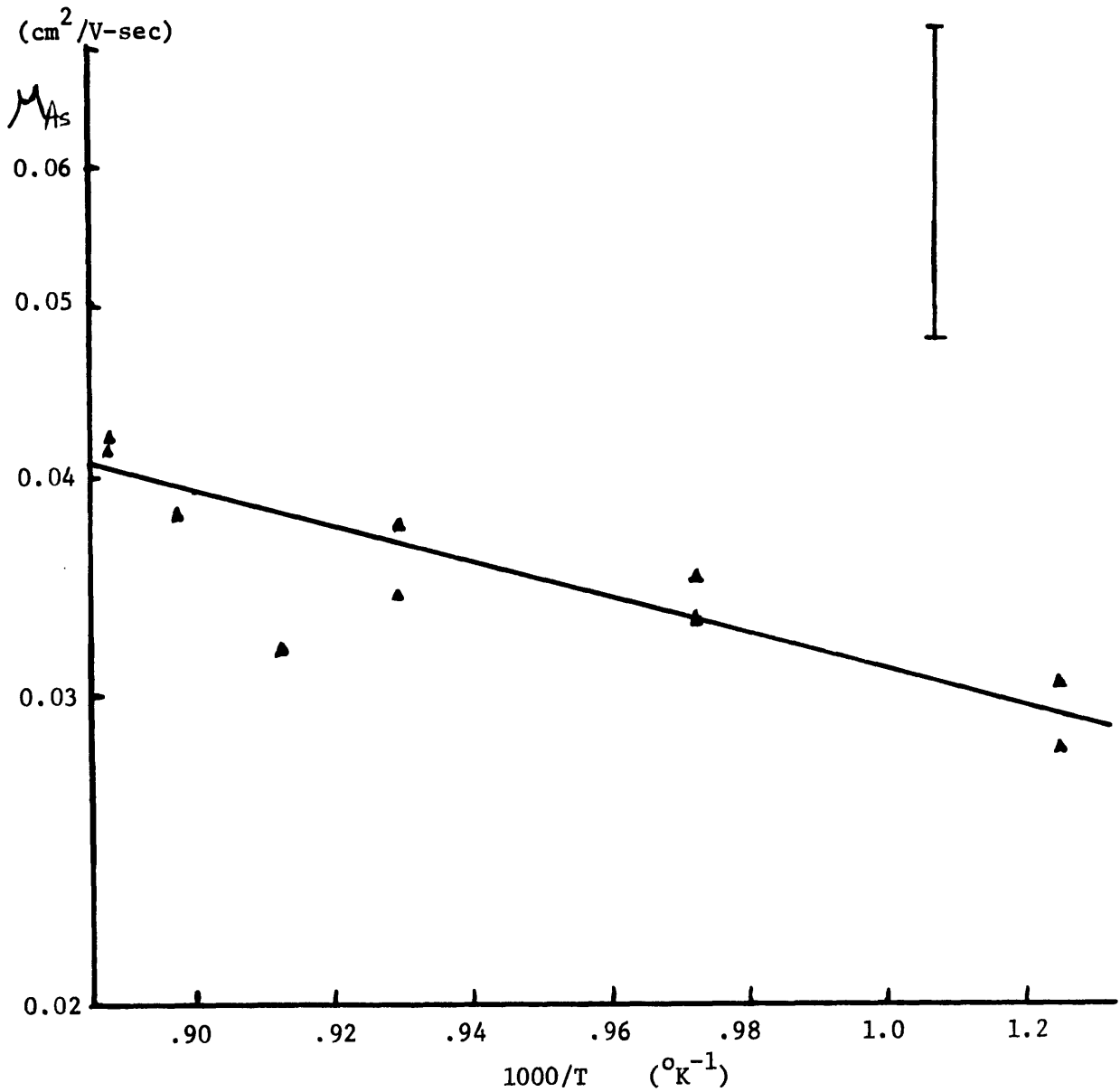
Figure 5.29: Differential electromigration mobility of As in Ga, (μ_{As}), versus inverse temperature as determined (using the current-controlled LPE model) from an analysis of growth rate behavior. The solid line, determined from regression analysis ($r^2 = 0.89$), is given by $\mu_{As} = 0.32 \exp[-2330/T]$ cm^2/V-sec. The uncertainty in all experimental points is ±20%.

Steady-state growth achieved under current-controlled conditions is of primary interest because of its control over growth rates and its associated segregation properties (refer to Chapter Six). Since the value of $\mu_{As}E$ is known for various temperatures, from the preceding results, it is now possible to analyze the mechanism of growth under conditions of constant growth rate. Experiments were conducted in which a GaAs source was present above the solution during current-controlled growth, in contrast to the previously described experiments. This was accomplished by two different approaches:

(1) an undoped wafer was positioned (during loading) on top of the gallium (see Section 4.1.2) and

(2) a film of polycrystalline GaAs was deposited on the upper Ga surface by cooling the pre-saturated solution.[102]

This latter procedure has the added advantage that it results at the same time in the formation of a buffer layer on the substrate (see Section 5.2.1). No difference was observed in the steady-state growth behavior of layers due to using one or the other of the above techniques. An example of steady-state growth thus achieved on a conventionally grown layer is shown in Fig. 5.30, with the two regions in the layer delineated by interface demarcation. Growth rates for two layers grown at different temperatures from solutions to which GaAs source material was added are plotted as a function of time in Fig. 5.31. It can be seen that the growth rates in both regions are constant (within measurements error)
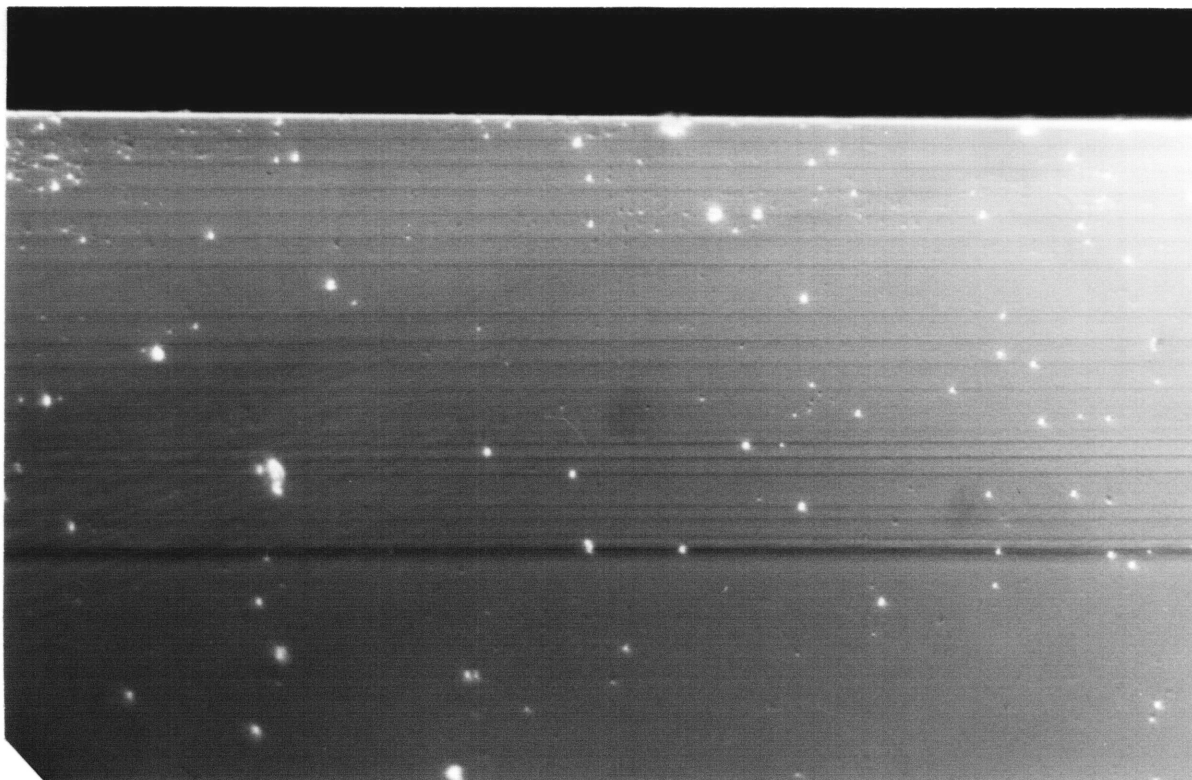
Figure 5.30: Micrograph of a layer grown by steady-state current-controlled LPE (+10 A/cm^2) at 850°C on a layer grown by conventional LPE (0.4°C/min). (107 μm thick).
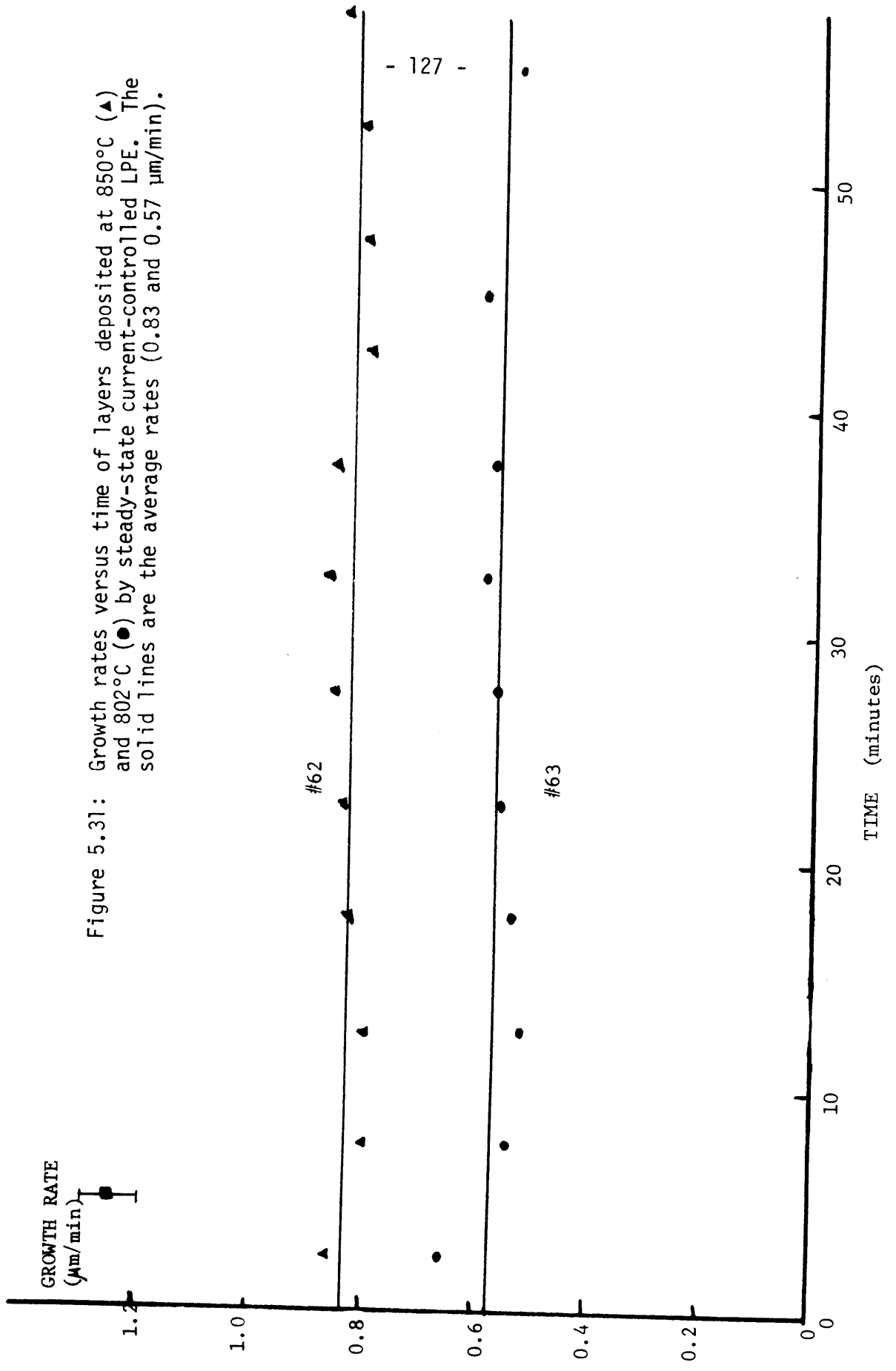
Figure 5.31: Growth rates versus time of layers deposited at 850°C (▲) and 802°C (●) by steady-state current-controlled LPE. The solid lines are the average rates (0.83 and 0.57 μm/min).

except for the initial growth, within the first demarcation period where the rates are slightly higher. No evidence is found in either layer for a decreasing growth rate which characterized growth from a depleted solution, and which would be expected under these experimental conditions to occur within the first thirty minutes of growth in the absence of a source.

The contribution of thermal effects to steady-state current-controlled growth is a function of the net temperature difference between the substrate and the source. Although Peltier cooling or Joule heating may change the temperature of the growth interface, these will only result in transient growth or dissolution, respectively. It is the thermal gradient which accompanies these effects that will, when superimposed on any existing gradients, affect the steady-state growth rate. Thus if the net thermal effect during current-controlled LPE results in the substrate being cooler than the source, there will be a contribution to growth. If the reverse thermal conditions are present, then the net growth rate (consisting of electromigration and diffusion fluxes) will be diminished and may result in dissolution of the substrate. The contribution of these thermal effects to the steady-state growth rate may be estimated from the above temperature difference present (ΔT) and the momentum boundary layer thickness δ as ΔR,

$$\Delta R = D \ \Delta T \ / \ 2 \ m \ C_s \ \delta \tag{5.33}$$

where m is the liquidus slope, D is the diffusivity of As in Ga, and C_s

is the concentration of As in the solid (0.5 at.frac.). Equation 5.35 assumes equilibrium conditions at both the substrate-solution and source-solution interfaces, as well as the same δ above and below the mixed region in solution. If ΔT, defined as the source's interface temperature minus the substrate's growth interface temperature, is positive, growth will be enhanced by the thermal conditions. If $\Delta T < 0$, the growth rate will be reduced from that expected by electromigration.

Constant growth rates from the layers depicted in Figure 5.31 and other layers deposited under steady-state conditions are plotted in Figure 5.32. The solid lines represent the growth rates calculated from equations 10.1 and 10.28 with values for μ_{As} determined previously (Fig. 5.24), current densities of 10 and 20 A/cm^2, and a ΔT of zero. The observed deviation of the data points (at 850°C) from the calculated rate curve is, under ideal conditions, the contribution of thermal effects (ΔR). It is noteworthy that all data points indicate that the substrate-solution interface is at a temperature greater than or equal to the temperature of the source-solution interface. Assuming an arbitrary δ of 0.05 cm, the temperature differences (ΔT) present during these experiments, calculated from equation 5.35, ranged from 0 to 1.8°C for 10 A/cm^2 and from 2.8 to 6.0°C for 20 A/cm^2.

The data on which Fig. 5.32 is based is presented in Table 5.3 with information on the substrate and its rear electrical contacts. The listed value of ΔR, obtained from the difference in the observed growth rate and the electromigration growth rate based on the results in Fig. 5.29, corresponds to the growth rate due to thermal effects. Unless otherwise

Figure 5.32: Steady-state growth rates from layers deposited on various
substrate types and with current densities of 10 A/cm^2
plotted versus inverse temperature. The solid lines are
rates derived for electromigration only (using the values of
μ_{As} in figure 5.29. The data point labels refer to Table
5.3 (p. 131) and the text.
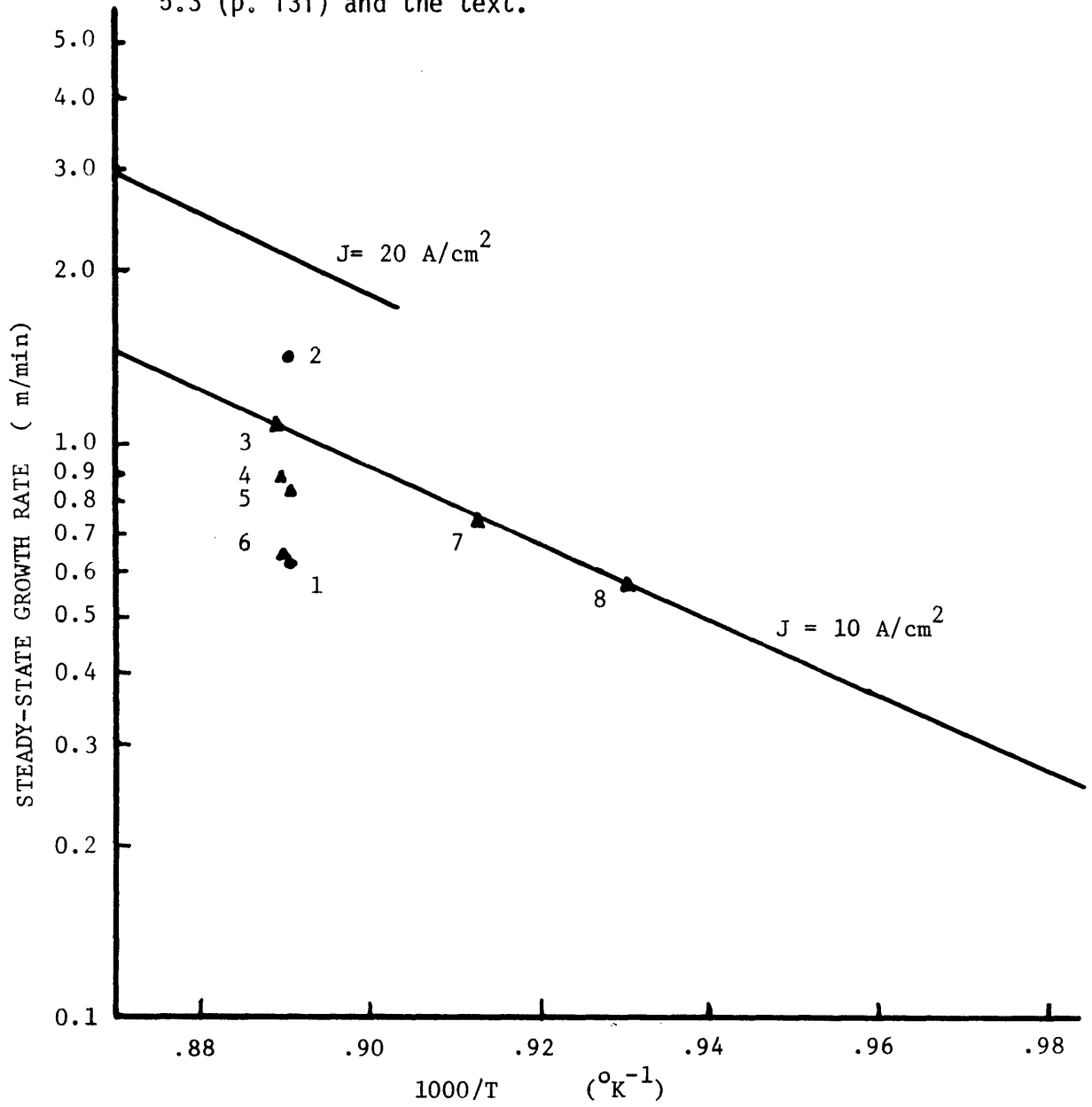
TABLE 5.3

Comparison of steady-state growth rates from current-controlled LPE to the predicted electromigration rates (Fig. 5.29).

Data Point (Fig. 5.22)	Sample	Growth Temp. (°C)	Solution Height (mm)	Exp. Growth Rate (μm/min)	Growth Rate Difference (μm/min)	Notes*
1	130	850	4.5	0.62	-1.50	20 A/cm^2 Zn-doped substrate (2 x 10^{18} cm^{-3})
2	126	850	4.5	1.42	-0.70	20 A/cm^2
3	124	852	4.5	1.09	0	
4	150	851	4.5	0.88	-0.20	
5	62	850	7.0	0.83	-0.23	
6	142	851	4.5	0.64	-0.44	Cr-doped substrate 320 μm thick
7	70	823	5.0	0.74	-0.02	Cr-doped substrate 820 μm thick
8	63	802	5.0	0.57	-0.01	

*Unless noted otherwise, the current density was 10 A/cm^2 and the substrates were n-type (2 x 10^{18} cm^{-3}) and 350 to 400 μm thick.

indicated all substrates were 350 to 400 µm thick, Te-doped 2×10^{17} cm^{-3}, and contacted by gallium-coated Ta foil; the normal growth current was 10 A/cm^2. Too few layers were grown to unambiguously allow the determination of the growth effect of the various experimental parameters, but several effects can be identified. (In the following discussion the data point number refers to Fig. 5.32 and Table 5.3.)

Data points one and two are from experiments using a current of +20 A/cm^2 (+ to substrate) and p- and n-type substrates, respectively. Since the substrates were of the same thickness and conductivity, the primary difference in the two experiments is the presence of Peltier heating at the growth interface of the p-type substrate, and the presence of Peltier cooling at the growth interface of the n-type substrate. If the difference in steady-state growth rates (of data points 1 and 2) is assumed to be due entirely to the Peltier effect, then it can be concluded that the Peltier effect plays a significant role in determining the growth rates during steady-state current-controlled growth. However, in the present circumstances, Peltier cooling does not cause growth but instead only lowers the tendency for dissolution caused by the other thermal effects. An estimate of the boundary layer thickness δ can be made by setting the difference in the observed growth rates for points 1 and 2, 0.80 µ/min, equal to ΔR in equation 5.33 for the expected temperature difference of 2°C (extrapolating measurements in Section 5.2.3 to 20 A/cm^2 and assuming that the thermal effects are additive). Using $D = 6 \times 10^{-5}$ cm^2/sec, a value for δ of 0.03 cm was obtained, and is reasonable (refer to Sections 5.1.4 and 5.2.1). For the lower current

density of 10 A/cm^2, the deviations are generally smaller, with data points 3, 4, 5, 7, and 8 (Fig. 5.32 and Table 5.3) all within 20% of the growth rates due to electromigration. Data point 6 represents growth on a thin (320 μm) semi-insulating substrate, of the same type shown previously. (in Table 5.2) to exhibit greater interface heating than an n-type substrate under similar conditions. It is of interest to note that growth on a thick (820 μm) semi-insulating substrate (data point 7) involved no net thermal effect. Because Peltier cooling is expected to differ with substrate doping, the above variations cannot be assigned to the Peltier or Joule effects. However, these observations indicate that the thermal characteristics of the growth interface and solution as determined by the Peltier and Joule effects have a significant effect on the steady-state growth rates of current-controlled LPE.

Dramatically different growth behavior has been presented for current-controlled LPE without a source in solution and for (steady-state) current-controlled LPE with a source in solution. Growth rates from the former process were in excellent agreement with the current-controlled LPE model (presented in Section 5.1.3), from which an analysis was made that determined values for the diffusivity and electromigration mobility of As as well as the contribution of each to the growth rate. Using experimentally determined values of μ_{As} to obtain a growth rate due to electromigration, an analysis was carried out on steady-state growth rates which showed that the thermal effects can significantly affect growth and in the present circumstances tended to reduce the steady-state growth rates. Examples of

individual experiments suggested that Joule heating and Peltier cooling are both important to steady-state growth.

5.2.3 <u>Temperature effects and characterization</u>

Thermal characterization is grouped into the two general categories of macroscopic gradients and microscopic variations in temperature. The former includes the effects of Joule heating and furnace cooling, while the latter involves the thermal behavior of the growth interface in conventional and current-controlled LPE systems. Temperature measurements were carried out with sheathed and ungrounded chromel-alumel thermocouples (described in Section 4.1.1) located above and below the growth interface as indicated schematically in Fig. 4.1.

Vertical gradients in the growth system were determined by taking the difference of the measurements from the two thermocouples assuming thermal symmetry with respect to the horizontal transverse direction (transverse to the furnace tube axis). These gradients were found to be routinely 0.2 to 0.6°C/cm and stabilizing next to the well containing the solution. They were found to be destabilizing during bakeout when the gallium was left uncapped.

Horizontal gradients (parallel to the furnace tube axis) within the graphite boat were determined by the upper thermocouple which was mobile within its graphite well that traversed the entire length of the boat. These gradients within the growth region were found to be 0.7°C/cm in early experiments but could be reduced to 0.01°C/cm by adjusting shunt resistances along the furnace windings. However, temperature measurements

showed that these horizontal gradients were a function of furnace temper-
ature; thus an initially small gradient (0.01°C/cm) increased to 0.84°C/cm
after 30°C cooling in one hour. This effect could be virtually eliminated
by suitable adjustment of the furnace shunt resistances but limited the
minimum gradient to 0.2°C/cm. The bulk of the conventional LPE growth
experiments were carried out with the constant horizontal gradient of
0.2°C/cm.

Isothermal current-controlled growth experiments were subjected to
these same horizontal and vertical thermal gradients. It was observed,
however, that the end of the boat to which the current carrying rods were
attached would heat-up 2°C with respect to the boat center when a current
of 7.1 A (10 A/cm^2) was applied at 850°C. Temperature measurements
showed that this Joule heating effect became noticeable only in experiments
with a small initial horizontal gradient (0.2°C/cm) and then would tend to
reduce it to less than 0.1°C/cm absolute. Furthermore, Joule heating
resulted in temperature rises of up to 2.4°C over the boat for an applied
current of 7.1 A. This thermal effect was found, as expected, to be
independent of substrate doping (n$^-$, n$^+$, p$^+$, or semi-insulating), sub-
strate thickness (0.3 to 0.8 mm), and solution doping (Te, Sn, or undoped).
To assess the distribution of Joule heating within the growth system,
resistivity measurements were carried out. It was found that the substrate
contributed virtually nothing to the overall resistance of the graphite
boat (150 - 200 mΩ at the rods). Using the thermocouple sheaths as vol-
tage probes, it was possible to eliminate the rod and rod/graphite contact
resistances which lowered the measured resistance to 8 mΩ. This value of

the resistance of the growth system, (two sheaths to graphite contacts, two graphite to gallium contacts, two gallium to GaAs contacts, and the associated bulk resistances), was linear for growth current densities from 0.1 to 10 A/cm^2 and constant over time. However, during growth by either steady-state current or furnace cooling, this resistance was found to increase by a factor of up to 2 for a growth period of one hour. Although this latter effect is not understood at the present time, the maximum amount of Joule heating expected from it near the growth interface is only 0.8 watts (at 7.1 A), as compared to the heating estimated at the rod-graphite contacts of 7.5 watts.

Temperature characterization of the substrate-solution interface was achieved through a series of temperature measurements with a thermocouple in contact with the substrate surface in the solution. The thermocouple was made of one mil chromel and alumel wires threaded into a twin bore quartz capillary (0.5 mm OD). The junction was coated with a cement of Al_2O_3 powder and a phosphate binder, with a maximum coating thickness later measured of 100 μm. The thermocouple was rigidly mounted in the upper part of the boat with the coated junction immersed in the solution and pressing on the substrate's growth surface. The thermal response time (90% recovery to a step-change in T) for the thermocouple and high impedance HP recorder was estimated to be less than one second. Temperature effects associated with current pulses of 5 to 20 second duration (1 to 10 A/cm^2) transmitted across the substrate-solution interface could thus be recorded.

Recorder tracings of the interface temperature of three pulses with current densities of 3, 6, and 9 A/cm^2 are shown in Fig. 5.33. It can be seen that the temperature reaches 90% of its maximum values less than two seconds after the current has been applied or terminated (with approximate rise/fall pulse times of 1 msec). The rate of heating while the current is on is roughly proportional to I^2, indicating that the Joule effect is responsible. The maximum temperature decreases which resulted from the applied pulses are presented in Fig. 5.34 as a function of the applied current density. In agreement with Peltier cooling reported in the literature[103] for this system, the cooling effect is small, reaching a maximum value of 0.5°C for a current density of 10 A/cm^2. A basic analysis of the Peltier effect is given in references (62) and (104).

5.2.4 Analysis of the nature and origin of non-uniform growth associated with conventional and current-controlled LPE

Interface demarcation has been used to study the substrate-solution interface morphology and its changes during conventional and current-controlled liquid phase epitaxy. A theoretical analysis of this technique, and its use and limitations are discussed in Section 5.1.5 and 5.1.6. In the section results on the characterization of thickness non-uniformities associated with growth are presented. This data, in turn, is used to determine the nature and origin of growth perturbations. Also discussed is the use of a buffer layer, grown by conventional LPE, as a substrate for steady-state current-controlled growth.

The thickness of a layer grown by cooling from 853 to 791°C in 127 minutes versus distance along a cleaved cross-section is plotted in

Figure 5.33: Thermal recordings of the growth interface temperature during applied current pulses of 3, 6, and 9 A/cm^2. The heating rate during the pulse duration is due to the Joule effect.
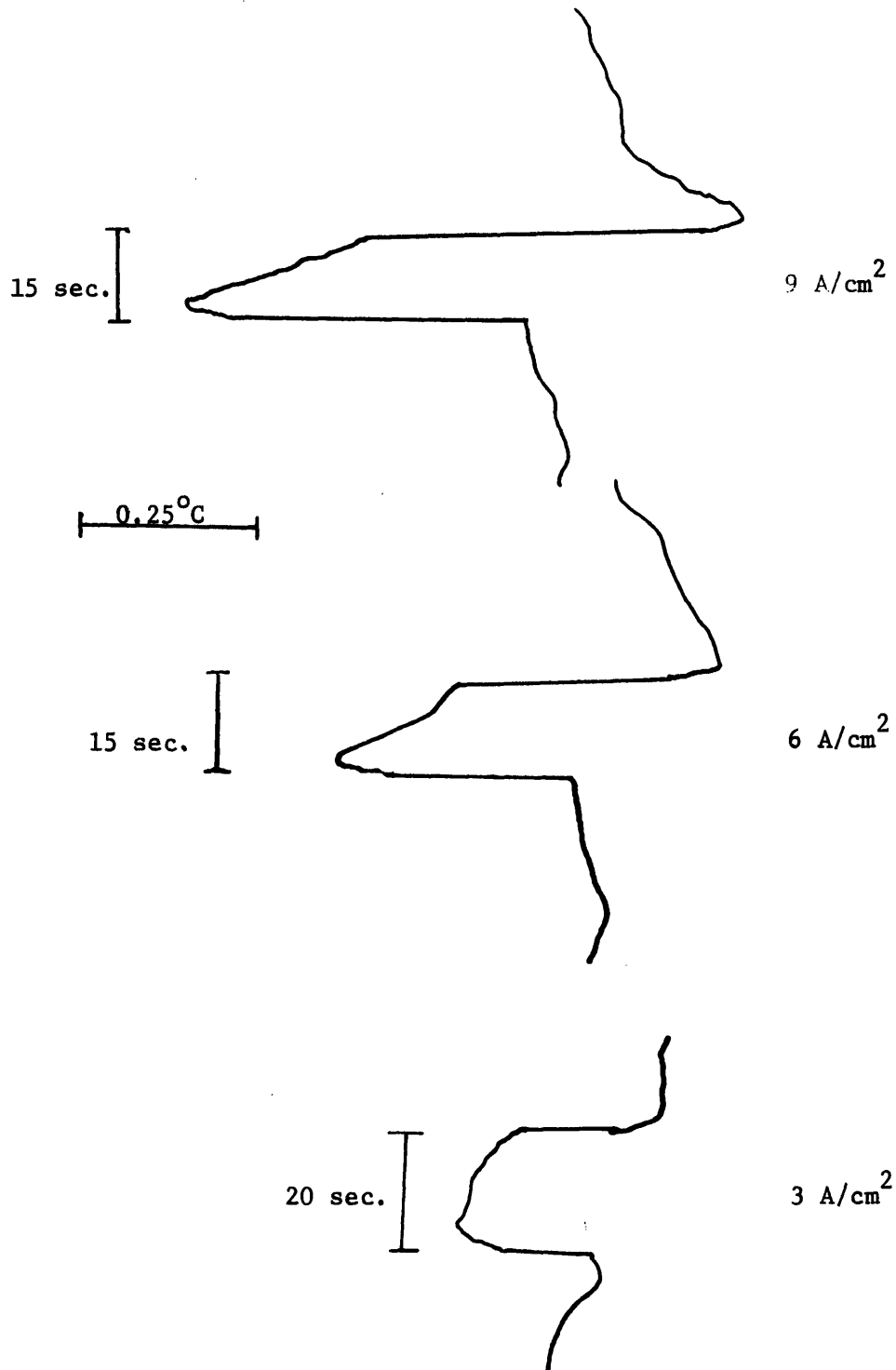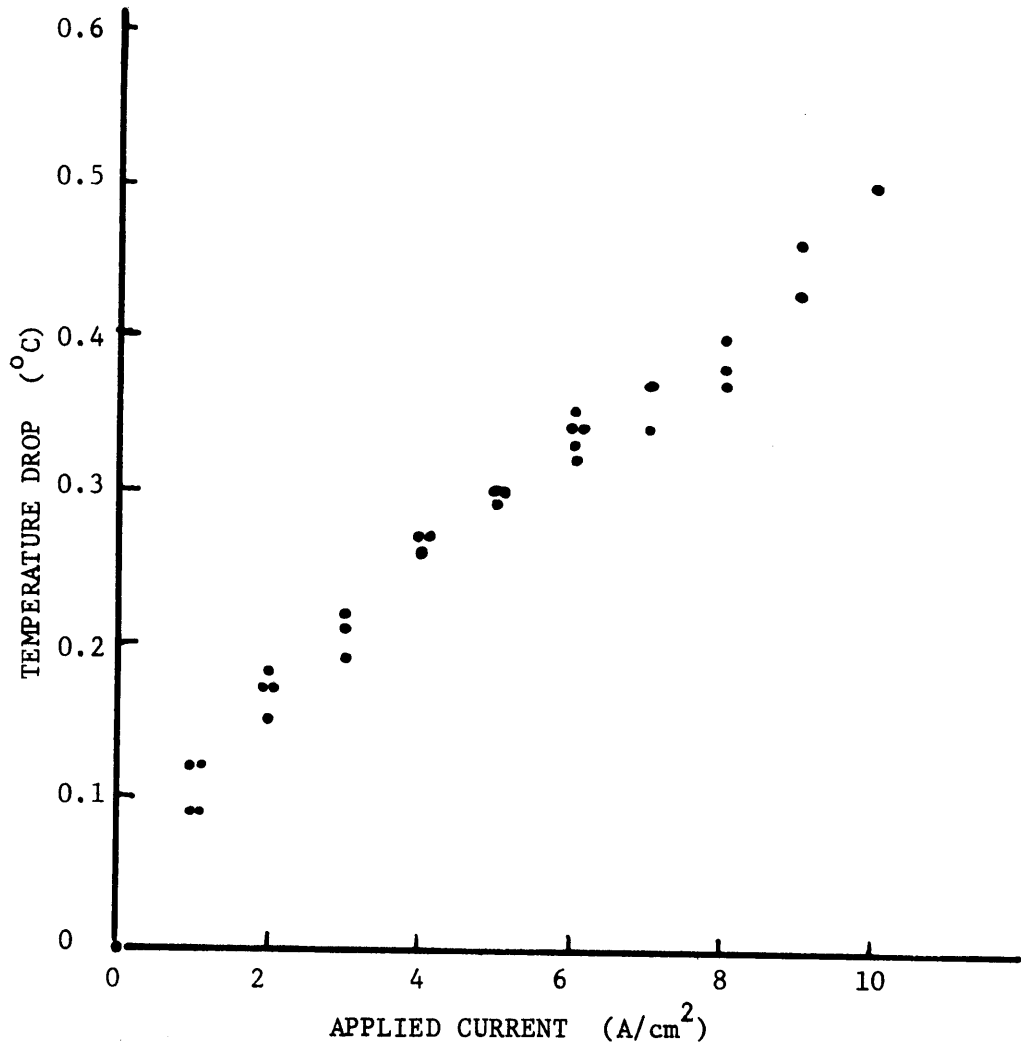
Figure 5.34: Maximum temperature drop measured at the Ga/GaAs
interface plotted versus the applied current density
at 850°C.

Fig. 5.35 for a number of intermediate growth times. The average thickness as determined from twenty-three measurements approximately 0.375 mm apart was found to be 104 μm. The standard deviation (5.3 μm) of the film thickness is typical for thick layers obtained by conventional LPE. Thickness measurements taken from a cleaved surface parallel to and 2 mm from the above averaged 102.4 μ ($\pm$3.8 μ) with the same general shape, indicating that the pattern in Fig. 5.31 is two-dimensional, to a first approximation. This assumption is reasonable since the orientation of the cleaved edge corresponds to the direction of the horizontal thermal gradient in the growth system. Figure 5.35 exhibits features which are typical of both thin and thick layers grown by conventional LPE. The lateral extent of the flat portion, over which thickness variations are less than $\pm$5%, was found to vary for different growth experiments, ranging from 40 to 90% of the layer cross-section. The region of increased thickness (on the left side of Fig. 5.35), when present, was also found to very in width, up to 50% of the total layer cross-section. The increase in thickness for this region was found to be normally less than 20% over the thickness of the flat region, and was located within the half of the layer grown in the cooler portion of the gradient. The layer edge on the warmer side of solution (right side of Fig. 5.35) shows accelerated growth in a very narrow region (< 400 μm), similar to the example in Fig. 5.12b. Micrographs of two regions of this layer depicted by A and B are presented in Figs. 5.14a and 5.14b, respectively. The motion of the solution during contacting and isolation was right to left with respect to Fig. 5.35.

The difference in growth behavior from one region to the next can be seen by comparing distances between the interface demarcation lines. From

Figure 5.35: Conventional LPE layer morphology taken from a cleaved cross-section with interface demarcation. Regions A and B refer to micrographs given in figure 5.14 (a and b).
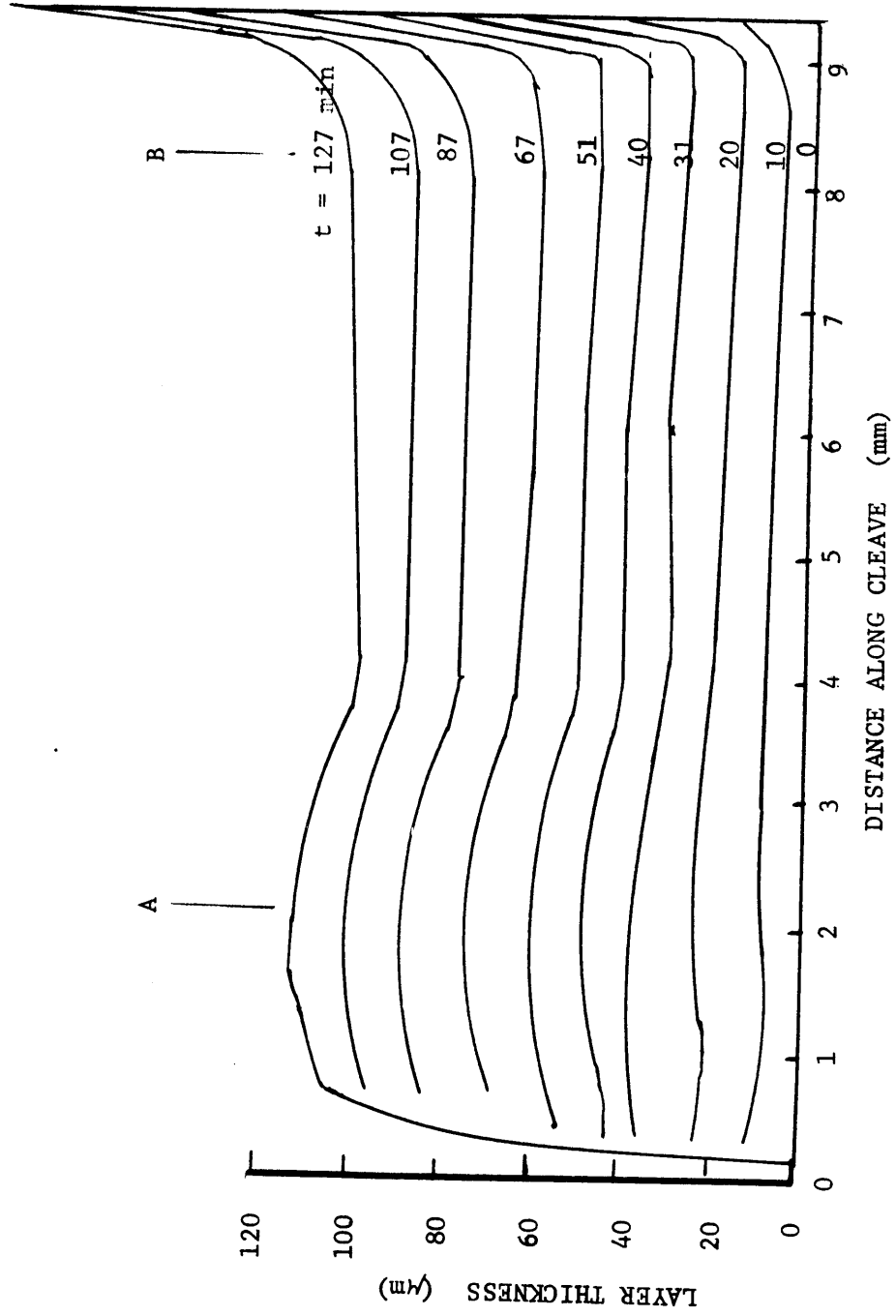
Fig. 5.35 it is clear that the variation in final layer thickness can be attributed to a different growth rate during the first forty minutes of growth in the two regions. This behavior is not expected to be caused by uneven cooling or initial supersaturation of the solution, but suggests, rather, that the boundary layer thickness in the solution is a function of distance along the interface. In regions A and B in Fig. 5.35 the thickness variation can be accounted for as different solute boundary layer thicknesses of approximately 0.3 and 0.7 mm, respectively. These values suggest the establishment of an asymmetric convective flow pattern in the solution, with a smaller momentum boundary layer on the cooler side of the solution. The growth nonuniformity due to the unavoidable lateral thermal gradient has been calculated from equation 5.8 and was found to modify the growth rate by less than 5%. It is of interest to note that the above interpretation of the growth behavior restricts growth at the solution edges since the boundary layer there must be expected to be large. It is therefore concluded that the observed accelerated growth at the layer periphery is not due to convection.

The thickness of a layer grown by a current density of 10 A/cm^2 for 65 minutes at 840°C is presented in Fig. 5.36 for several intermediate growth times. The bulk of the layer is flat (±5% of average), which is typical of layers grown on substrates that were contacted by a germanium pedestal (as in this instance) or tantalum foil. Unlike conventionally-grown layers, the only correlation between thicknesses measured from parallel cleavage faces of current-controlled epilayers is this flat region with its average thickness. The growth perturbations tend to be
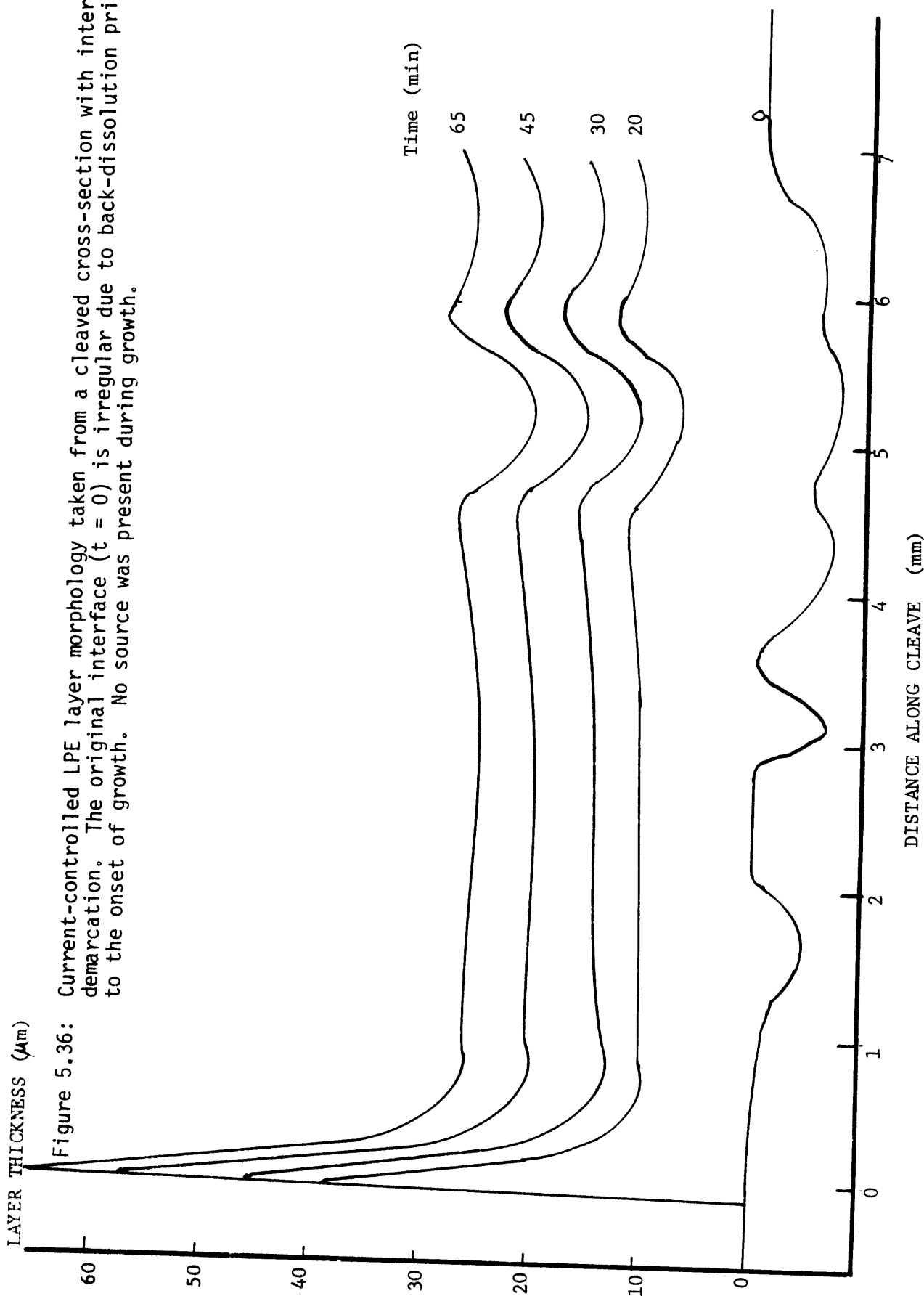
Figure 5.36: Current-controlled LPE layer morphology taken from a cleaved cross-section with interface demarcation. The original interface (t = 0) is irregular due to back-dissolution prior to the onset of growth. No source was present during growth.

localized in positions irrespective of the growth configuration. It can be seen that accelerated growth up to 250% in excess of the average rate took place at both edges of the layer.

There are two important features demonstrated in Fig. 5.36. First, during the initial twenty minutes of growth much of the irregularity of the original interface morphology was eliminated as indicated by the relatively flat interface demarcation line. Second, the depression in the layer that persisted to twenty minutes of growth propagated through the remainder of the layer without any interface flattening effect seen at all. The distinguishing growth characteristic between the first twenty minutes and last forty-five minutes of growth was obtained from the current-controlled growth model of Section 5.1.3: the latter portion of growth was predominantly due to electromigration, while the initial portion was due to Peltier cooling and its associated thermal type of growth.

It was previously shown in Section 5.1.6 that conventional (or thermal) LPE exhibits a tendency of the interface to flatten with time. This is consistant with the morphology of the initial portion of the layer in Fig. 5.36. The lack of such a mechanism in the latter stages of growth suggests that either the perturbation is being maintained by a non-uniform growth effect or the mechanism does not exist for the type of growth taking place. Because the growth rate in the latter stages of deposition is constant over both the flat region of the layer and the entire depression, the current density is uniform and the former possibility above is eliminated. Thus it is concluded that growth due entirely to electromigration will exhibit a constant interface morphology.

The difference in growth behavior between conventional and current-controlled LPE is neatly summarized by the use of Fig. 5.37. It shows the cross-section of a layer grown initially by current (10 A/cm^2) for thirty minutes, followed by one interface demarcation pulse (the dark line) and furnace cooling at a rate of 0.66°C/min. The lower bright line is the original interface, the bright line just above it being a result of the cleave only. The morphology of the interface does not change significantly during current-controlled growth, but does flatten during deposition of an equally thick conventionally (thermally) grown layer.

This finding has been applied in the growth of steady-state current-controlled layers that were deposited on conventional LPE layers as a substrate (or buffer layer). This procedure resulted in the elimination of areas of retarded growth, non-wetting, and faceting, leading to a flat morphology. An example of a cross-section of such a layer is given in Fig. 5.38. After intentional dissolution of the substrate by heating the system, the temperature was lowered 15°C over forty minutes. The cooling program was stopped and the furnace held at 850°C while a current density of +20 A/cm^2 was applied across the growth interface for an additional thirty minutes. Because GaAs source material was present above the solution, the growth rate was constant during the application of current, and convection was present in solution. From an asymmetric dissolution interface, the morphology of the conventionally-grown layer changed, appearing as the example in Fig. 5.35. During the steady-state current-controlled growth, the interface morphology continued to undergo change, approaching a flat interface. This behavior suggests that a portion of the growth is
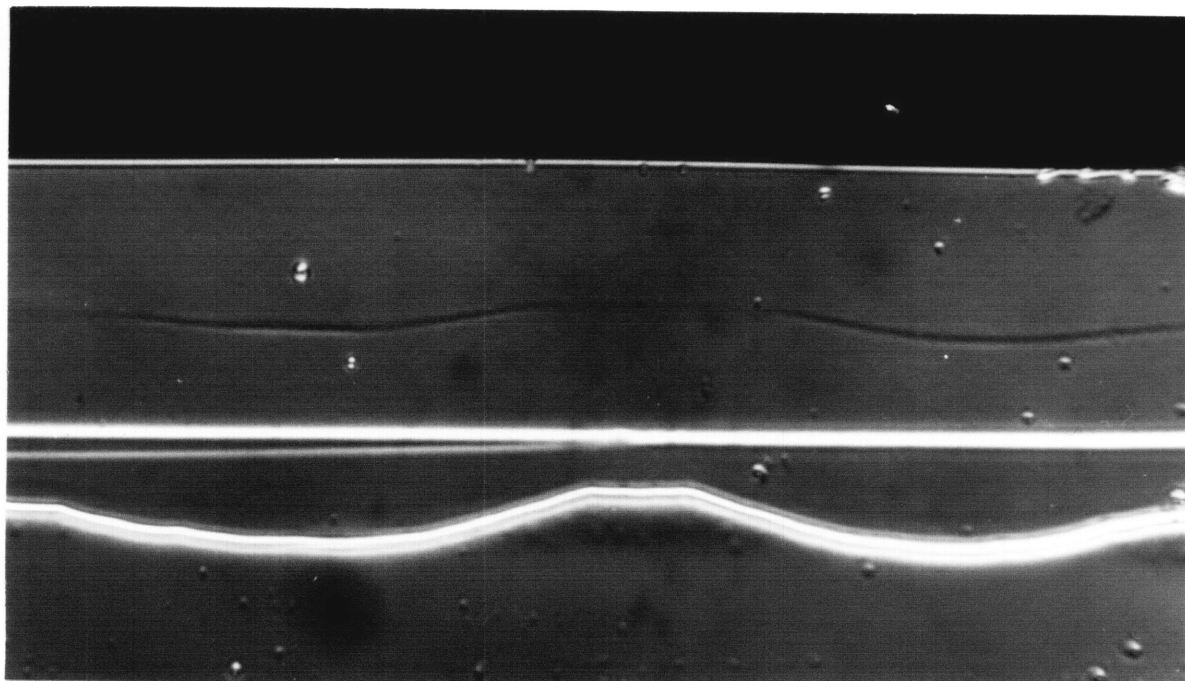
Figure 5.37: The maintenance by current-controlled LPE of a constant
layer morphology and the changes resulting from conven-
tional LPE. The dark line (ID) depicts the interface
between current-controlled LPE without a source (lower)
and conventional LPE (upper). The straight bright line
is a result of the cleave only.

Figure 5.38: Morphology of a steady-state current-controlled LPE layer deposited on a conventional LPE layer. After 40 minutes of growth by cooling 0.4°C/min, the furnace was maintained at 850°C while 20 A/cm² was applied for 30 minutes more.
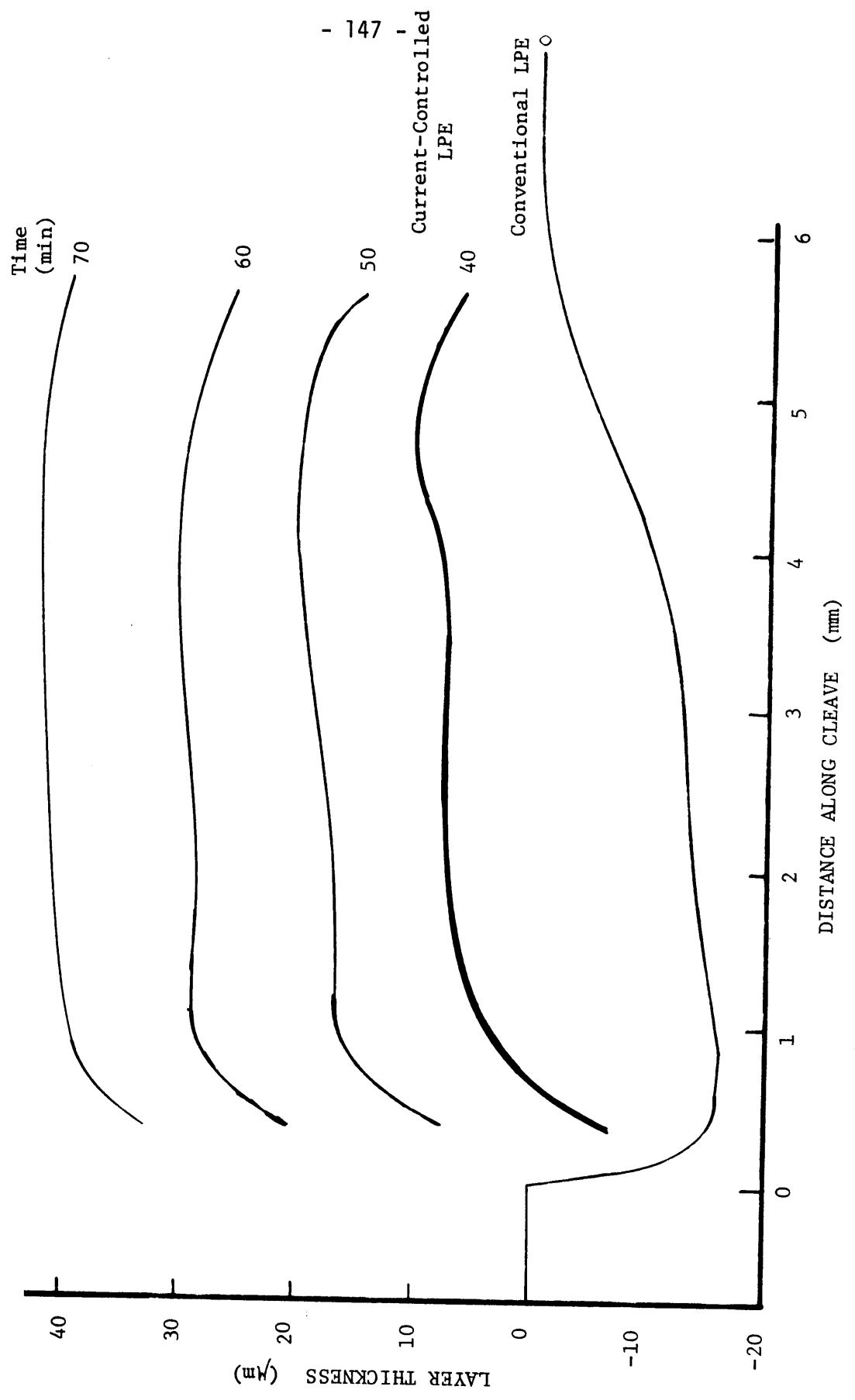
due to Peltier cooling, although the presence of a boundary layer may also affect the morphology.

The use of a buffer layer had two advantages. As shown in Fig. 5.38 the interface morphology improved significantly. In addition, electrical measurements carried out on these layers provided an accurate comparison of segregation during the two types of growth.

5.3 Discussion of Growth Behavior and Layer Morphology

The analysis of conventional LPE layers with the growth model of Section 5.1.2 has demonstrated excellent agreement between experimental and theoretical growth rates for conditions of local equilibrium at the growth interface. It has also indicated the presence not only of convection but of competitive growth sites. The former effect has generally been reported for LPE of GaAs in dipping and tilting systems,[2-5] and in geometries where GaAs is positioned above the solution.[6,7] The presently used system contains small horizontal thermal gradients that have been qualitatively shown to control the initial transient through the establishment of a momentum boundary layer. The average growth rate during conventional LPE, however, has been found to depend only on the rate of cooling and the solution height. The presence of alternate growth sites is predicted from the comparison of experimental growth rates with the conventional LPE model (Section 5.1.2), as well as by maximum layer thicknesses from finite cooling experiments. It is unlikely that these sites are within the solution for the following reasons:

(1) Convection will limit, for the cooling rates (0.03 to 1.6°C/min) and solution heights used ($\ell \leq 8$ mm), the maximum amount of undercooling in the solution (estimated in Section 5.1.2 as less than 5°C). The maximum undercooling before the onset of homogeneous nucleation in a Ga solution at 800°C has been reported to be 9°C.[5,21]

(2) Convection will disperse any precipitates into
the entire mixed region in the solution, effec-
tively reducing the volume of solution supplying
the layer with As. The growth efficiency will
thus be significantly less than 50%.

If nucleation and growth do not occur within the solution, the competitive
growth sites must exist at the solution surface (graphite-gallium inter-
face). This is consistent with observations of solutions cooled to room
temperature: the GaAs precipitates as a shell around the gallium. How-
ever, experimental growth rates for small cooling rates indicate the
presence of competitive growth sites for solution undercooling of less
than 1°C, and thermal measurements characterize the top of the solution as
warmer than the layer-solution interface. Thus, although their effects
have been characterized, the nature and origin of these sites have not
been determined.

The growth behavior of current-controlled LPE layers deposited from
solutions without a GaAs source present has been found to be of equal
complexity as conventional LPE. Since the current-controlled growth model
(of Section 5.1.3) was used to analyze this growth behavior, it is of
interest to determine the suitability of the model by first examing its
premise and then its conclusions. The two basic assumptions of the model
are a constant arsenic concentration in solution at the interface, and an
electromigration flux proportional to the arsenic concentration, applied
electric field, and a mobility. The former can be deduced from the
constant growth rates obtained from steady-state current-controlled LPE.

The latter assumption has been experimentally confirmed from the thermal behavior of current-induced growth rates obtained after neglecting initial and final transients (Fig. 5.27). The above proportionality of growth rate on arsenic solubility also indicates the interface is at or near equilibrium.

The results of the analysis of growth rates using the current-controlled LPE model lend further support for its applicability to experiment. Values obtained for the diffusivity and electromigration coefficients of As in Ga, and for the Peltier cooling of Ga/GaAs are in excellent agreement with reported values. Diffusivities reported for As between 700 and 850°C are compared to values obtained in the present work in Fig. 5.39. As previously indicated the presently determined values are in the lower range of reported values, which implies the absence of convection during the current-controlled experiments made without a GaAs source during growth. The present results are, however, in excellent agreement with work carried out at 800°C,[14,16,17] based on comparisons of theory and experimental growth thicknesses. It is noteworthy that the use of interface demarcation allowed the determination of a value for D at one temperature from the data of one layer.

The value for μ_{As} at 850°C (0.040 cm^2/V-sec) obtained in a similar manner as the diffusivity is in agreement with the values of Jastrzebski and coworkers of 0.049[58] (corrected for E) and 0.018[88] cm^2/V-sec. The presently obtained value is also in excellent agreement with the results of independent electromigration experiments reported and discussed in Chapter seven.
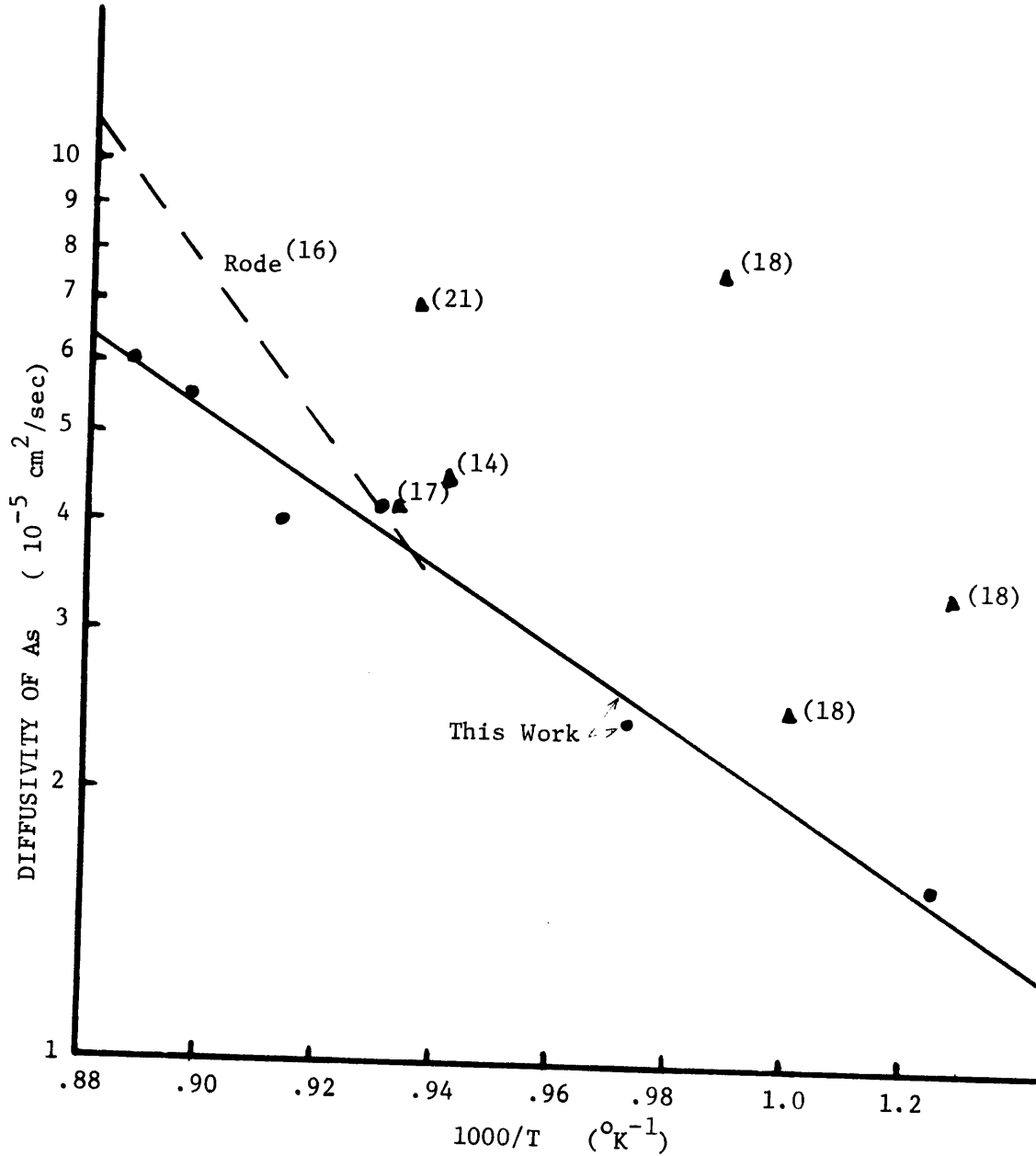
Figure 5.39: Diffusivity of As in Ga for temperatures from 700 to 850°C. Reported values (▲) are referenced; values presently determined are taken from figure 5.28 (p. 122).

Although the effect on Peltier cooling of substrate thickness was not studied extensively in the present work, comparisons between initial growth transients of layers deposited on substrates supported by a germanium pedestal and by a graphite pedestal approximately indicate a 2°C difference in the effective cooling of the interface. This affect is in agreement with Lawrence and Eastman[57] who reported using an n-type GaAs pedestal to remove from the proximity of the growth interface the Peltier heating on the rear of the n-type substrate. Theoretical[62] and experimental[61] work indicates that a 2°C difference in Peltier cooling of GaAs results from an increase of substrate thickness from 0.40 to 2.0 mm (at 830°C, 12 A/cm^2). While this increase is for a GaAs substrate, it is nevertheless close to the thickness of the Ge pedestal used (1.5 mm).

It is therefore concluded from the confirmation of both results and assumptions that the current-controlled LPE model presented in Section 5.1.3 represents and applies to current-controlled growth in the absence of a GaAs source and convection. The following implications of the model must also apply to this type of growth:

(1) Growth is predominantly due to electromigration of As;

(2) The net change in the interface temperature due to the Peltier and Joule effects induces, through equilibrium conditions, a concentration change at the interface that dominates over the early stages of growth only;

(3) The solution becomes depleted of As until a

concentration gradient (destabilizing under

the present conditions) is established that

creates a diffusive flux equal and opposite

to the electromigration flux.

When these results were applied to steady-state current-controlled

LPE (growth in the presence of a GaAs source), it was observed that the

Peltier and Joule effects detracted from the growth rate with amounts

varying from 0 to 70% of the R predicted solely by electromigration.

Since all growth in this manner did not utilize a pedestal, these results

are not inconsistent with the values of μ_{As} obtained. It is believed that

the thermal conditions of the system are extremely important for this type

of growth because of the presence of the source material. The GaAs source

will compete with the layer if the growth interface is at a higher temper-

ature than the source. Since the source material is polycrystalline and

may not completely cover the top of the solution, it cannot be assumed

that Peltier heating is present at the source. Thus, the applied current

does not necessarily impose a thermal gradient on the solution, but instead

contributes Peltier and Joule effects to the existing thermal conditions.

These thermal effects are not important during current-controlled LPE

without a source for two reasons. First, the absence of convection limits

the amount of solute transport due to concentration gradients. Second,

the absence of a source signifies that the arsenic concentration in the

solution is determined by the temperature at the growth interface. If the

interface temperature increases or decreases with respect to the saturation

temperature of the solution, dissolution or growth, respectively, super-imposed on the electromigration flux is independent of the thermal con-ditions normally encountered in LPE away from the interface. Nucleation and growth at the solution surface which might be expected to occur under normal conditions are suppressed to some degree by the electromigration flux away from the upper surface.

The influence of the thermal conditions on the morphology of the two types of current-controlled LPE is also observed to differ. Layers grown by the steady-state technique exhibit similar morphological characteristics as conventional LPE layers. The thickness non-uniformities of these layers have been attributed to a variation in the boundary layer thickness. There is also present during the growth of these layers an unidentified mechanism that tends to flatten the growth interface. A similar mechanism has been observed in the early stages of growth by current-controlled LPE without a source, but is not evident in the layer after the initial transient. It is therefore believed that the "interface flattening" mechanism is associated with the kinetics of thermal growth (cooling).

6. SEGREGATION BEHAVIOR

6.0 Introduction

This chapter is primarily concerned with the segregation behavior of tin and tellurium during conventional and current-controlled liquid phase epitaxy. Effects contributing to dopant incorporation are first considered from a theoretical standpoint, and then treated on the basis of carrier concentration measurements made on layers grown in several different manners. These experimental results are subsequently compared with theory and with work reported in the literature.

6.1 Background and Theory of Segregation

6.1.0 General considerations for LPE of GaAs

The addition of a dopant to the gallium solution creates a ternary system. The behavior of the dopant species is then determined by kinetic and thermodynamic conditions that are not independent of the behavior of the other elements present. Thermodynamic considerations are taken into account by an interface distribution coefficient (Section 6.1.1), while diffusion, convection and the growth rate determine the dopant profiles in the solution (Section 6.1.2). In addition, the presence of an electric field during current-controlled growth also affects the behavior of the dopant (Sections 6.1.3, 6.1.4).

Use is made throughout this chapter of various segregation coefficients which are all ratios of dopant concentrations of the liquid to the solid. The equilibrium constant k_0 can be determined from the relevant phase diagram, and describes a solid-liquid system in equilibirum. The interface distribution coefficient k_i is the ratio of dopant concentrations in the two phases at the interface. The effective distribution coefficient k_{eff} uses the average dopant concentration in the solution. However, complications arise when defining the dopant concentration in GaAs. The distribution coefficients for a dopant in a Ga site differs from k for the same species in an As site, which of course differs from k for the total dopant concentration independent of site. Techniques used for determining dopant concentrations usually rely on electronic properties, yielding none of the above. In order to avoid this ambiguity in the discussion of the experimental results, another distribution coefficient,

k^*_{eff}, has been defined as the ratio of carrier concentration in the solid (given directly by the C-V measurement) to the average dopant concentration in the solution. The relationship of k^*_{eff} to k_{eff} is treated in Section 6.1.5.

6.1.1 Temperature dependence of the distribution coefficients of Sn and Te in GaAs

Kang and Greene[6] have reported values for k^*_{eff} of Sn and Te in GaAs in the temperature range from 650 to 850°C. Layers were grown isothermally by the imposed thermal gradient technique, with carrier concentrations from 5×10^{16} to 5×10^{17} cm^{-3} measured by the C-V technique. They found in the grown layers constant carrier concentration profiles whose values were proportional to the amount of solution doping used. The temperature dependence of k^*_{eff} was empirically found to be

$$k^*_{eff} = A \, e^{-E_a/kT} .$$
(6.1)

The values of the constants A and E_a were determined from their experimental data as 0.88 and 0.80 eV for tin, and 1.08×10^{-6} and -1.0 eV for tellurium, respectively. The negative activation energy in the latter case reflects a k^*_{eff} which increases with decreasing growth temperature. The difference in the behavior of the two dopants has been reported[6,64] as due to the change in chemical potential of As with temperature[105] having an opposite effect on Sn in a Ga site than on Te in an As site.

The expression 6.1 was presently used to determine the expected variation of k_{eff}^* for conventional LPE as a function of layer thickness. Referring to known growth conditions of a particular layer, the function k_{eff}^* (time) could be obtained from k_{eff}^* (T) with the recording of the solution temperature during growth. Using interface demarcation to identify layer thickness as a function of time, k_{eff}^* (time) could be converted to k_{eff}^* (thickness). This allows a direct comparison to be made between segregation behavior predicted by equation 6.1 and the experimental concentration profile (see Sections 6.2.2 and 6.2.3). It should be realized, however, that the empirical behavior given by equation 6.1 represents an experimental result and not a theoretical result.

6.1.2 Growth rate dependence of dopant incorporation: kinetic effects

The dopant segregation behavior during crystal growth in binary systems has been reported[48,106] along with theory for diffusion-limited growth and conditions of partial mixing in the melt. The results of these studies are presently applied to conventional LPE with the assumption of isothermal conditions and a constant rate of growth (R), so as to permit an estimate of the theoretical dopant accumulation in the solute boundary layer at the substrate-solution interface. It is presently further assumed that the interface distribution coefficient is equal to the equilibrium distribution coefficient, k_o.

The effective distribution coefficient for a dopant in a diffusion-limited system as a function of distance (x) from the original growth interface is given as:[106]

$$k_{eff} = (1 - k_0) \{1 - \exp (-k_0 Rx/D)\} + k_0 \qquad (6.2)$$

where R is the growth rate and D is the dopant diffusivity in solution. If a value of D is assumed to be 5×10^{-5} cm^2/sec (the same magnitude of D_{As} in Ga), then a typical LPE growth rate ($R \approx 1.3 \times 10^{-6}$ cm/sec) and layer thickness ($x \approx 10^{-2}$ cm) will lead to a maximum value of k_{eff} for x = 100 μm of $k_0 \cdot (1 + k_0/4000)$ for $k_0 < 1$. This means that no appreciable accumulation layer is formed and $k_{eff} \approx k_0$.

The effective distribution coefficient for a dopant in a system with a convectively induced and controlled solute boundary layer is given by[48]

$$k_{eff} = k_0 \{k_0 + (1 - k_0) \exp (-R\delta/D\}^{-1} \qquad (6.3)$$

where δ is the boundary layer thickness beyond which complete mixing in the solution is assumed. For a typical value for δ (0.1 cm), this expression reduces to

$$k_{eff} = k_0 \{1 + (1 - k_0) / 400\} \qquad (6.4)$$

which, as in the previously discussed diffusion controlled case, indicates that $k_{eff} \approx k_0$ and dopant accumulation within the established boundary layer is negligible.

This present theoretical result may seem to be incongruous with diffusion-controlled growth, as the dopant has been assumed to have the same diffusivity as the solute (As). There are, however, two major differ-

ences in the constraints, or boundary conditions, imposed upon the dopant and upon As. First, the dopant distribution coefficient is assumed to be less than one, while k_o for As is 13.5 at 850°C (Section 5.1.1). Second, dopant accumulation is determined by the growth rate, which in turn is determined by the As profile in solution. The accumulation of dopant at the advancing interface is therefore scaled down by a factor of 13.5 from the As depletion at the interface. In addition, the amount of As depletion at the interface at 850°C is only 5% of the arsenic concentration for 5°C undercooling of the solution. Thus, the accumulation of dopant estimated for the above conditions is less than 0.4% of the dopant concentration in solution.

This analysis indicates that the segregation behavior of dopants with $k_o < 1$ (such as Sn and Te at 850°C) should be independent of growth rates normally encountered in LPE.

6.1.3 Dopant segregation in the presence of an electric field

An applied electric field may have two possible direct effects on dopant incorporation during LPE:

(1) it may result in electromigration of the dopant species; and

(2) it may result in the establishment of localized non-equilibrium conditions at the interface.

The former is a kinetic process which may affect the dopant concentration in the solution adjacent to the growth interface. The latter constitutes

the effect of the electric field on the chemical potential of the dopant elements.

An estimate of the maximum change in the interfacial dopant concentration due to electromigration can be obtained through the basic equations of state in Appendix 10.1. Thus, by substituting conservation of mass (of the dopant) for the boundary condition at the interface, the concentration of the dopant at the interface, C_i^d, is obtained as a function of the average dopant concentration C_o^d in solution (in the absence of convection):

$$C_i^d = C_o^d \; \eta_d \; \ell \; (1 - \exp[-\eta_d \ell])^{-1} \tag{6.5}$$

where ℓ is the solution height, $\eta_d \equiv \mu_d E/D$, μ_d and D are the electromigration and diffusion coefficients respectively of the dopant, and E is the electric field. For $\eta_d \ell \ll 1$, equation 6.5 reduces to

$$C_i^d = C_i^d \; (1 + \eta_d \ell/2) \tag{6.6}$$

which is the maximum increase in dopant concentration at the interface due to electromigration. It should be pointed out that electromigration of the dopant will not result in a sudden change in the dopant concentration at the interface, but causes a gradual increase to the maximum given by equation 6.6 over a period of time greater than ℓ^2/D (typically one hour or more). The effect of convection in solution is to reduce the maximum accumulation to $C_o^d \cdot (1 + \eta_d \delta)$ which is reached after a time $\ell\delta/D$.

The effect of an electric field on the chemical potential of the dopant species can be estimated by treating the solution/layer interface as a Schottky diode. At 850°C, the ideal reverse saturation current density of a diode was calculated from an expression in Sze[74] to be 2×10^5 A/cm^2 (a minimum value) for V > 3kT/q and a barrier height of 0.75 V. For an applied current of 10 A/cm^2, the voltage across the junction (interface) is estimated to be 30 μV, which is three and one-half orders of magnitude smaller than kT/e. A change in chemical potential of the dopant on the order of 30 μV can be neglected.

From the present analysis, the only effect on segregation behavior directly expected from an applied electric field is a slow increase in dopant incorporation dependent on the differential electromigration mobility of the dopant in solution.

6.1.4 Segregation associated with interface demarcation

The presence of interface demarcation lines in etched layer cross-sections is evidence of a segregation effect associated with the application of an applied electric current across the solution-layer interface. The instantaneous nature of this effect rules out electromigration as a cause, and suggests that it is a kinetic effect associated with the large growth rates accompanying the change in current density. Theoretical growth rates during demarcation, presented in Section 5.1.5, indicate exceptionally rapid growth that may result in a temporary dopant accumulation at the interface. This explanation predicts a segregation effect

for both cooling and heating pulses as well as for an increase in current density across the interface.

Further analysis of interface demarcation requires a quantitative evaluation of the experimental characteristics of this effect, which is not within the scope of the present work.

6.1.5 Application of capacitance-voltage measurements to compositional analysis

Any quantitative treatment of dopant segregation associated with epitaxial growth requires a knowledge of the dopant concentrations in both the solid and liquid phases. Because the C-V technique measures differential charge carrier concentrations, it is necessary to first establish the relationship between the measured quantities and the actual dopant concentrations in the solid.

The capacitance-voltage technique, described in Section 4.3, basically measures the difference in the density of ionized donors and acceptors located in a plane at a certain distance (given by the depletion width) below the junction.[67] Thus, the measured carrier concentration constitutes an average over the area sampled by the junction. To insure the determination of meaningful carrier concentrations within a given plane, measurements were taken in several locations at the same depth. The presently adopted procedure, described in detail in Section 4.3, yielded data reproducibility of better than 5% due in part to constant lateral carrier concentrations in all epitaxial layers.

To relate the measured carrier concentrations to dopant concentrations, both the compensation ratio (N_A/N_D) and the degree of dopant ionization must be known. This latter quantity is a function of the Fermi level, density of dopant atoms, and the donor and acceptor energy levels within the band gap. Using a graphic procedure,[74] the theoretical fraction of ionized dopant atoms for Sn and Te in GaAs was determined for different doping densities. It was thus found that a measured carrier concentration of 10^{17} cm^{-3} corresponds to 77% ionization, which decreases to 61% for $n = 2 \times 10^{17}$ cm^{-3}. It is therefore concluded that proportionality between carrier concentration and dopant concentration is maintained over small concentration ranges only. This limitation is of no significant consequence to the present study. The compensation ratio for Sn in GaAs grown at 860°C is 1/2.2,[107] and at 700°C is 1/3.6.[40] The latter value is reported to be independent of carrier concentration.[40] Hall mobility data of Sn-doped layers grown in the present work at 850°C indicate compensation ratios from 0.4 to 0.5. Thus, both N_D and the sum ($N_D + N_A$) can be taken as proportional to the measured carrier concentration.

In the present study the carrier concentrations measured by the C-V technique are considered proportional to the dopant concentration.

6.2 Experimental Results on Segregation

6.2.0 Introduction

Experiments were conducted to determine the effect of growth parameters on segregation for conventional and current-controlled LPE of GaAs. Growth solutions were intentionally doped with either tin or tellurium such that the resulting doping in layers was in excess of background impurity levels. Carrier concentrations were measured by the capacitance-voltage technique described in Section 4.3.

Intentionally doped layers were grown by one or more combinations of conventional (thermal cooling) and current-controlled LPE at or near 850°C. One type of variation used was the superposition of thermal cooling on an applied current of either polarity. The other type of variation used was growth of an initial portion of a layer by conventional LPE followed by growth due to an applied current with or without further cooling. The advantage of depositing two such layers on one substrate is in the direct comparison of segregation behavior obtained from a carrier concentration profile through the layer. Multiple layers were also grown with different current densities.

The use of interface demarcation enabled the identification of the growth temperature and type of growth of a specific portion of the layer, as well as the microscopic growth rate. A reverse procedure to the one described in Section 6.1.1 was adopted, whereby an interface demarcation line in a layer pinpointed the time of growth. By referencing the time of growth to the temperature recording of the solution, the growth temperature and type of growth, corresponding to the interface demarcation, were found.

6.2.1 Background doping level

The purity of the growth system was periodically monitored by growing undoped conventional LPE layers on semi-insulating substrates and subsequently determining their carrier concentration and Hall mobility. Carrier concentrations in undoped layers corresponding to contaminants were determined from Van der Pauw measurements and ranged from 3×10^{14} to 6×10^{16} cm^{-3} (n-type). These layers had Hall mobilities from 3200 to 6800 cm^2/V-sec (at 20°C). If an undoped layer exhibited a mobility below 4000 or a carrier concentration in excess of 5×10^{15} cm^{-3}, all layers grown after the previous purity check were treated as questionable. In addition, steps were taken to purify the system which was tested again for contamination before doped layers were again deposited.

To assess the effect of re-using a solution on the background doping level of layers, a series of growth experiments was conducted in which layers were consecutively deposited on four substrates from a single undoped solution. Hall mobility and carrier concentration of the four layers are presented in Fig. 6.1. Hall mobility decreased from 5500 cm^2/V-sec in the first run to 3500 in the fourth, while the carrier concentration increased from 7×10^{14} cm^{-3} to 3×10^{15} cm^{-3}. The total density of ionized donors and acceptors calculated from this data is 10^{16} cm^{-3} in the first two layers, increasing to about 3×10^{16} cm^{-3} in the third and greater than 7×10^{16} cm^{-3} in the fourth layer. It is believed that the contamination is introduced each time that a new substrate is loaded.
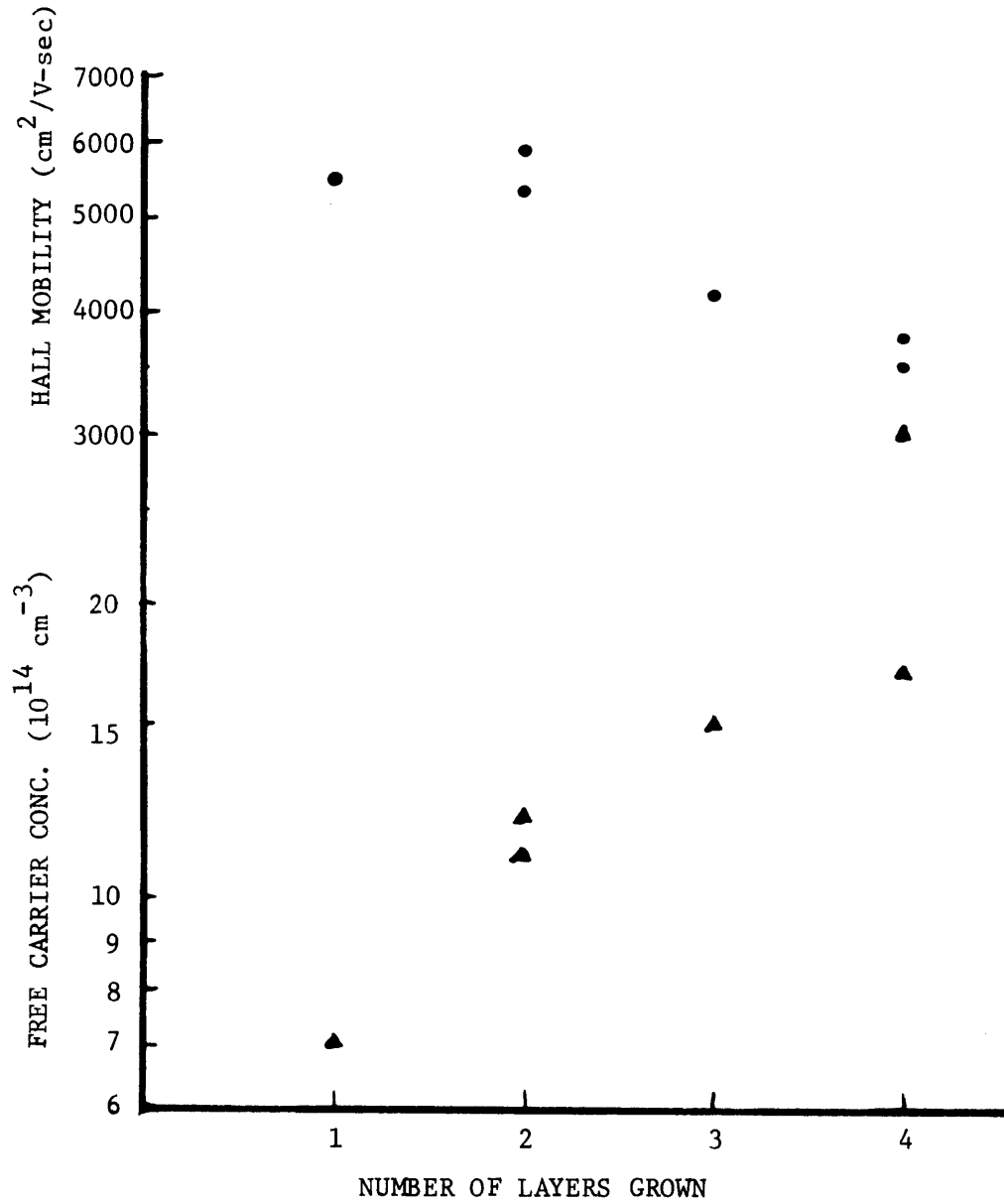
Figure 6.1: Hall mobility (●) and free carrier concentration (▲) of undoped layers grown by conventional LPE at 850°C from the same solution (determined from Van der Pauw measurements).

It is concluded that a solution could not be re-used more than twice in the present growth system to deposit layers that are to be the subject of this segregation study.

6.2.2 Segregation behavior of tin in GaAs

Layers were grown from solutions doped with 0.4 to 4.1 atomic % tin as described in Section 6.2.0. Carrier concentration profiles of each layer were constructed from series of C-V measurements (Section 4.3) and related to the microscopic growth rate and type of growth involved. Profiles are also compared to the segregation behavior predicted by equation 6.1.

To determine the effect that an applied steady-state current (with a source in the solution) has on segregation during cooling, a layer was grown from 859°C with a cooling rate of 0.4°C/min. After 25 minutes of growth a current density of +10 A/cm^2 was applied across the growth interface for an additional twenty minutes after which the solution was isolated from the layer. The total temperature drop at the solution was 20°C. From the one interface demarcation applied during growth at the onset of the current, it was determined that the initial portion of the layer was 10.2 μm thick and the latter portion 18.0 μm thick. These correspond to average growth rates of 0.41 μm/min for the conventionally grown layer, and 0.9 μm/min for the part of the layer deposited with cooling and current present. The carrier concentration profile for this layer, shown as points in Fig. 6.2, decreases with layer thickness from 3.9 x 10^{17} cm^{-3} initially to 3.3 x 10^{17} cm^{-3} near the surface. The behavior predicted by equation
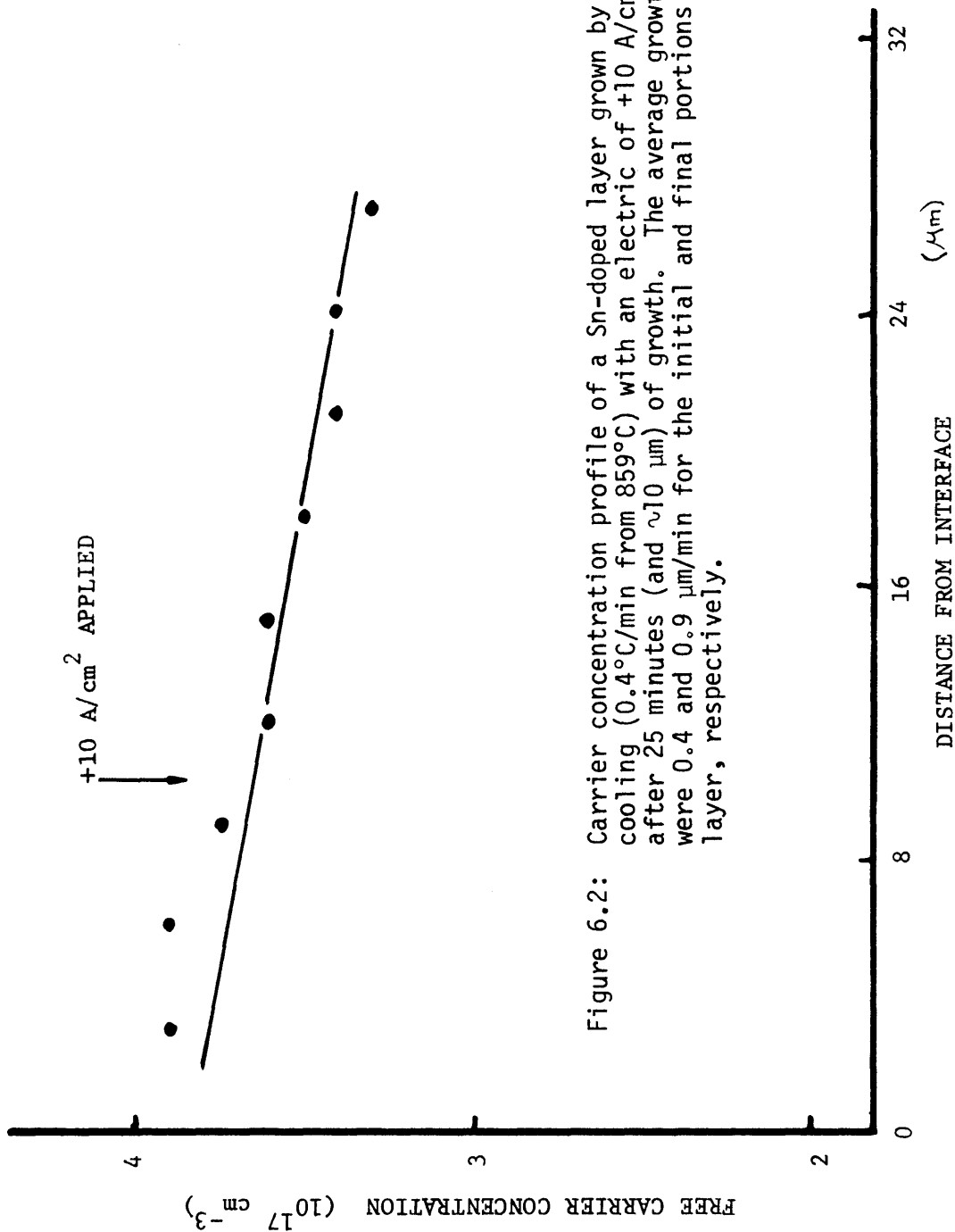
Figure 6.2: Carrier concentration profile of a Sn-doped layer grown by furnace cooling (0.4°C/min from 859°C) with an electric of +10 A/cm² applied after 25 minutes (and ∿10 μm) of growth. The average growth rates were 0.4 and 0.9 μm/min for the initial and final portions of the layer, respectively.

6.1 is plotted as the solid line, and is in excellent agreement with the experimental points. Implications of this agreement in this layer and others yet to be analyzed are discussed in Section 6.3.

The carrier concentration seems to be unaffected by the application of the current, in spite of a resulting increase in the growth rate of 120%. The growth rate change alone was not expected to produce a change in carrier concentration (refer to Section 6.1.2), and it can therefore be concluded that the change in segregation behavior of Sn for the applied current density of +10 A/cm^2 is negligible.

The effect of steady-state isothermal current-controlled growth on segregation was studied in a layer deposited at 850°C by a current density of +10 A/cm^2. The carrier concentration measured was a constant 1.7 ($\pm$0.1) x 10^{17} cm^{-3} for thirty microns in the layer deposited at a constant growth rate of 0.75 μm/min ($\pm$5%) (Fig. 6.3). The decrease by a factor of two in the carrier concentration at the surface is discussed presently where it is found not to be a segregation effect. The flat concentration profile in Fig. 6.3 demonstrates the ability of current-controlled growth to provide uniform doping at reasonable growth rates. It should be noted in comparison to Fig. 6.2 that it is the isothermal condition that appears necessary for the flat profile.

The depth of the observed decrease in carrier concentration at the surface was found to depend on the length of time that the layer spent at elevated temperatures after isolation from the solution. The measured depths varied from four to less than one micron for after-growth times (where T > 600°C) of four hours to ten minutes. Profiles were taken of

Figure 6.3: Carrier concentration profile of a Sn-doped layer grown isothermally at 850°C by current-controlled LPE (+10 A/cm²) with a source. The growth rate was constant at 0.75 μm/min (±5%).
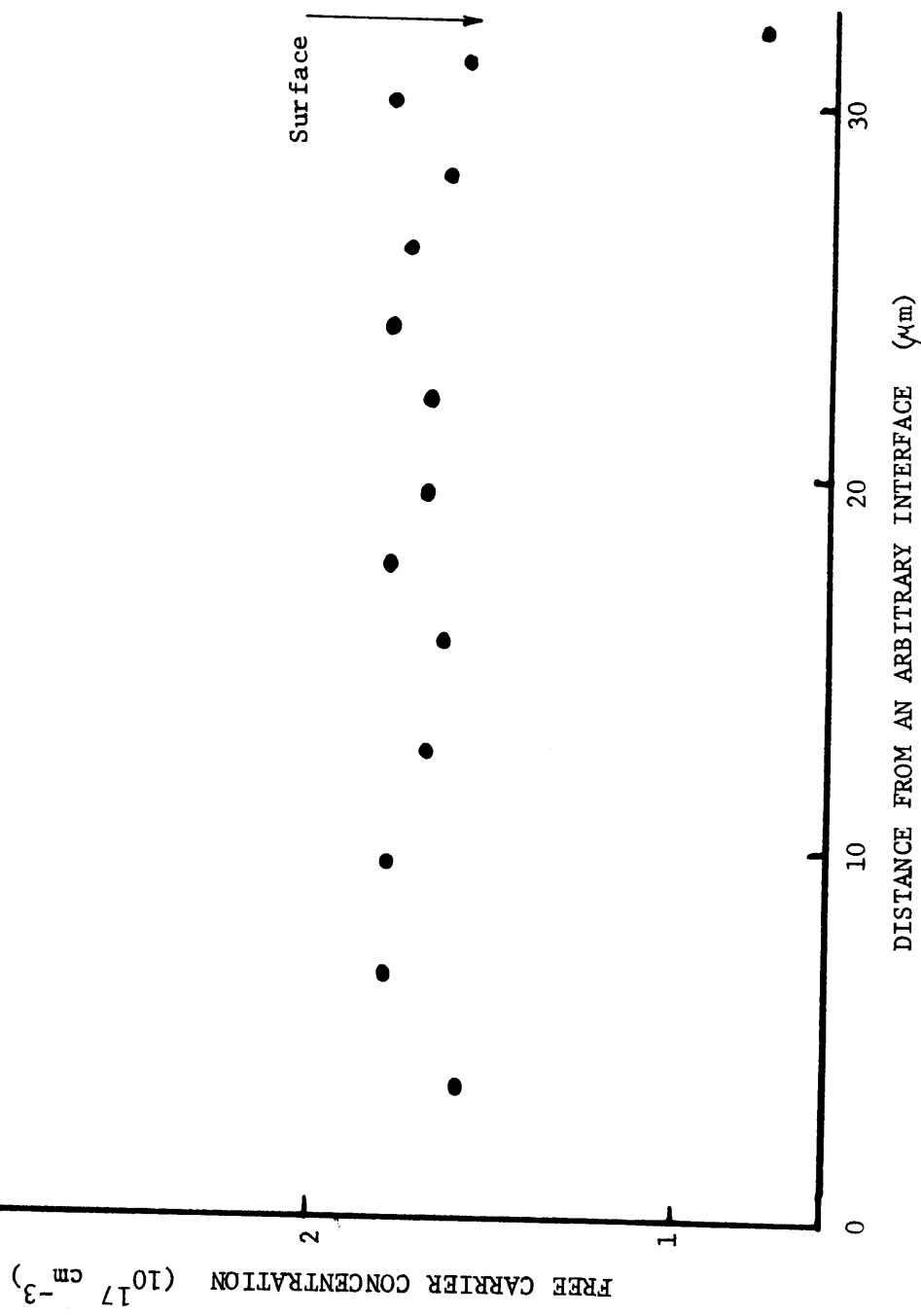
a layer whose surface was partially covered with excess GaAs deposited from a drop of solution not wiped off after growth. The carrier concentration at the exposed surfaces of both layer and excess exhibited a drop in value from the bulk. However, the carrier concentration at the layer-excess interface was not lower than the bulk values. Therefore, the decrease in carrier concentration at the layer surface is due to exposure to the ambient at high temperatures after growth. It is believed that arsenic is lost to the gas phase at the surface, creating As vacancies which then diffuse into the layer. Since As vacancies act as electron acceptors, they would compensate the layer toward p-type material.

By simultaneously using current-controlled growth with furnace cooling of 0.46°C/min, it was possible to grow a layer in the presence of a dissolution current of -10 A.cm^2 (- polarity to the substrate). Growth was conducted from 850°C to 836°C in thirty minutes with interface demarcation used only at the start and finish of growth. The average growth rate was 0.60 μm/min, which is comparable to growth rates of conventional LPE layers with similar cooling rates. The carrier concentration profile of this layer, given in Fig. 6.4, decreases with layer thickness from 4.1 to 3.6 x 10^{16} cm^{-3}. In addition to the surface depletion effect, there appears to be a perturbation near the original interface. This latter effect is believed to be due to the Schottky diode not being parallel to the original interface during the last few C-V measurements. The broken line again represents equation 6.1, and again there is excellent agreement between it and the experimental points. From a comparison of Figs. 6.4 and 6.2 there appears to be no difference in the decreasing trend of the

Figure 6.4: Carrier concentration profile of a Sn-doped layer grown by furnace cooling in the presence of an applied heating current of -10 A/cm2 (- to substrate). The average growth rate was 0.6 μm/min during cooling from 850 to 836°C.
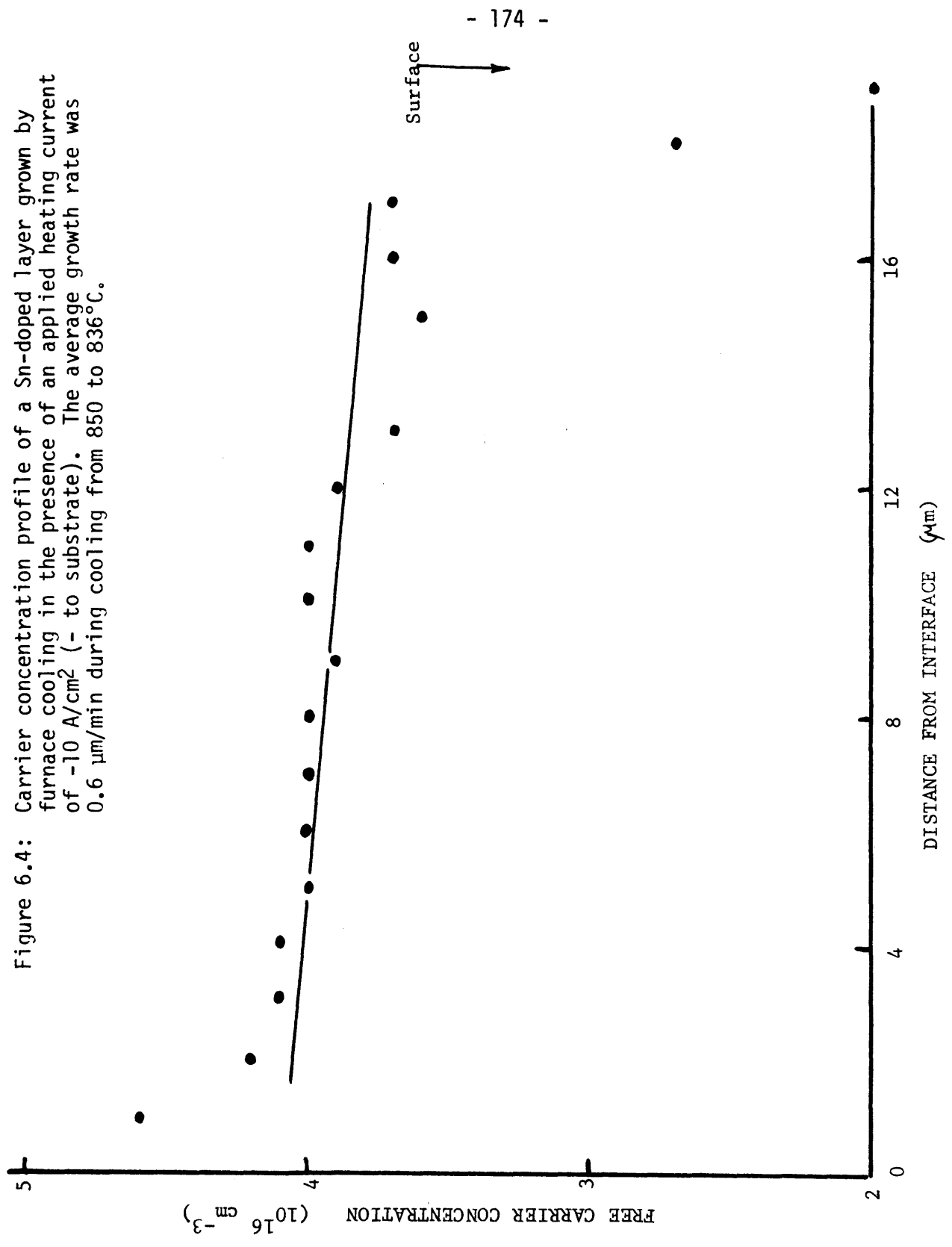
carrier concentrations for increasing layer thickness. In particular, there is no evidence that an applied current density of 10 A/cm^2 of either polarity has caused a dopant accumulation as predicted by equation 6.6 for dopant electromigration. Assuming that a 10% deviation from the observed behavior can be detected by the present methods, the quantity $\mu E\delta/D$ in equation 6.6 is less than 0.1. With the electric field equal to 5.5×10^{-4} V/cm for a current density of 10 A/cm^2 and with typical values of δ and D of 0.1 cm and 5×10^{-5} cm^2/sec respectively for the present system, the differential electromigration mobility of Sn in GaAs at 850°C is less than 0.1 cm^2/V-sec.

To determine the effect of a changing current density on Sn segregation, a layer was grown isothermally at 853°C by a current whose magnitude varied as a sin wave from 0 to +16 A/cm^2. The period of this growth current was two minutes, chosen such that the expected layer thickness corresponding to one cycle of current was comparable to the maximum depletion depth in C-V measurements (1 μm). The growth duration was 18 minutes (9 cycles) and the layer thickness was 16.9 μm, for an average thickness grown of 1.9 μm per cycle. Visual inspection of the etched layer cross-section under interference microscopy failed to provide any indication of the cyclic nature of growth. Carrier concentration measurements were taken of several areas at several layer depths, with individual C-V profiles extending from 0.2 to 0.9 μm under the applied diodes. In no circumstance did these individual profiles contain any variation from a constant carrier concentration. In addition, there was excellent agreement between all measurements taken. The change in applied current therefore

did not apparantly affect Sn segregation, for the conditions of finite growth rate studied. This experimental analysis is sensitive to instantaneous segregation changes that are thermodynamic in origin, such as changes in the chemical potential of Sn due to the applied current. The absence of any observable effect by both C-V measurements and etching/ optical characterization indicates that the solid and solution are in equilibrium locally at the interface.

The distribution ceofficient k^*_{eff} (Sn) was calculated from carrier concentration measurements for conventional and current-controlled LPE layers (k^*_{eff} is defined in Section 6.1.0). Layer carrier concentrations varied from 4×10^{16} to 4×10^{17} cm^{-3}, and tin concentrations in solution ranged from 0.43 to 4.1 atomic %. Layers were grown by conventional LPE, current-controlled LPE, and combinations of these, with cooling rates ranging from 0.03 to 1.8°C/min, current densities from -10 to +1 to +10 A/cm^2, and growth rates from 0.02 to 2.1 m/min. The results for k^*_{eff} (Sn) at 850°C are plotted versus growth rate in Fig. 6.5 The solid line is given by k^*_{eff} (Sn) = 2.3×10^{-4}, and is in excellent agreement with the experimental data. It is concluded from this figure that for R ≤ 2.1 µm/min and at 850°C:

(1) there is no growth rate dependence for Sn segregation in conventional LPE layers; and

(2) there is no growth rate dependence for Sn segregation in current-controlled LPE layers.
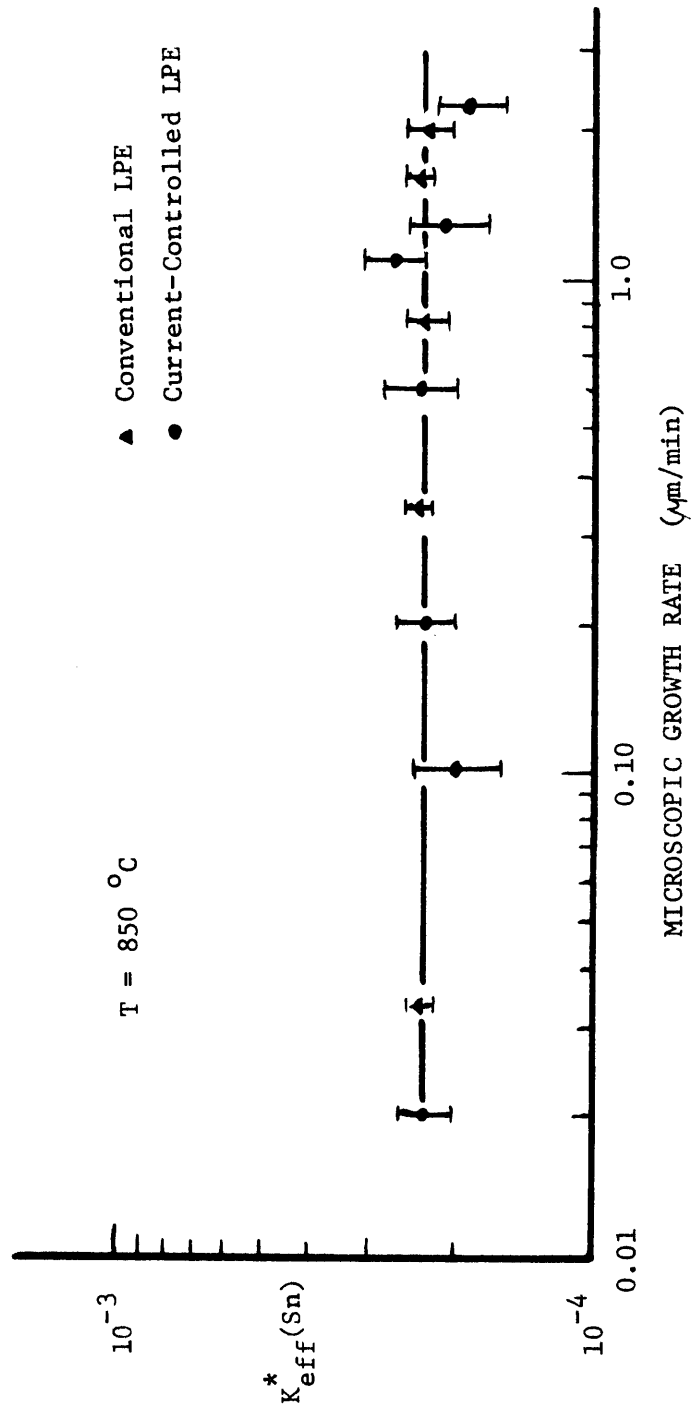
Figure 6.5: Growth rate dependence of k_{eff}^* [Sn] (ratio of free carrier conc. in the solid to the average dopant conc. in solution) at 850°C in both conventional (▲) and current-controlled (●) LPE layers.

6.2.3 Segregation behavior of tellurium in GaAs

Several layers were grown from Te-doped solutions (with GaAs sources present) at or near 850°C, and their dopant segregation behavior characterized by C-V measurements. Because of the large distribution coefficient encountered for Te ($k^*_{eff} \approx 0.3$ in the present experiments), it was necessary to use small amounts of dopant (10 - 50 μgm) to obtain layer carrier concentrations near 10^{17} cm^{-3}. The amounts of powdered Te added to the solutions introduced a large potential error in any subsequent determinations of k^*_{eff}, which necessitated the use of a buffer layer as a basis of comparison for carrier concentrations (Section 6.2.0).

Two layers were grown from the same solution at 864°C, and cooled at a rate of 0.4°C/min for thirty-five minutes (estimated layer thickness: 20 μm). For sample 125, cooling was contained from 850°C with an applied current density of -10 A/cm^2 for an additional 52 minutes. For sample 124, furnace cooling was terminated at 850°C and the second portion of the layer grown isothermally by a current density of +10 A/cm^2 for 55 minutes. Interface demarcation was applied in both layers from which microscopic growth rates were obtained. Carrier concentration profiles and microscopic growth rates for these layers are presented in Fig. 6.6. The growth rate behavior in the conventional (buffer) layer of sample 124 is similar to that given by the conventional growth model in Section 5.1.2, with an average R of 0.5 μm/min. When the cooling is terminated and the growth current applied (at 17.2 μm thickness), the growth rate initially peaks at 1.03 μm/min and then assumes a steady-state value of 0.7 μm/min to the layer surface (50 μm). The carrier concentration for sample 124 increases

Figure 6.6: Microscopic growth rates and carrier concentrations of two Te-doped layers grown by conventional and current-controller LPE. For each layer, the asterisks (*) indicate the application of a direct current (+10 for #124 and -10 A/cm² for #125).
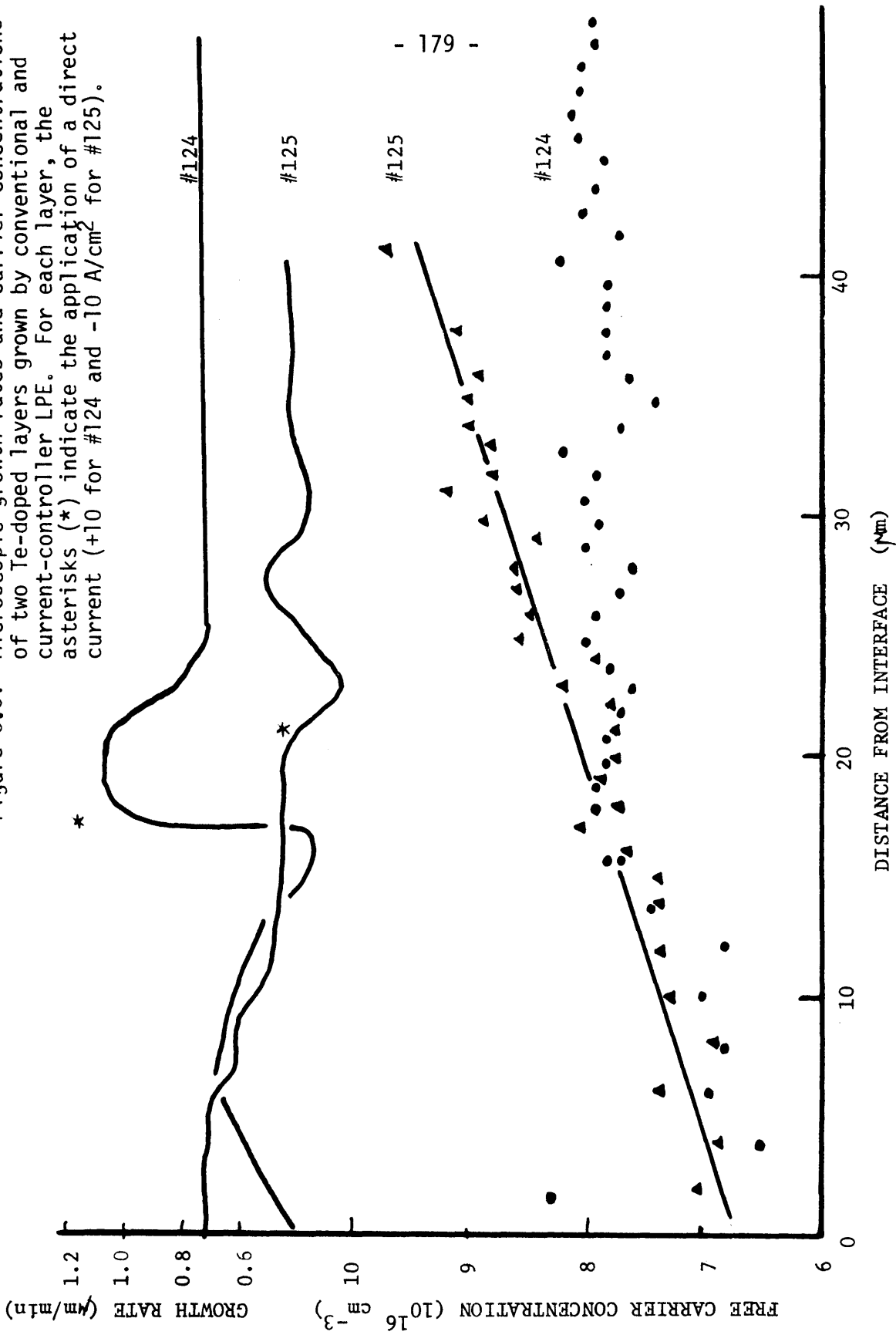
from 6.5 x 10^{16} to 7.8 x 10^{16} cm^{-3} in the buffer layer and remains fairly

constant at 7.8 x 10^{16} cm^{-3} in the latter portion of the layer deposited

isothermally by steady-state current-controlled LPE. The growth rate

behavior in the conventional layer of sample 125 is similar to that of the

previous sample, and has the same average growth rate of 0.5 μm/min. When

a dissolution current is applied (thickness: 20 μm), the growth rate drops

from 0.43 to 0.23 μm/min in ten minutes of growth, and then recovers to

0.42 μm/min in the remainder of the layer (to 41 μm). The carrier concen-

tration in this layer increases from 6.8 x 10^{16} to 9.2 x 10^{16} cm^{-3} with

layer thickness, with no apparent change in behavior as a result of the

applied current. The solid line represnts segregation behavior predicted

by equation 6.1, and is in good agreement with the experimental data of

sample 125 and of the conventionally grown portion of sample 124. The

slope of this line has the opposite sign from the tin segregation behavior

because of the different temperature dependencies for Sn and Te (refer to

Section 6.1.1). This thermal behavior is discussed in Section 6.3.

The behavior of the carrier concentrations with respect to the type of

growth and growth rates in samples 124 and 125 is similar to the results

of Sn segregation. The application of a dissolution current (-10 A/cm^2)

did not apparently affect the segregation behavior of Te. Isothermal

current-controlled LPE provided a flat carrier-concentration profile over

30 μm thick, due to Te doping. Changes in the microscopic growth rate,

in the limited range from 0.23 to 1.03 μm/min, had no apparent effect on

segregation behavior of Te.

To assess the effect of Te segregation of an increase in current

density during steady-state current-controlled LPE, a layer was grown by

first cooling 14°C to 850°C, and then applying a current density of $+5$ A/cm^2 for 11 minutes, $+10$ A/cm^2 for 14 minutes, and $+20$ A/cm^2 for 11 minutes. Microscopic growth rates for the three current-grown regions were 0.33, 0.70, and 1.4 μm/min respectively. The carrier concentration profile was measured for the final portions of the layer including part of the layer grown with $+5$ A/cm^2, shown in Fig. 6.7. The carrier concentration is constant over a 20 μm region to within $\pm 8\%$ with a value of 9.3×10^{16} cm^{-3}. There is no effect seen for the increase in growth rate accompanying the increase in current density to $+20$ A/cm^2. The scatter of the data points near the surface was due to random lateral variations in layer carrier concentration which were not present four microns underneath the surface. It is believed that these variations were caused by inter- face instability, such as facet formation, developing under the $+20$ A/cm^2 applied current density.

These results indicate that there is no net effect on Te segregation of a sudden increase in growth rate from 0.6 to 1.85 μm/min. This obser- vation is consistent with the theoretical behavior predicted in Section 6.1.2. There is also no apparent effect of the increase in current density from $+10$ to $+20$ A/cm^2 on Te segregation. From the previous results on Te it can be concluded that the change in chemical potential of Te for an applied current density of 10 A/cm^2 is also negligible. Thus, the inter- face is in local equilibrium, justifying the assumption of the same made previously.
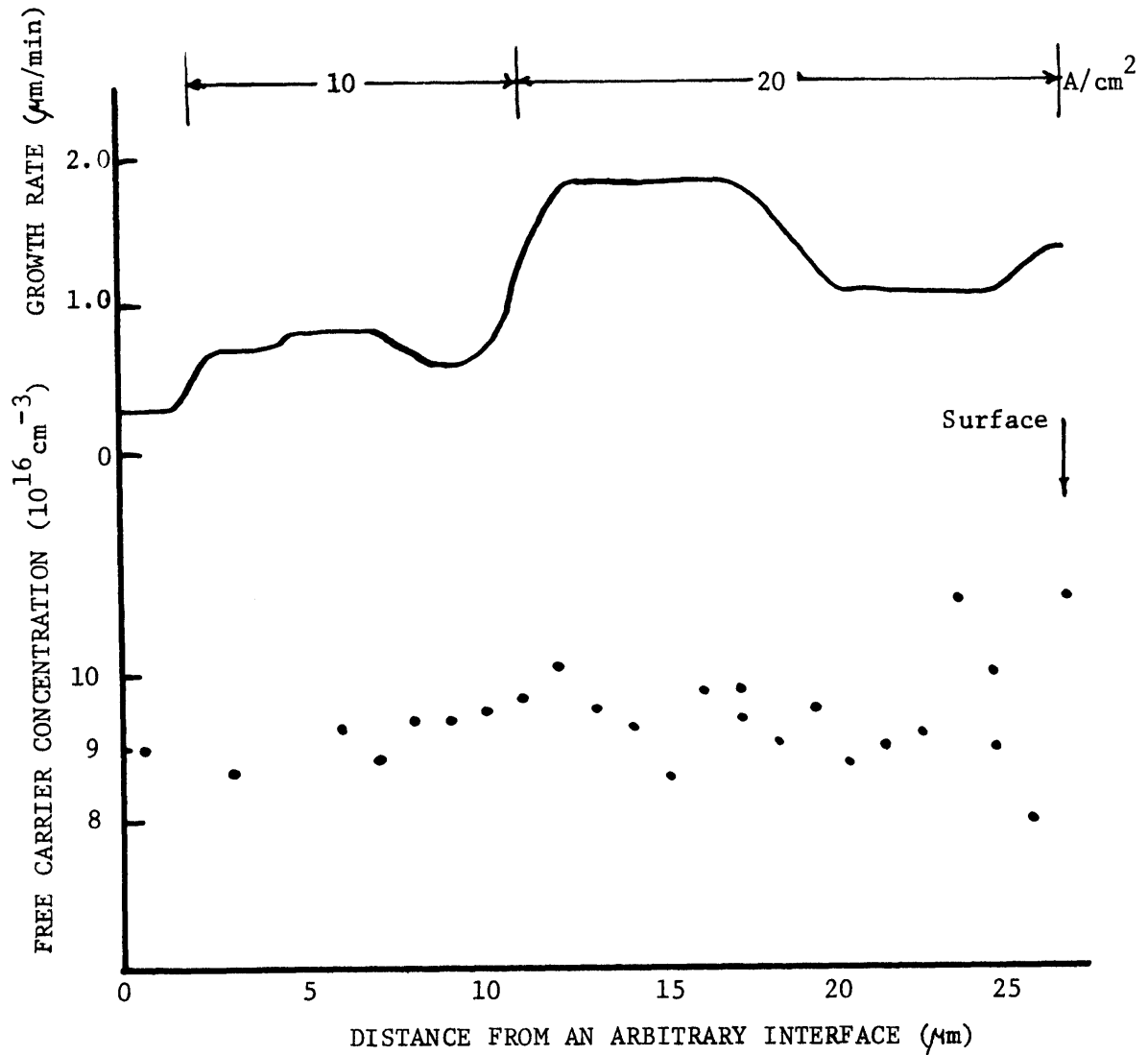
Figure 6.7: Microscopic growth rate and carrier concentration profile
of a Te-doped layer grown isothermally at 850°C by current
densities of +5, +10, and +20 A/cm².

6.3 Discussion of Segregation Behavior

The value of k^*_{eff} (Sn), the effective distribution coefficient

relating to free carrier charge concentration in the solid (Section 6.1.0),

was found to be 2.3 ($\pm$0.3) x 10^{-4} in GaAs grown at 850°C. This value is

in good agreement with reported values of 2.1 x 10^{-4}[6] and 1.2 x 10^{-4}.[107]

It is of interest to determine from k^*_{eff} the dopant distribution coef-

ficient k_{eff} (Sn) via the compensation ratio (0.4 from Section 6.1.5) and

the fraction of ionized impurities ($\approx$0.8 from Section 6.1.5). Thus the

ratio of tin atoms in the compound to the number of free carriers n is

approximately 2.9 at 850°C for n = 10^{17} cm^{-3}, which leads to a value for

k_{eff} (Sn) of 6.7 x 10^{-4}. Because k^*_{eff} was found to be independent of

growth rate in conventional LPE layers, it is concluded that the equilib-

rium and effective distribution coefficients are equal, and therefore

k_0 (Sn) = 6.7 x 10^{-4} at 850°C in GaAs.

The temperature dependence of k^*_{eff} given empirically by equation 6.1

with coefficients determined by Kang and Greene[6] has been shown to be in

excellent agreement with the carrier concentration profiles in Sn- and

Te-doped layers. The difference in the sign of the profile slopes for Sn

and Te segregation indicates that (1) the temperature dependence is

responsible for the observed behavior, and (2) that the experimental tech-

nique is capable of detecting real changes in the carrier concentration.

These are supportive of the conclusions drawn in the previous sections,

that the application of a current density up to 20 A/cm^2 for Te-doping and

to 10 A/cm^2 for Sn-doping has a negligible effect on the segregation

behavior for the conditions studied. Specifically, the following effects

were tested for and not observed: dopant electromigration, departure from equilibrium conditions at the interface, and growth rate dependence of segregation. The important implication of this conclusion is that Sn and Te dopant modulation is not possible by current densities that are small enough to yield reasonable growth areas without interference from Joule heating.

The present results on segregation during current-controlled growth are consistent with the steady-state behavior reported by Lawrence[108] for Te- and Sn-doping of GaAs (10^{15} cm^{-3} range) grown at 700°C by steady-state current-controlled LPE. He found that the net change in carrier concentration (after a transient) due to a step-increase in the current density of +10 A/cm^2 was +2% to +6% in Sn-doped layers, and +6% to +8% in Te-doped layers. Of these increases, from 11 to 38% were attributed to the background doping behavior. The transient behavior reported[57,60,108] corresponding to the onset of an increase in current density varied from 1 to 4 μm thick and entailed a 20 to 47% maximum increase in carrier concentration for both Sn and Te. Lawrence also reported that there was no segregation transient effect observed for a decrease in the current density.

This transient behavior is presently believed to be a result of the exceptionally high growth rates associated with a temperature drop at the interface. This hypothesis, stated in Section 6.1.4, is supported by the absence of a transient reported for a current density decrease, and adequately explains interface demarcation. The fact that these transients were not observed in layers in the present work could be due to the small

thickness of the effect (from Peltier cooling of less than 1°C: Section 5.2.3) in combination with the diode not being exactly parallel to the interface during the measurement. The presence of a segregation effect associated with interface demarcation was also undetected by C-V measurements in the present work.

The only other work reporting on segregation in current-controlled LPE was done by Jastrzebski and Gatos.[59] They reported growing Te-doped layers (4-6 x 10^{18} cm^{-3}) at 850°C and Sn-doped layers (5-7 x 10^{17} cm^{-3}) at 950°C with current densities from 0.5 to 40 A/cm^2. They observed that carrier concentrations, obtained from Van der Pauw/Hall measurements, increased an average of 10% in Te-doped layers and 8.5% in Sn-doped layers for an ·increase in current density of 10 A/cm^2.

The results of the present work on segregation suggest that the effects that Jastrzebski et al observed[59] are high by a factor of 2. However, differences in the growth temperatures, doping densities, and measurement techniques may account for the discrepancy. It is therefore of interest to estimate the minimum values of parameters that can be detected by the present approach to segregation. In order to effect a 10% change in the steady-state carrier concentration of a layer grown at 850°C,

> (1) the interface temperature must be changed
>   15°C for Sn-doping and 11°C for Te-doping,
>   predicted by the temperature dependence of
> k^*_{eff};

(2) the growth rate must be 30 μm/min and 100 μm/min for a Sn- and Te-doped layer, respectively [from eq. 6.3 with k_o (Sn) = 10^{-3} and k_o (Te) = 0.7];

(3) the electromigration mobility of the dopant species must be 0.09 cm^2/V-sec (eq. 6.6 with $D = 5 \times 10^{-5}$ cm^2/sec, δ = 0.1 cm) for a change in the current density of 10 A/cm^2 or,

(4) the change in the applied current density must be 30 A/cm^2 (eq. 6.6 with the above conditions and $\mu_d = \mu_{As}$ from Section 5.3).

At temperatures higher than 850°C, the last three requirements become more stringent because of an increase in the dopant diffusivity. Only the temperature change for a 10% difference in Sn-segregation decreases (to 11°C at 950°C). On the other hand, at lower temperatures most of these requirements will ease somewhat, i.e., any segregation changes due to these effects will be more pronounced.

In summary, it is found that Sn and Te segregation behavior is controlled solely by the temperature at the growth interface which is in local equilibrium, for the conditions studied. Thermal, or conventional, LPE results in layers with changing carrier concentrations given empirically by eq. 6.1, while isothermal current-controlled growth yields layers with flat carrier concentration profiles. Segregation effects due to an applied current density of 10 A/cm^2 for Sn-doped layers and of 20 A/cm^2 for Te-doped layers are found to be less than 10% at 850°C. Carrier con-

centrations of these layers were independent of microscopic growth rate from 0.02 to 2.0 μm/min caused by either conventional or current-controlled LPE. It is suggested that the high growth rates associated with a rapid drop of the interface temperature are responsible for inter-face demarcation.

7. ELECTROMIGRATION

7.0 Introduction

The effect of electromigration (EM) on epitaxial growth is in addition to any thermal effects present in the system (such as furnace cooling or the Joule or Peltier effects). The maximum thickness of a layer grown from an equilibrated solution with no source present is limited by the solution height, the ultimate temperature drop during growth, and the final arsenic concentration (or the slope of the liquidus of the equilibrium phase diagram). When layers were grown isothermally (constant furnace temperature) by a current flow across the solution-solid interface, the layer thicknesses were significantly greater than those expected with a temperature drop of one or two degrees centrigrade, predicted from the Peltier cooling at the interface.[103] The driving force for growth under the given conditions could not be attributed to Peltier cooling alone. On the basis of the above argument, and of surface migration experiments, the question of electromigration was raised by Jastrzebski et al,[58] while other workers[62] maintained that growth was due to Peltier cooling at the interface.

Since this controversy was based on results of current-controlled growth experiments, it was decided to conduct a series of simple experiments without growth that could determine the EM mobility of As in Ga at 850°C. The procedures used are described in Section 4.5.

7.1 Theoretical Treatment of Electromigration in a Dilute Metallic Solution

Electromigration is the directed displacement of a component of a solution in the presence of an applied electric field.[98] In most cases the resulting force on a species is due to either an interaction of the charge of the species with the field,[49] or an interaction between conducting electrons and the species.[51,52] The net movement or migration depends on the species' size, mass, concentration, and environment (e.g., other components of the solution).

The transport of metallic species under the influence of an applied potential was treated extensively in the literature some ten years ago. Verhoeven[49] gives a general expression for the flux of a dilute species due to an applied electric field E as

$$J_1^{EM} = C_0 \, C_2 \, \overline{V}_2 \, \mu_1^2 \, E \tag{7.1}$$

where C_1 and C_2 are the concentrations of species 1 and 2 respectively, $\overline{V}_2$ is the partial molar volume of component 2, and μ_1^2 is the differential mobility (velocity/unit field) of component 1 in component 2. In the present work, the solutions contained between 0.96 and 0.98 mole-fraction gallium, and for simplification both C_2 and $\overline{V}_2$ were set equal to 1. The flux of arsenic due to electromigration (EM) can then be written as (dilute solution approximation)

$$J_{As}^{EM} = C_{As} \, \mu_{As} \, E \tag{7.2}$$

When this flux is added to the diffusion flux and interface velocity (due to growth), the continuity equation, a one-dimensional system, is given as:

$$\frac{\partial C_{As}}{\partial t} = D \frac{\partial^2 C_{As}}{\partial x^2} + R \frac{\partial C_{As}}{\partial x} - \mu_{As} E \frac{\partial C_{As}}{\partial x} \tag{7.3}$$

where R is the growth rate (interface velocity), and D is the mutual diffusion coefficient ($C_{As} D_{Ga} + C_{Ga} D_{As}$), which is for the present system approximated as D_{As}.

These electromigration experiments were in closed systems with no growth or moving interfaces, and therefore the growth rate R in equation 7.3 is zero. Because the value of D_{As} is not known precisely, the use of time dependent solutions of (7.3) involving D_{As} was avoided (a derivation of the time dependent solution is given in Appendix 10.1). The two solutions to (7.3) of interest to the present experiments are the short-time approximation (neglecting the diffusion term) and the steady-state solution (corresponding to infinite times).

The steady-state distribution of arsenic is obtained from

$$0 = D_{As} \frac{\partial^2 C_{As}}{\partial x^2} - \mu_{As} E \frac{\partial C_{As}}{\partial x} \tag{7.4}$$

with boundary conditions corresponding to a closed system (i.e., the flux at the system boundaries is zero) of

$$J\Big|_{o,\ell} = D \frac{\partial C}{\partial x}\Big|_{o,\ell} - \mu E C\Big|_{o,\ell} = 0 \qquad (7.4a)$$

Upon integrating twice and substitution of (7.4a), equation 7.4 becomes

$$C_{As}(x) = C_{As}(0) \, e^{-\mu_{As} E x / D_{As}} \qquad (7.5)$$

where $C_{As}(0)$ is the arsenic concentration at $x = 0$. In experiment EM-7 this concentration was fixed at the As liquidus concentration by excess GaAs at $x = 0$. The arsenic distribution given by (7.5) is such that at every point $0 \leq x \leq \ell$, the diffusive flux is equal and opposite to the electromigration flux. It is of interest to note that the distribution of Bi in Sn as reported by Wagner et al[100] fits solution (7.5). However, in the present experiments only the endpoints of the distribution, i.e., $C_{As}(0)$ and $C_{As}(\ell)$ were measured.

The short-time approximation to equation 7.3 is obtained by assuming that the flux in equation 7.2 is constant:

$$\Delta M_{As} = J_{As}^{EM} \cdot A \cdot t \cdot (AW_{As}) \qquad (7.6)$$

where ΔM_{As} is the mass of arsenic transported in time t across an interface of area A, and AW_{As} is the atomic weight of arsenic. Since this approximation assumes that the changes in C_{As} are small, an average concentration $\bar{C}_{As}$ is used in J_{As}^{EM} to yield

$$\mu_{As} = \frac{\Delta M_{As}}{A \, \bar{C}_{As} \, E \, t \, (AW_{As})} \qquad (7.7)$$

Equation 7.7 is used to obtain values of μ_{As} for these EM experiments. A first order approximation of the error due to the omission of the diffusion term in the total flux was derived from the diffusion flux J_{As}^D as

$$\frac{J_{As}^D}{J_{As}^{EM}} = \frac{D \, \Delta C_{As} \, / \, 2}{\mu_{As} \, E \, \overline{C}_{As}} \tag{7.8}$$

where ΔC_{As} is the difference in As concentrations as $x = 0$ and $x = \ell$. This equation may be used to correct for diffusive fluxes of either direction.

7.2 Experimental Results

Visual inspection of the reservoirs after separation showed that the GaAs precipitated at the surface of the two solutions only: no GaAs was visible through the quartz capillary. However, after dissolution of the gallium in the capillary small crystals of GaAs were seen and when weighed, corresponded closely to the GaAs expected from the average As concentration in the system. Because the presence of convection during the ten minute quenching was expected to deplete the As concentration in the capillary, it is felt that no convection was present. Thus the results are a function only of electromigration and diffusion.

The electric field in the Ga solutions was calculated from the resistivity measured and the current density applied. Figure 7.1 gives the resistivity of the system as a function of temperature with good agreement of the value at 30°C with one reported by Williams and Appapillai.[109]

The value of ρ of 55 $\mu\Omega$-cm was obtained by extrapolation to 850°C and with 20 A/cm^2 leads to an electric field of 1.1×10^{-3} V/cm for these EM experiments.

After separation of the GaAs, final concentrations in both reservoirs and the capillary were calculated, ranging from 0.0301 to 0.0388 mole fraction As. Since the solubility of As in Ga at 850°C is 0.0371 (Section 5.1.1), GaAs precipitates were usually present in one reservoir during the experiments. The total amount of GaAs measured indicated that 7 to 9% of the As was lost to the ambient.

It was found that in three experiments there was considerable movement of Ga from one well to the other. This was believed to be caused by
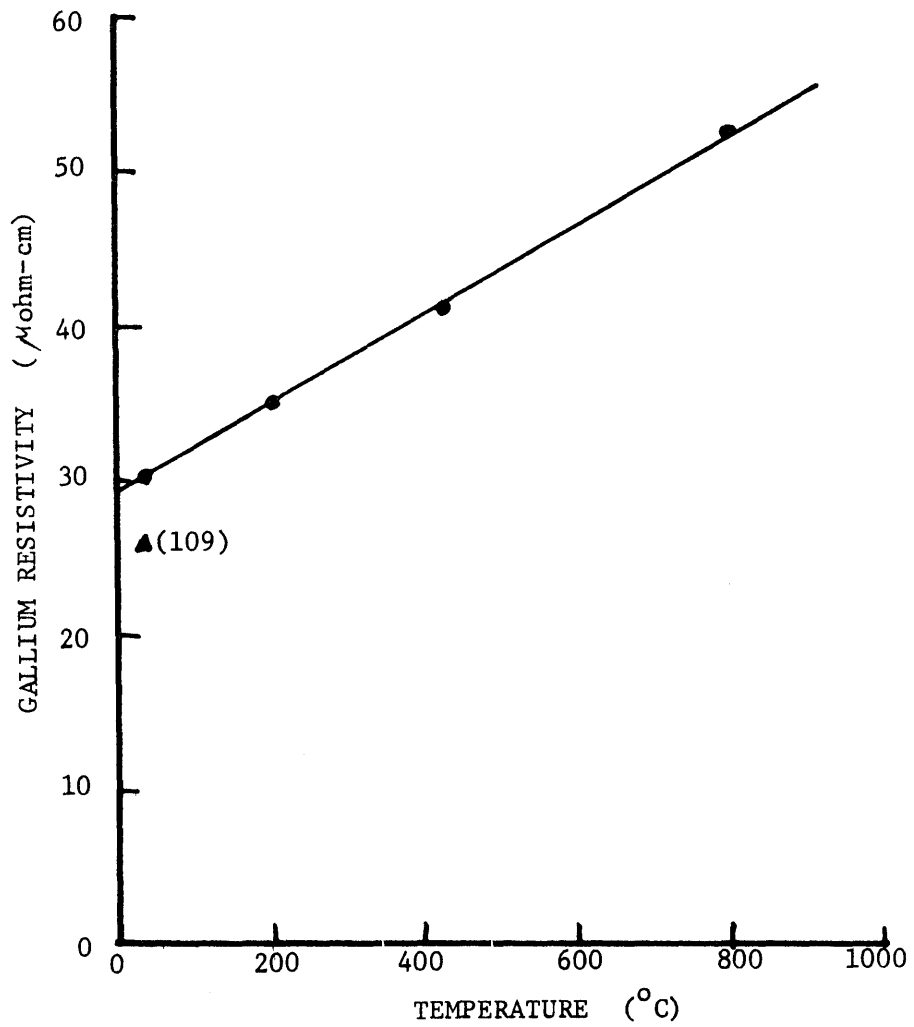
Figure 7.1: Resistivity of an arsenic saturated gallium solution as a function of temperature.

insertion of the system into the furnace tube, and was eliminated in the last experiment by special handling of the system (TLC). Thus, although each reservoir started with the same amount of As, the initial concentrations of As in the left-hand and right-hand reservoirs (C_L and C_R, respectively) were not necessarily equal. In order to take this disparity into account in the determination of μ_{As}, a correction term ΔM_{As}^* was calculated from equation 7.6 for the equilibration time with the diffusive flux (used instead of J_{As}^{EM}) due to the maximum concentration difference between the reserviors. The initial As concentrations in the reservoirs were obtained from the initial amounts of GaAs added and the final amounts of Ga measured after the experiments, assuming that no movement of Ga took place at elevated temperatures. Another correction term ΔM_{As}^{**} was introduced to allow for the As diffusive flux during the experiment by using equations 7.6 and 7.8 with both the initial and final concentrations in each reserviors.

The results of four electromigration experiments are presented in Table 7.1. Current densities of both polarities were 20 A/cm^2 across the capillary, for 12.5 hour duration. The mass of GaAs recovered after the experiments indicated a net As transport to the anode. The correction terms previously defined range from 1 to 12% of the difference in masses of As, and tend to subsequently reduce the value of μ_{As} calculated from equation 7.7. The spread in three of the calculated values of μ_{As} can be attributed to the experimental technique and the degree of uncertainty in the calculations (ΔM_{As}^* and ΔM_{As}^{**}). The cause of the low value for μ_{As} in

TABLE 7.1

Results of the electromigration experiments.

| Exp # | Capillary current density (A/cm²)+ | Average arsenic conc. (mole-frac) | Mass of GaAs recovered from reservoirs (g) | | Net mass transfer of arsenic (mg) | Mass Corrections++ | | Corrected mass transfer of As(mg) | μ_{As} at 850°C (cm²/V-sec) |
			Left	Right		M^*_{As} (mg)	M^{**}_{As} (mg)		
EM-7	+20	0.0336	0.185	0.164	10.9	-0.3	-1.0	9.6	0.030
EM-8	-20	0.0362	0.185	0.198	-6.7	+0.1	+0.3	-6.3	0.018
EM-9	-20	0.0343	0.176	0.203	-14.0	+0.3	+1.2	-12.5	0.037
EM-10	+20	0.0360	0.189	0.1615	14.2	-0.01	+0.01	14.2	0.040

++ Refer to text for definitions of mass corrections.

+ Polarity is with respect to the left-hand reservoir.

experiment EM-8 has not been ascertained. It is therefore not possible to define a value of μ_{As} with less than ±40% uncertainty.

7.3 Discussion

These experiments all confirmed the presence and direction of electro-migration of As in Ga at 850°C in the absence of epitaxial growth and the associated Peltier effect. The values of μ_{As} calculated from these experiments are in excellent agreement with the value of 0.040 cm^2/V-sec[58] (corrected for E) and 0.018 cm^2/V-sec[88] reported in the literature. In addition, there is excellent agreement between the value of μ_{As} determined by growth experiments in the present work (Section 5.2.2), and the value determined from these EM experiments that were independent of growth. It is therefore concluded that As in a Ga solution will migrate under an applied electric field toward the anode with an approximate mobility of 0.036 cm^2/V-sec.

8. SUMMARY AND CONCLUSIONS

The growth and segregation behavior of epitaxial GaAs deposited by conventional and current-controlled LPE were studied through a characterization of the microscopic growth rates given by interface demarcation, and through charge carrier concentration profiles given by the capacitance voltage technique. A model was proposed which accounts for the contributions of various growth parameters to current-controlled LPE. From the data obtained during this investigation, the following conclusions are made:

(1) Conventional LPE growth in the present system is characterized by 50% to 60% efficient deposition, with the efficiency being independent of growth rates, cooling rates and the extent of convection. This finding suggests the presence of growth sites other than the substrate. It was also found that during conventional LPE conditions of local equilibrium do exist at the GaAs-solution interface for growth rates smaller than 2 μm/min and cooling rates smaller than 2°C/min.

(2) The results indicate that, for current-controlled LPE without the use of a source in the temperature range from 700 to 850°C, growth is predominantly due to electromigration of As. The temperature change at the growth interface due to Peltier cooling and Joule heating results in an equilibrium concentration change at the interface (given by the Ga-As phase diagram), which appears as a transient in the growth rate behavior, becoming negligible after 10 to 20 minutes of growth.

(3) The growth rate due to electromigration was experimentally found to be proportional to the arsenic solubility, as given by the dilute solution approximation of Verhoeven.[49]

(4) The value of the diffusivity and electromigration mobility of arsenic in gallium was determined by comparisons of the experimental growth rates with theory. It was found that $D = 0.32 \exp(-9700/T)$ cm^2/V-sec for $973°K \leq T \leq 1123°K$ with an uncertainty of less than 30%. The diffusivity at 800°C is 3.9×10^{-5} cm^2/sec. The EM mobility in the above temperature range was determined to be $\mu_{As} = 0.32 \exp(-2330/T)$ cm^2/V-sec. The value of μ_{As} at 850°C (0.040 cm^2/V-sec) was also determined by independent measurements of electromigration in the absence of growth.

(5) The thermal conditions in the present growth system during current-controlled LPE with a source above the solution were found to control the departure from the expected electromigration flux of the steady-state growth behavior. The important thermal parameter for growth is believed to be the temperature difference between the substrate-solution and source-solution interfaces, which is controlled by existing thermal gradients and the Peltier and Joule effects.

(6) Different morphological characteristics were observed in conventional and current-controlled LPE without a source. Thickness variations in conventional LPE could be attributed to variations in the thickness of the momentum boundary layer, while in current-controlled LPE morphological variations could be explained as a result of variations in the original interface morphology. It was observed that during conventional LPE and the initial transient of current-controlled LPE, a significant reduction occurred in the amplitude of the morphological varations of the layers.

(7) Tin and tellurium segregation in layers deposited by conventional or steady-state current-controlled LPE at 850°C was found to be

virtually independent of the rate of growth (for R < 2 μm/min).

(8) The segregation behavior of Sn and Te has been found to be unaffected by the application of an electric current (up to 10 A/cm^2 for Sn, to 20 A/cm^2 for Te).

(9) The growth interface temperature was determined to be the controlling parameter for segregation of Sn and Te. Variations in layer carrier concentrations could be attributed solely to changes in the interface temperature.

(10) The values of k_{eff}^* (Sn), the effective distribution coefficient relating to the free charge carrier concentration in the solid (Section 6.1.0), was found to be 2.3 ($\pm$0.3) x 10^{-4} in GaAs grown at 850°C. This value has been correlated to the equilibrium distributuion coefficient which was thus calculated to be 6.7 x 10^{-4} at 850°C.

9. RECOMMENDATIONS FOR FURTHER STUDY

The present work has resolved several of the issues concerned with current-controlled LPE and has also raised several questions. It has been suggested that Joule heating, along with Peltier cooling, plays an important role in steady-state current-controlled growth. In addition, the contribution of existing thermal gradients has not yet been determined, nor has the extent or origins of convection in the steady-state configuration. The different morphologies observed are of interest in the growth of both smooth layers and opto-electronic structures.[110] Several layers presently grown by current-controlled LPE have exhibited reductions of several orders of magnitude in etch pit densities. This may be due to a difference in the interface kinetics or the use of interface demarcation to interrupt growth.[111] Finally, limited control over the segregation behavior may be possible by using temperature changes in conjunction with an applied current.[112] Based on these issues, the following recommendations for further study are presented:

(1) The effects of substrate thickness and doping on current-controlled LPE without a source should be investigated, along with its implications to Peltier cooling.

(2) Thermal effects including Peltier cooling, Joule heating, and existing gradients should be characterized in the steady-state configuration and related to growth behavior.

(3) The origins and extent of convection during LPE should be established.

(4)   The mechanisms responsible for the differences in interface morphologies should be identified.

(5)   The defect structure in current-controlled LPE layers should be investigated.

(6)   The effect of an electric current on segregation of other dopants used in LPE of GaAs and on the composition of ternaries should be characterized.

(7)   The segregation effect associated with interface demarcation should be further investigated. Specifically, interface demarcation should be optimized to allow for maximum detectability and minimum interference to growth to allow for more accurate microscopic growth rate determination in transient regions.

10.1 APPENDIX

DERIVATION OF A THEORETICAL MODEL FOR
CURRENT-CONTROLLED LPE IN A FINITE SOLUTION

Two theoretical models are presented which describe the growth rate characteristics and layer thickness as well as the solute concentration profile for an LPE system under the application of an electric current across the solution and solution-substrate interface. For growth with no mixing in solution an exact theoretical treatment is given in section 10.1.1 while growth with mixing in solution is treated as an approximation in section 10.1.2. The resulting expressions for growth with mixing are used primarily to predict the final transient of growth rates. Two basic assumptions are made in both treatments :

1. The solute concentration at the growth interface
   remains constant once a potential is applied;

2. The applied field results in an electromigration
   flux proportional to the solute concentration,
   as given by Verhoeven[49] (see eq. 7.2).

The effect of Peltier heating or cooling on the interface concentration is discussed in section 5.1.3, together with other assumptions necessary to make the model applicable to experiments. The basic growth configuration shown in Fig. 5.1 is used which limits growth or dissolution to the substrate surface at $x = 0$, and provides uniform one-dimensional current flow.

10.1.1 Current-controlled growth with no mixing in a finite solution

For dilute solutions the flux J of solute (concentration C) is the sum of diffusion and electromigration:

$$J = -D \frac{\partial C}{\partial x} - C\mu E, \quad (0 \le x \le \ell) \tag{10.1}$$

where D is the solute diffusivity, μE is the product of a differential electromigration mobility (EM) and the applied electric field, and ℓ is the solution height. The solid-solution interface is at x = 0, indicating solute transport to the interface for fields of positive polarity. The continuity equation obtained from the above flux is simplified by assuming that the diffusivity D and the EM drift velocity μE are independent of solute concentration and are slowly varying functions of temperature:

$$\frac{\partial C}{\partial t} = D \frac{\partial^2 C}{\partial x^2} + E \frac{\partial C}{\partial x}, \quad (0 \le x \le \ell) \tag{10.2}$$

The following boundary conditions are used:

$$C(0,t) = C_i \tag{10.3}$$

and

$$D \frac{\partial C}{\partial x}\bigg|_{x=\ell} + \mu E \, C(\ell,t) = 0 \tag{10.4}$$

where C_i is the interfacial solute concentration. While the initial condition may be arbitrarily set to any distribution $C_0(x)$, it is useful to assume equilibrium conditions at t = 0, thus making C_0 constant:

$$C(x,0) = C_0 \tag{10.5}$$

For the given boundary conditions the steady state solution to eq. 10.2 is readily seen to be an exponential:

$$C(x) = C_i \, e^{-\mu E x/D} \tag{10.6}$$

where $\mu E/D \equiv \eta$ has units of inverse length. In the determination of $C(x,t)$ the motion of the growth interface (which is small compared to solute velocities) is neglected.

Equation 10.2 is solved using separation of variables after first dividing through by D. The time dependent factor of C is exponentially decreasing with time,

$$c^{(t)} = A \, e^{-k^2 Dt} \tag{10.7}$$

where k^2 and A are real constants. The accompanying equation for the position dependence of C [i.e., $c^{(x)}$] is

$$\frac{\partial^2 c^{(x)}}{\partial x^2} + \eta \frac{\partial c^{(x)}}{\partial x} + k^2 \, C(x) = 0 \tag{10.8}$$

Taking $c^{(x)} = B \exp(px)$ the characteristic equation and its solution are

$$p^2 + \eta p + k^2 = 0 \tag{10.9}$$

$$p = \frac{\eta}{2} \pm \sqrt{\frac{\eta^2}{4} - k^2} \tag{10.10}$$

Combining the time and x dependent solutions, the concentration is a sum of terms in k_n^2, each of which satisfies equation 10.2:

$$C(x,t) = \sum_n e^{-\eta x/2 - k_n^2 Dt}$$
$$\cdot (A_{1n} e^{x\sqrt{\eta^2/4 - k_n^2}} + A_{2n} e^{-x\sqrt{\eta^2/4 - k_n^2}}) \tag{10.11}$$

The conditions 10.3 - 10.6 are now invoked to determine the constants A_{1n}, A_{2n} and k_n^2. For large t values (10.6), C(x) is finite and non-zero; therefore one k_n^2 must be equal to zero. If $k_o^2 \equiv 0$, equation 10.11 reduces to 10.6 if $A_{1,0} = 0$ and $A_{2,0} = C_i$. The concentration at x = 0 now becomes

$$C(o,t) = C_i + \sum_n e^{-k_n^2 Dt} (A_{1n} + A_{2n}) \qquad (10.12)$$

where the application of boundary condition 10.3 requires that the summation equal zero for all time, or for each n,

$$A_{1,n} = - A_{2,n} . \qquad (10.13)$$

The term $(n^2/4 - k_n^2)^{1/2}$ in 10.11 is assumed imaginary and a new symbol, λ_n, is used:

$$\lambda_n = (k_n^2 - n^2/4)^{1/2} \qquad (10.14)$$

where λ_n is real and positive. The validity of this assumption is established by the self-consistency of the resulting solution and the determination of k_n^2. With 10.13 and 10.14 the concentration C(x,t) reduces to the Fourrier series :

$$C(x,t) = C_i e^{nx} + e^{-nx/2} \sum_n e^{-k_n^2 Dt} b_n \sin \lambda_n x \qquad (10.15)$$

where b_n are constants. Equation 10.4 is a boundary condition of the third kind,[113] and results in a non-linear equation for λ_n when 10.15 is substituted into 10.4:

$$e^{-n\ell/2} \sum_n b_n e^{-k_n^2 Dt} \{\tfrac{n}{2} \sin \lambda_n \ell + \lambda_n \cos \lambda_n \ell\} = 0 \qquad (10.16)$$

The terms in the brackets must sum to zero for each n allowing λ_n to be obtained from

$$\lambda_n \cos \lambda_n \ell = - \tfrac{n}{2} \sin \lambda_n \ell \qquad (10.17)$$

which can be solved numerically from

$$\tan \lambda_n \ell = - (\lambda_n \ell) / (n\ell/2) \, . \qquad (10.18)$$

There is a solution to 10.18 within each period of $\tan \lambda_n \ell$ which can be represented by

$$\lambda_n = \frac{(n-1/2)\pi}{\ell} + \sigma_n \, , \, n = 1, 2, 3... \qquad (10.19)$$

where $0 < \sigma_n < \pi/2$ and the limit of σ_n ($n \to \infty$) is zero. The constants k_n^2 are now determinable from equation 10.14 as

$$k_n^2 = \frac{n^2}{4} + \lambda_n^2 \qquad (10.20)$$

which increases as n^2 for large values of n.

The constants b_n can be obtained by evaluating the initial conditions (10.5) with the expression for C(x,t) from 10.15:

$$C(x,0) = C_0 = C_i e^{-nx} + e^{-nx/2} \sum_n b_n \sin \lambda_n x \qquad (10.21)$$

which can be reduced by multiplying both sides by $\sin \lambda_m x$ and integrating over x from 0 to ℓ. Using the orthogonality properties of the sine

function, all integrals in the summation are zero except for n = m :

$$\int_0^\ell \sin \lambda_n x \, \sin \lambda_m x \, \partial x = 0 \quad \text{for } n \neq m \qquad (10.22)$$

$$= N_n \quad \text{for } n = m \ . \qquad (10.23)$$

The normalization constant N_n can be evaluated by integration and a subsequent substitution of equation 10.17 to

$$N_n = \frac{\ell}{2} + \frac{n}{4\lambda_n^2} \sin^2 \lambda_n \ell \qquad (10.24)$$

The integration of the right side of equation 10.22 after the multiplication of $\sin \lambda_m x$ yields

$$b_n = \frac{1}{N_n} \left[\frac{C_0 e^{nx/2}}{n^2/4 + \lambda_n^2} \left(\frac{n}{2} \sin \lambda_n x - \lambda_n \cos \lambda_n x \right) \right.$$

$$+ \frac{C_i e^{-nx/2}}{n^2/4 + \lambda_n^2} \left(\frac{n}{2} \sin \lambda_n x + \lambda_n \cos \lambda_n x \right) \Big]_0^\ell \qquad (10.25)$$

which after substitution for x becomes:

$$b_n = \frac{1}{N_n k_n^2} \{ C_0 \, e^{n\ell/2} \left(\frac{n}{2} \sin \lambda_n \ell - \lambda_n \cos \lambda_n \ell \right) + C_0 \, \lambda_n$$

$$+ C_i \, e^{-n\ell/2} \left(\frac{n}{2} \sin \lambda_n \ell + \lambda_n \cos \lambda_n \ell \right) - C_i \, \lambda_n \} \ . \qquad (10.26)$$

On the basis of equation 10.17 this expression simplifies to

$$b_n = \frac{1}{N_n k_n^2} \{C_0 e^{n\ell/2} \sin \lambda_n \ell + (C_0 - C_i) \lambda_n\} \tag{10.27}$$

The final form of $C(x,t)$ is thus

$$C(x,t) = C_i e^{-nx} + e^{-nx/2} \sum_{n=1}^{\infty} \frac{e^{-k_n^2 Dt} [nC_0 e^{n\ell/2} \sin_n \ell + (C_0 - C_i)\lambda_n]}{k_n^2 (\ell/2 + \frac{n}{2\lambda_n^2} \sin^2 \lambda_n \ell)} \sin \lambda_n x \tag{10.28}$$

where k_n^2 and λ_n are given by equations 10.20 and 10.18. This series converges for all $t \geq 0$ and for $0 \leq x \leq \ell$, primarily because λ_n has a value within each period π/ℓ which alternates the sign of $\sin \lambda_n x$.

The growth rate R can be obtained by scaling the flux at $x = 0$ to the concentration of the solid C_s:

$$R = - \frac{J (x=0)}{C_s - C_i} . \tag{10.29}$$

Using equation 10.28 to evaluate the flux J from 10.1 at $x = 0$:

$$R = \frac{D}{C_s - C_i} \sum_{n=1}^{\infty} \frac{\lambda_n e^{-k_n^2 Dt} [nC_0 e^{n\ell/2} \sin\lambda_n \ell + (C_0 - C_i)\lambda_n]}{(\ell/2 + \frac{n}{4\lambda_n^2} \sin^2 \lambda_n \ell) k_n^2} \tag{10.30}$$

which converges for all $t > 0$ but diverges for $t = 0$ with $(C_0 - C_i) \neq 0$, as expected from the onset of a step-change in interfacial concentration. The layer thickness d is the integral of R from $t = 0$ to t,

$$d = \sum_{n=1}^{\infty} \frac{\lambda_n [nC_0 \, e^{n\ell/2} \sin \lambda_n \ell + (C_0 - C_i) \lambda_n]}{(C_s - C_i) k_n^4 (\ell/2 + \frac{n}{4\lambda_n^2} \sin^2 \lambda_n \ell)} (1 - e^{-k_n^2 Dt})$$

(10.31)

which is finite for all times.

10.1.2 Current-controlled growth with convection in a finite solution

The growth configuration is the same as in the previous section (Fig. 5.2) with convection being treated as a source of mixing in the solution (Fig. 5.2b). The boundary layer limits solute transport to diffusion and electromigration only, while beyond $x = \delta$ the solution is assumed to be completely mixed. The resulting boundary conditions are

$$C(0,t) = C_0 - C_i$$

(10.32)

and

$$C(\delta,t) = C(\ell,t) = C_0 - dC_s/\ell$$

(10.33)

where ℓ is the solution height, d the epitaxial layer thickness, and C_s the As concentration in the solid. Equation 10.33 represents conserva-

tion of mass, equating the decrease of the solute in solution to the amount of solute in the grown layer. The initial condition is

$$C(x,0) = C_0 . \qquad (10.34)$$

The flux through the boundary layer is comprised of an electromigration term and a diffusion term:

$$J = - C\mu E - D \left[\frac{C(\delta,t) - C(0,t)}{\delta} \right] \qquad (10.35)$$

The growth rate R is proportional to the flux at x = 0,

$$R = - \frac{1}{(C_s - C_i)} J \bigg|_{x=0} = \frac{C_i \mu E}{C_s - C_i} + \frac{D}{\delta} (C_0 - dC_s/\ell - C_i)/C_s \qquad (10.36)$$

which can be rearranged to

$$R = \frac{C_i \mu E}{C_s - C_i} + (C_0 - C_i) \frac{D}{(C_s - C_i)} - \frac{Dd}{\delta\ell} \qquad (10.37)$$

Taking $\delta\ell/D \equiv \tau$, it can be shown that d and R are exponentials of the following forms:

$$d = \tau \left[\frac{\mu E}{C_s - C_i} C_i + (C_0 - C_i) D/\delta (C_s - C_i) \right] \{1 - e^{-t/\tau}\} \qquad (10.38)$$

and

$$R = [\frac{\mu E}{C_s - C_i} C_i + (C_o - C_i) \, D/\delta \, (C_s - C_i)] \, e^{-t/\tau} \qquad (10.39)$$

The above expressions satisfy the previous conditions applied to describe a growth system with convection. The conditions used are an approximation of growth once a boundary layer is established, and as such the model is not valid for the initial growth period $(t < \frac{\delta^2}{D})$. An alternate approach to the effect of convection on growth is to use the behavior of the preceding model where it is most valid, at time $t \gtrsim \delta\ell/D$, to establish an effective solution height ℓ_c such that the diffusion model of 10.1.1 may be used to describe the same behavior. The diffusion model predicts similar behavior for large values of t, but has the advantage of describing initial growth transients exactly while the boundary layer is being established. This is important when step changes in interface temperature or composition are present, and the initial growth rate approaches $\pm \infty$.

The effective solution height ℓ_c can be roughly determined by equating the exponentials in expressions 10.39 and 10.30 (first term only),

$$- k_1^2 \, Dx = - Dx/\ell\delta \qquad (10.40)$$

and approximating k_1^2 as $4\ell_c^2 k^2$ (good for $n\ell < 1$). If growth rates can be described by equation 10.30 for a particular ℓ_c, the boundary layer δ can be determined from

$$\delta = 4\ell_c^2/\ell\pi^2 \qquad (10.41)$$

where ℓ is the measured solution height. A more accurate determination of δ from ℓ_c can be made by equating the maximum thickness of layers calculated by the diffusion and convection models. In the notation used previously these thicknesses are, for the diffusion case,

$$d_{max} = \frac{(C_0 - C_i)}{(C_s - C_i)} \ell_c + \frac{\mu E\ C_i}{2D\ (C_s - C_i)} \ell_c{}^2 \qquad (10.42)$$

and for the convection case,

$$d_{max} = \frac{(C_0 - C_i)}{(C_s - C_i)} \ell + \frac{\mu E\ C_i}{D\ (C_s - C_i)} \delta\ (\ell - \frac{\delta}{2}) \qquad (10.43)$$

where ℓ_c has been substituted for ℓ in the former equation.

By equating these two expressions, δ is obtained as:

$$\delta = \ell - [\ell^2 - \ell_c{}^2 + \frac{2(C_0 - C_i)}{\eta\ C_i} (\ell - \ell_c)]^{1/2}. \qquad (10.44)$$

This expression can be simplified for $(C_0 - C_i)$ values normally encountered with Peltier cooling or heating:

$$\delta = \ell - (\ell^2 - \ell_c{}^2)^{1/2}. \qquad (10.45)$$

It can be shown that 10.45 approaches 10.41 for $\ell_c{}^2 \ll \ell^2$,

$$\delta \approx \ell_c{}^2/2\ell \qquad (10.46)$$

A discussion of the magnitude of δ expected from fluid dynamic considerations of the Ga/GaAs system is presented in section 5.1.4 and 5.3.

10.2 Appendix: The Effect on LPE of Local Variations in the Layer-Substrate Resistivity

An example was given in section 5.1.4 of a layer thickness variation due to a local variation in the applied current density, which may be due to the substrate's rear contact, growth interface wetting conditions, or defects in the substrate or layer. Without specifying the cause, the effects on current density of the resistivity of a region in the solid are calculated, as well as the heat evolved per unit volume due to the current.

The solid is assumed to be of average resistivity ρ_0 through which is passed an average current density J_0, leading to an applied field $V_0 = J_0\rho_0$ across the solid. This voltage is also applied across a volume V (area A, length ℓ) with an arbitrary resistivity ρ, leading to a localized current density J,

$$J = J_0\rho_0/\rho \qquad (10.47)$$

The Joule heat evolved per unit volume, Q_J , is given by

$$Q_J = I^2R/V = J^2\rho$$

where $I = JA$ and $R = \ell\rho/A$. By substitution of equation 10.47 into 10.48, the Joule heating per unit volume is obtained with the average heating for the solid, $Q_0 = J_0^2\rho_0$, as

$$Q_J = Q_0 \left(\frac{\rho_0}{\rho}\right) \qquad (10.49)$$

Thus, more heating is present in volumes of lower resistivity than the average, accompanying the larger currents. The above effect on growth may be partially offset by Peltier cooling which is proportional to the density.

BIBLIOGRAPHY

1. M. Kumagawa, A. F. Witt, M. Lichtensteiger, and H. C. Gatos, J. Electrochem. Soc. 120 (1973) 583.

2. H. Nelson, RCA Review 24 (1963) 603.

3. H. Rupprecht, J. M. Woodall, K. Konnerth, and D. G. Pettit, Appl. Phys. Lett. 9 (1966) 221.

4. E. A. Geiss, J. D. Kuptsis, and E. A. D. White, J. Cryst. Growth 16 (1972) 36.

5. M. G. Astles, J. C. H. Birbeck, C. J. Laversuch, and M. C. Rowland, J. Cryst. Growth 34 (1976) 24.

6. C. S. Kang and P. E. Greene, 1968 Symposium on GaAs, pp. 18-21.

7. S. I. Long, J. M. Ballantyne, and L. F. Eastman, J. Cryst. Growth 26 (1974) 13.

8. M. B. Panish, I. Hayashi, and S. Sumski, IEEE J. Quantum Elec. QE-5 (1969) 210; Met. Trans. 2 (1971) 795.

9. H. F. Lockwood and M. Ettenberg, J. Cryst. Growth 15 (1972) 81.

10. J. M. Blum and K. K. Shih, J. Appl. Phys 43 (1972) 1394.

11. W. A. Tiller and C. S. Kang, J. Cryst. Growth 2 (1968) 345.

12. M. B. Small and J. F. Barnes, J. Cryst. Growth 5 (1969) 9.

13. H. Minden, J. Cryst. Growth 6 (1970) 228.

14. I. Crossley and M. B. Small, J. Cryst. Growth 11 (1971) 157.

15. R. Ghez, J. Cryst. Growth 19 (1973) 153.

16. D. L. Rode, J. Cryst. Growth 20 (1973) 13.

17. J. J. Hsieh, J. Cryst. Growth 27 (1974) 49.

18. R. L. Moon and J. Kinishota, J. Cryst. Growth 21 (1974) 149.

19. A. Doi, T. Asano, and M. Migitaka, J. Appl. Phys. 47 (1976) 1589.

20. R. L. Moon and S. I. Long, J. Cryst. Growth 32 (1976) 68.

21. M. Mihara, N. Toyoda and T. Hara, Appl. Phys. Lett. 27 (1975) 131.

22. S. Long, J. Ballantyne, and L. F. Eastman, J. Cryst. Growth 32 (1976) 95.

23. R. Ghez and J. S. Lew, J. Cryst. Growth 20 (1973) 273.

24. R. Deitch, J. Cryst. Growth 7 (1970) 69.

25. J. Crossley and M. B. Small, J. Cryst. Growth 19 (1973) 160.

26. R. H. Saul and D. D. Roccasecca, J. Appl. Phys. 44 (1973) 1983.

27. E. Bauser, M. Frik, K. S. Loechner, L. Schmidt, and R. Ulrich, J. Cryst. Growth 27 (1974) 148.

28. B. L. Mattes and R. K. Routes, J. Cryst. Growth 27 (1974) 131.

29. R. L. Moon, J. Cryst. Growth 27 (1974) 62.

30. W. A. Tiller, J. Cryst. Growth 2 (1968) 69.

31. W. W. Mullins and R. F. Sekerka, J. Appl. Phys. 35 (1964) 444.

32. R. Ghez and E. A. Giess, Mat. Res. Bull. 8 (1973) 31.

33. R. Solomon, 1968 Symposium on GaAs, 1968, pp. 11-17.

34. D. L. Rode, J. Cryst. Growth 27 (1974) 313.

35. J. J. Van Vechten, J. Cryst. Growth 38 (1977) 139.

36. M. B. Small and J. Crossley, J. Cryst. Growth 27 (1974) 35.

37. C. S. Kang and P. E. Greene, Appl. Phys. Lett. 11 (1967) 171.

38. J. C. Carballis, D. Diguet, and J. Lebailly, Proc. of the Second Int. Symposium on Gallium Arsenide (1968) pp. 28-35.

39. K. H. Zschauer, 1972 Symposium on GaAs, pp. 3-10.

40. J. Vilms and J. P. Garrett, Solid State Elec. 15 (1972) 443.

41. H. G. B. Hicks and P. E. Greene, 1970 Symposium on GaAs,

42. H. Morkoc and L. F. Eastman, J. Cryst. Growth 36 (1976) 109.

43. P. E. Greene, Solid State Comm. 9 (1971) 1299.

44. A. R. Goodwin, C. D. Dobson, J. Franks, Proc. of the Second Int. Symposium on GaAs (1968), pp. 36-40.

45. P. D. Sudlow, A. Mottram, and A. R. Peaker, J. Mat. Sci. 7 (1972) 168.

46. K. H. Zschauer and A. Vogel, 1970 Symposium on GaAs

47. G. Pfann and R. S. Wagner, Trans. AIME 224 (1962) 1139.

48. J. A. Burton, R. C. Prim, and W. P. Slichter, J. Chem. Phys. 21 (1953) 1987.

49. J. D. Verhoeven, Trans. AIME 223 (1965) 1156.

50. O. P. Sinha, Phys. Letters 38A (1972) 193.

51. S. G. Epstein and A. Paskin, Phys. Letters 24A (1967) 309.

52. S. G. Epstein, Conf. on Prop. of Liquid Metals (1967) 325.

53. W. G. Pfann, K. E. Benson, and J. H. Wernick, J. Electron 2 (1957) 597.

54. R. Singh, A. F. Witt, and H. C. Gatos, J. Electrochem. Soc. 115 (1968) 112.

55. M. Lichtensteiger, A. F. Witt, and H. C. Gatos, J. Electrochem. Soc. 118 (1971) 1013.

56. G. M. Blom, J. J. Daniele, T. Kyros, and A. F. Witt, J. Electrochem. Soc. 122 (1975) 1541.

57. D. J. Lawrence and L. F. Eastman, J. Cryst. Growth 30 (1975) 267.

58. L. Jastrzebski, H. C. Gatos, and A. F. Witt, J. Electrochem. Soc. 123 (1976) 1121.

59. L. Jastrzebski and H. C. Gatos, Inst. Phys. Conf. Ser. No. 33b (1977) 88.

60. D. J. Lawrence and L. F. Eastman, J. Elec. Mat. 6 (1977) 1.

61. A. Abul-Fadl and E. K. Stefonakos, J. Cryst. Growth 39 (1977) 341.

62. J. J. Daniele and C. Michel, Inst. Phys. Conf. Ser. No. 24 (1975) 155.

63. L. Jastrzebski, H. C. Gatos, and A. F. Witt, J. Electrochem. Soc. 124 (1977) 633.

64. H. Kressel, J. Elec. Mat. 3 (1974) 747.

65. G. M. Blom, S. L. Blank, and J. M. Woodall, Eds., Liquid Phase Epitaxy, Special Issue J. Cryst. Growth 27 (1974).

66. C. J. Herman, Private communication.

67. J. Hilibrand and R. D. Gold, RCA Review (June 1960) 245.

68. A. M. Goodman, J. Appl. Phys. 34 (1963) 329.

69. J. A. Copeland, Trans. Elec. Devices. 16 (1969) 445.

70. P. H. LadBrooke and J. E. Carroll, Int. J. Elec. 31 (1971) 149.

71. G. L. Miller, Trans. Elec. Dev. 19 (1972) 1103.

72. B. J. Gordon, H. L. Stover, and R. S. Harp, Proceedings ASTM Symp. Si Dev. (1970) 273.

73. F.D. Hughes, R. F. Headon, and M. Wilson, J. Phys. E5 (1972) 241.

74. S. M. Sze, Physics of Semiconductor Devices, N.Y.: Wiley-Interscience, 1969.

75. P. Wu, E. C. Douglas, and C. W. Mueller, Trans. Elec. Devices 22 (1975) 319.

76. E. H. Hall, Am J. Math. 2 (1879) 287.

77. L. J. Van der Pauw, Philips Res. Reports 13 (1958) 1.

78. G. A. Rozgonyi and D. C. Miller, Thin Solid Films 31 (1976) 185.

79. E. S. Meieran, Trans. Met. Soc. AIME 242 (1968) 413.

80. M. Halliwell, J. B. Childs, and S. O'Hara, 1972 Symposium on GaAs, pp. 98-105.

81. B. K. Tanner, X-Ray Diffraction Topography, New York: Pergamon Press, 1976.

82. G. A. Rozgonyi and S. E. Haszko, J. Electrochem. Soc. 117 (1970) 1562.

83. A. M. Vejux, Ph.D. Thesis, M.I.T., Sept. 1972.

84. M. S. Abrahams and C. J. Buiocchi, J. Appl. Phys. 36 (1965) 2855.

85. R. N. Hall, J. Electrochem. Soc. 110 (1963) 383.

86. M. Rubenstein, J. Electrochem. Soc. 113 (1965) 752.

87. C. D. Thurmond, J. Phys. Chem. Solids 26 (1965) 785.

88. L. Jastrzebski, J. Lagowski, and H. C. Gatos, to be published.

89. J. R. Carruthers, J. Cryst. Growth 2 (1968) 1.

90. J. R. Carruthers, Unpublished.

91. G. K. Batchelor, Quart. Appl. Math. 12 (1954) 209.

92. S. Ostrach, to be published, 1978.

93. E. P. Martin, Ph.D. Thesis, M.I.T., June 1977.

94. M. J. Stewart and F. Weinberg, J. Cryst. Growth 12 (1972) 217.

95. M. J. Stewart and F. Weinberg, J. Cryst. Growth 12 (1972) 228.

96. A. Doi, T. Asano, and M. Migitaka, J. Cryst. Growth 39 (1977) 353.

97. R. D. Gold, Japan. J. Appl. Phys. 2 (19) 131.

98. D. K. Belashchanko, Russian Chem. Rev. 34 (1965) 219.

99. D. R. Hay and E. Scala, Trans. Met. Soc. AIME 223 (1965) 1153.

100. R. S. Wagner, C. E. Miller, and H. Brown, Trans. Met. Soc. AIME 236 (1966) 554.

101. J. D. Verhoeven, Trans. Met. Soc. AIME 239 (1967) 694.

102. J. J. Daniele, Private communication.

103. E. K. Stefanakos, A. Abul-Fadl, and M. D. Workman, J. Appl. Phys. 46 (1975) 3002.

104. J. T. Thompson, Jr., M.S. Thesis, M.I.T., June 1976.

105. J. S. Harris, Y. Nannichi, G. L. Pearson, and G. F. Day, J. Appl. Phys. 40 (1969) 4575.

106. W. A. Tiller, K. A. Jackson, J. W. Rutter, and B. Chalmers, Acta Met. 1 (1953) 428.

107. J. S. Harris and W. L. Snyder, Solid State Elec. 12 (1969) 337.

108. D. J. Lawrence, Ph.D. Thesis, Cornell Univ., 1977.

109. A. R. Williams and M. Appapillai, J. Phys. F3 (1973) 772.

110. T. Fukui, K. Wakita, Y. Hocikoshi, Japan. J. Appl. Phys. 16 (1977) 1043.

111. R. H. Saul, J. Electrochem. Soc. 118 (1971) 793.

112. L. Jastrzebski and H. C. Gatos, J. Cryst. Growth 42 (1977) 309.

113. P. W. Berg and J. L. McGregor, Elementary Partial Differential Equations, San Francisco: Holden-Day, 1966.

BIOGRAPHICAL NOTE

The author was born on August 26, 1950, in Flushing, New York. He attended Cornell University from which he received a Bachelor of Science degree in May, 1972, and a Master of Engineering degree in May, 1973, in the Department of Applied and Engineering Physics, School of Engineering. While attending Cornell he became a member of Tau Beta Pi, and was a recipient of the New York State Regents Scholarship.

The author entered the Massachusetts Institute of Technology in September, 1973, and has been working under the supervision of Professor A. F. Witt as a Research Assistant in the Electronic Materials Group of the Department of Materials Science and Engineering. He has been elected to Sigma Xi and was an IBM Fellow during 1976-77.